May 17, 1974

To the Graduate Council:

I am submitting herewith a thesis written by Arnold Stephen Grot entitled "Time-Temperature-Precipitation Studies of Titanium-Modified Type 316 and Type 321 Stainless Steels." I recommend that it be accepted for nine quarter hours of credit in partial fulfillment of the requirements for the degree of Master of Science, with a major in Metallurgical Engineering.

J. E. Spruiell
Major Professor

We have read this thesis
and recommend its acceptance:

Dan L. Olver

E. C. Hansbury

Accepted for the Council:

Hilton A. Smith
Vice Chancellor for
Graduate Studies and Research

TIME-TEMPERATURE-PRECIPITATION STUDIES OF TITANIUM-MODIFIED TYPE 316 AND TYPE 321 STAINLESS STEELS

A Thesis

Presented to

the Graduate Council of

The University of Tennessee

In Partial Fulfillment

of the Requirements for the Degree

Master of Science

---

by

Arnold Stephen Grot

June 1974

ABSTRACT

The present research was undertaken in order to provide a relatively complete and systematic picture of the microstructural stability in both titanium-modified type 316 (316TiM) and type 321 stainless steels. These studies encompass a range of pretreatment conditions and include investigation of the recovery and recrystallization behavior of the steels as well as the phase stability.

The use of bulk extraction and x-ray diffraction techniques enabled the characterization of the precipitation activity and determination of time-temperature-precipitation diagrams between 450 and 950°C for up to 4000 hours for each pretreatment of both steels. Optical metallography allowed the study of recrystallization behavior and phase distribution. The detailed morphology and identification of the various carbides (TiC and $M_{23}C_6$) and intermetallic phases (sigma and chi) were determined by transmission electron microscopy.

These studies reveal that the early nucleation of TiC and $Ti_4S_2C_2$ is an important factor in the phase stability of types 316TiM and 321. This influence is related to the carbon content in the matrix. The precipitation of $M_{23}C_6$ is delayed and its growth retarded by TiC. Sigma is preferentially precipitated in type 316TiM due to the low carbon content in the matrix. Chi formation is retarded by

1146941

early sigma formation. Cold work accelerates the precipitation of $M_{23}C_6$, enhances sigma growth provided recrystallization refines the grain size, and suppresses chi nucleation and growth if sigma growth is accelerated. Recrystallization in type 316TiM occurs earlier and proceeds more rapidly than in types 316 and 321. The observation that type 321 is more stable than type 316TiM is explained by the differences in composition.

TABLE OF CONTENTS

CHAPTER		PAGE
I.	INTRODUCTION	1
	Background of the Problem	1
	Basic Metallurgical Principles of Stainless Steels	4
II.	PREVIOUS STUDIES OF MICROSTRUCTURAL STABILITY IN AUSTENITIC STAINLESS STEELS	8
	Phases Precipitated in Austenitic Stainless Steels	8
	General Characteristics of Phase Instabilities in Austenitic Stainless Steels	11
	Phase Stability of Types 321 and 316	14
III.	EXPERIMENTAL PROCEDURE	20
	Materials, Pretreatments, and Aging Conditions	20
	Experimental Techniques	23
IV.	RESULTS AND DISCUSSION	27
	Characterization of As-Pretreated Samples	27
	Effect of Aging Treatments-Precipitation Behavior as Determined by X-Ray Diffraction of Bulk Extracted Residues	33
	Effect of Aging Treatment-Phase Morphology and Recrystallization Behavior	49
	Hardness Measurements	74

CHAPTER PAGE

Further Discussion 83

V. CONCLUSIONS 91

LIST OF REFERENCES 93

APPENDIXES 97

Appendix A 98

Appendix B 107

Appendix C 108

VITA 109

LIST OF TABLES

TABLE		PAGE
I.	Crystal Structure and Composition of Phases Reported in Types 316, 316L, and 321 Stainless Steels	9
II.	Chemical Analysis of Titanium-Modified Type 316 and Type 321 Austenitic Stainless Steels	21
III.	Pretreatment Conditions for the Time-Temperature-Precipitation Studies of Titanium-Modified Type 316 and Type 321 Stainless Steels	22
IV.	Aging Treatments Investigated for Each Pretreatment	24
V.	The Ratios of d-Spacings in Face-Centred Cubic Systems	107
VI.	Interplanar Spacings of Austenite	108

LIST OF FIGURES

FIGURE PAGE

1. Microstructures of As-Pretreated Type 316TiM Stainless Steel. (a) Solution Treated, (b) 10% Reduced, (c) 20% Reduced, (d) 40% Reduced 28
2. Electron Diffraction Patterns of As-Pretreated 20% Reduced Type 316TiM Stainless Steel in Figure 1(c). (a) Acicular Structure, (b) Cellular Structure 30
3. Microstructures of As-Pretreated Type 321 Stainless Steel. (a) Solution Treated, (b) 10% Reduced, (c) 20% Reduced 32
4. Weight Percent of Particles Extracted from Type 316TiM as a Function of Reduction in Area by Swaging and Aging Time. (a) Aged at 550°C, (b) Aged at 650°C, (c) Aged at 750°C, (d) Aged at 850°C 34
5. Weight Percent Extracted Residue Plotted Versus Aging Temperature for Aging Times of (a) 0.2 Hours, (b) 2 Hours, (c) 200 Hours 38
6. X-Ray Pattern from Extracted Residue Illustrating the Resolution of Diffraction Lines from Five Different Phases 41
7. X-Ray Patterns from the Extracted Residue from Solution Treated Samples Aged at 650°C, (a) Aged 20 Hours, (b) Aged 2000 Hours, (c) Aged 4000 Hours. . 43

FIGURE PAGE

8. Time-Temperature-Precipitation Diagram for Solution Treated Type 316TiM Stainless Steel 44

9. Time-Temperature-Precipitation Diagram for Type 316TiM Stainless Steel Given 10% Reduction in Area by Swaging Prior to Aging 45

10. Time-Temperature-Precipitation Diagram for Type 316TiM Stainless Steel Given 20% Reduction in Area by Swaging Prior to Aging 46

11. Time-Temperature-Precipitation Diagram for Type 316TiM Stainless Steel Given 40% Reduction in Area by Swaging Prior to Aging 47

12. Time-Temperature-Precipitation Diagram for Solution Treated Type 321 Stainless Steel 50

13. Time-Temperature-Precipitation Diagram for Type 321 Stainless Steel Given 20% Reduction in Area by Tube Drawing Prior to Aging 51

14. Type 316TiM Stainless Steel Reduced 20% and Aged at 650°C for (a) 20 Hours, (b) 200 Hours, (c) 2000 Hours, and (d) 4000 Hours 53

15. Type 316TiM Stainless Steel Reduced 10% and Aged at 750°C for (a) 0,2 Hours, (b) 2 Hours, (c) 20 Hours, and (d) 200 Hours 54

16. Type 316TiM Stainless Steel Reduced 40% and Aged at 750°C for (a) 0,2 Hours, (b) 2 Hours, and (c) 20 Hours 55

FIGURE PAGE

17. Recrystallization Behavior of Type 316TiM Reduced 40% by Swaging Compared with Type 316 Reduced 50% by Rolling 56

18. Recrystallization Starting Times for Type 316TiM Reduced by Swaging and Type 321 Reduced by Tube Drawing 57

19. Type 316TiM Stainless Steel Aged 200 Hours at 850°C. (a) Initially Solution Treated, (b) 10% Reduced, (c) Reduced 20%, (d) Reduced 40% 59

20. Transmission Electron Micrographs of Type 316TiM. (a) Solution Treated and Aged 4000 Hours at 550°C, (b) 10% Reduced and Aged 2 Hours at 750°C, (c) 20% Reduced and Aged 20 Hours at 750°C, (d) Solution Treated and Aged 2000 Hours at 850°C. . . 61

21. Transmission Electron Micrographs of Type 316TiM. (a) 10% Reduced and Aged 4000 Hours at 550°C, (b) 10% Reduced and Aged 20 Hours at 750°C, (c) 20% Reduced and Aged 2000 Hours at 750°C, (d) Solution Treated and Aged 2000 Hours at 750°C. . . 65

22. Type 321 Stainless Steel. (a) Solution Treated and Aged 4000 Hours at 650°C, (b) Reduced 20% and Aged 4000 Hours at 650°C, (c) Solution Treated and Aged 200 Hours at 850°C, (d) Solution Treated and Aged 2000 Hours at 850°C 70

FIGURE PAGE

23. Type 321 Stainless Steel Reduced 20% and Aged at 750°C for (a) 2 Hours, (b) 200 Hours, and (c) 2000 Hours 71

24. Figure 24. Transmission Electron Micrographs of Type 321. (a) Reduced 20% and Aged 200 Hours at 750°C, (b) Solution Treated and Aged 200 Hours at 650°C 72

25. Diamond Pyramid Hardness of Type 316TiM as a Function of Reduction in Area and Aging Time. (a) Aged at 550°C, (b) Aged at 650°C, (c) Aged at 750°C, (d) Aged at 850°C 75

26. Diamond Pyramid Hardness of Type 321 as a Function of Reduction in Area and Aging Time. (a) Aged at 650°C, (b) Aged at 750°C, (c) Aged at 850°C . . 80

27. A Simple Electron Diffraction Camera 99

CHAPTER I

INTRODUCTION

I. BACKGROUND OF THE PROBLEM

Austenitic stainless steels are widely used in industry. At high temperatures, these steels undergo changes which result in important variations of mechanical and chemical properties. These changes must be understood for safe, efficient use. The loss of impact resistance in austenitic steels at elevated temperatures is of prime concern for application in steam generating plants as piping and superheater tube material (1,2). Considered of equal importance are changes in corrosion resistance (3) and weldability (1,2) due to exposure to high temperatures. When used in nuclear reactors these steels must withstand the effects of irradiation as well as high temperatures (4-10).

The general suitability of the austenitic stainless steels for application as fuel cladding and other components of nuclear reactors has been realized for several years (6,7). This suitability is based upon high-temperature strength properties, resistance to corrosion by liquid sodium, compatibility with uranium-plutonium oxides, and a low neutron capture cross section. A major concern, however, is the low elevated temperature creep ductility that results from irradiation to high fluences (8). At high irradiation

and test temperatures, a loss of ductility due to helium embrittlement is observed. At somewhat lower temperatures observed increases in strength and decreases in ductility have also been attributed to and correlated with lattice hardening (10). This results at least in part from the formation of a high density of interstitial dislocation loops which apparently form from the supersaturation of interstitials created by the neutron bombardment. Precipitation of interstitials also leads to an imbalance in the number of vacancies and interstitials so that recombination is not complete. This leads to the agglomeration of vacancies to form voids and results in a second problem, namely the swelling of the stainless steel (9). Recent studies have shown that the presence of a high sink density such as is produced by cold working may delay the onset and/or reduce the magnitude of the swelling due to the formation of the void-dislocation structure generated by fast neutron bombardment (9). Such a reduction in swelling is desirable if these alloys are to be used for fast-reactor cladding and structural components.

Bloom and Stiegler (10,11) have shown that the addition of titanium to type 304 and type 316 stainless steels leads to improvement in post-irradiation ductility. The increased post-irradiation ductility is attributed to the decreased tendency for grain-boundary fracture. This decreased tendency may be due to the titanium combining with

sulfer and thereby removing it from the grain boundaries. It is also possible that titanium may have some benefit in reducing swelling or shifting the temperature range in which it occurs. As a result, titanium-modified type 316 (316TiM) stainless steel and other titanium containing austenitic stainless steels are prime potential candidate materials for nuclear application.

At the present time, little information is available on the elevated temperature phase stability in such steels with or without the added effect of neutron irradiation. The precise knowledge of the out-of-pile phase reactions is required as a basis for a rational prediction of the microstructural changes under reactor environment and the effect of these changes on mechanical, physical, and corrosion properties (4).

While investigators at Oak Ridge National Laboratory are interested in long range studies of mechanical properties, particularly creep tests of 316TiM as a function of various pretreatment, aging, and irradiation conditions, they do not plan to do a systematic study of the precipitation reactions occurring in this steel over a wide range of aging temperatures.

The classical titanium-bearing commercial stainless steel is type 321, and this steel is also of interest for nuclear applications (12). Experimental characterization of phase stability in type 321 austenitic stainless

steel has been sparsely conducted and findings are inconsistent for similar time-temperature ranges.

The present research was undertaken in order to provide a relatively complete and systematic picture of the microstructural stability in both type 316TiM and type 321 stainless steels. These studies encompass a range of pretreatment conditions and include investigation of the recovery and recrystalliqation behavior of the steels as well as the phase stability.

II. BASIC METALLURGICAL PRINCIPLES OF STAINLESS STEELS

Stainless steels are classified on the basis of the primary phase resulting from heat treatment. Correspondingly, they may be divided into three groups; martensitic, ferritic, and austenitic stainless steels. Martensitic and ferritic alloys are nickel free or of low nickel content. While martensitic steels are hardenable by the austenite-martensite transformation, ferritic steels are not. In practice, these two types of stainless steels are distinguished by their free chromium content, where the free chromium is defined as the chromium which can not be combined with the carbon in the steel (free chromium content = % Cr-(17 x %C)). If the free chromium content is greater than 12.5 weight percent then the steel is ferritic. If the free chromium content is less than 12.5 weight percent then the steel is martensitic. Austenitic stainless steels include

those alloys that contain at least 24 percent combined chromium, nickel, and manganese, and in which the amount of chromium is at least 18 percent.

The basic 18% Cr-8% Ni austenitic stainless steel, as typified by type 304 (0.08% C maximum), is corrosion resistant to many environments. However, this alloy is subject to intergranular corrosion, due to the depletion of chromium adjacent to the grain boundaries, if it becomes "sensitized." "Sensitization" is caused by the precipitation of chromium-rich carbides at the grain boundaries. An austenitic alloy can be desensitized by heat treatment in the temperature range where the carbides are dissolved by the austenite (980-1200°C).

In many cases, heat treatment of a component is not possible. Another way of controlling the formation of chromium-rich carbides is to reduce the carbon content in the alloy to below 0.03%, as in type 304L. With type 304L the rate of sensitization is reduced so that short exposures in the sensitization temperature range are not seriously detrimental and the alloy can be used below the range of sensitization temperatures. The alternative to reducing the carbon content to the low values of 0.03% or less is to add strong carbide forming elements which will combine with the carbon and lessen the possibility of chromium depletion by precipitation of the chromium-rich carbide. The two most frequently used elements for this purpose are titanium (type

321) and nobium (type 347. These are known as stabilized stainless steels and permit, with few exceptions, welding without decrease in corrosion resistance near the welds and without heat treatment after welding.

Also of consideration in the choice of composition of stainless steel components for service at elevated temperatures is their long time structural stability. If the service temperature is in the range of 650-816°C, the precipitation of sigma phase can cause embrittlement which is manifested in low values of room-temperature notched impact strength after exposure (1). Since creep-rupture strength and rupture ductility are increased by the presence of sigma (2), the purpose of limiting sigma is to protect equipment against fissuring during repair welding, cracking because of thermal shock, or accidental mechanical impacts when the components cool down after a long period of exposure in the embrittlement temperature range.

Pit corrosion can be of concern to some engineering applications of austenitic stainless steels when failure of components by this type of corrosion is critical. It has been found that the addition of 3% molybdenum will prevent serious pitting even in a 10% aqueous solution of ferric chloride. Type 316 is the standard molybdenum bearing austenitic stainless steel and type 316L is the low carbon grade.

Formability is sometimes a major consideration in

the choice of component material. Before the behavior of any grade in cold forming operations can be predicted, the change in ductility as well as in strength must be considered. For example, a steel that has a low rate of increase in tensile strength may break in a forming operation despite good retention of ductility. The ideal condition would be a combination of high strength, high work hardening rate, and high ductility. Austenitic stainless steels exhibit good adaption to severe deformation by cold working. This results from the slow rate at which the tensile and yield strengths converge due to work hardening, and the rate at which their ductility is lowered by cold deformation.

In material application, service conditions ultimately determine the choice of material. The properties of austenitic stainless steels show that these alloys can be used in many cases where other alloys would fail. In particular, the choice for using austenitic steels is influenced by their high temperature properties, corrosion resistance, and formability.

CHAPTER II

PREVIOUS STUDIES OF MICROSTRUCTURAL STABILITY IN AUSTENITIC STAINLESS STEELS

I. PHASES PRECIPITATED IN AUSTENITIC STAINLESS STEELS

The literature lists numerous examples of long time exposure of austenitic steels to elevated temperatures resulting in the decomposition of the austenitic matrix to various carbide and intermetallic phases (3-5,13-37). The phases commonly observed in the grades of stainless steel under investigation in this study are given in Table I. Information on composition and crystal structure of these phases, their amount, morphology and composition are observed to vary with alloy composition, pretreatment, and aging conditions. These dependencies are discussed in detail in parts II and III of this chapter with regard to the total precipitation process. A discussion of two of the individual phases widely studied because of their importance in engineering applications, follows.

Investigations in the 1950's showed the dependency of sigma formation on composition in the standard grades of austenitic stainless steels. Nicholson et al. (14) studied the effect of alloying elements on the sigma-forming tendencies of these steels and demonstrated that composition influences sigma formation. Tisinai et al.(13) demonstrated that

TABLE I

Crystal Structure and Composition of Phases Reported in

Types 316, 316L, and 321 Stainless Steels

Phase	Crystal Structure	Lattice Parameters, Å	Composition	Steel[a]
$M_{23}C_6$	fcc	a_o = 10.569 to 10.680	$(Cr_{16}Fe_5Mo_2)C_6$ $(FeCr)_{23}C_6$	316, 316L (4,5) 321 (3,22,28)
M_6C	fcc	a_o = 10.95 a_o = 11.195	$(Cr,Co,Mo,Ni)_6C$ $(Ti,Ni)_6C$	316, 316L (4) 321 (28)
TiC	fcc	a_o = 4.32		321 (3,27,28)
Sigma (σ)	Tetragonal	a_o = 8.828 to 9.188 c_o = 4.572 to 4.812	$(Fe,Ni)_x(Cr,Mo)_y$	316, 316L (4,5) 321 (28)
Chi (χ)	bcc	a_o = 8.86 to 8.92	$(FeNi)_{36}Cr_{18}Mo_4$	316, 316L (4,5)
Laves (η)	Hexagonal	a_o = 4.73 to 4.75 c_o = 7.72 to 4.74	Fe_2Mo	316, 316L (4,5)
$Ti_4S_2C_2$	Hexagonal	a_o = 3.20 c_o = 11.195		321 (27)
Matrix Austenitic	fcc	a_o = 3.59-3.598		316, 316L, 321

[a]Numbers in parentheses refer to list of references.

the nucleation times for sigma varied among the different grades of stainless steels. The work of Tisinai also showed the dependence of sigma nucleation time on temperature and confirmed the conclusion of Koh (15) that cold working the material accelerated the precipitation process of sigma.

While the dependency of sigma formation on composition, temperature, and cold work has been observed experimentally, the mechanism for sigma formation is not well established. Goldschmidt (16) suggested that decarburization of $M_{23}C_6$ could result in sigma formation. Lismer et al. (17) proposed that grain-boundary $M_{23}C_6$ coalesces with aging time, and that when a critical particle-size is reached, the carbide breaks down to form sigma. Singhal and Martin (18) and Duhaj (19) observed that sigma forms via a metastable b.c.c. ferrite phase when this phase is present. Lewis (20) proposed that sigma nucleated by the dissociation of dislocations punched out by residual carbide particles which result in stacking faults that act as nucleation sites. Martin and Singhal (21) were able to unify these theories into one mechanism of sigma formation. They noted that sigma nucleation required high energy interfaces, such as high-angle grain boundaries, incoherent twin boundaries, or high energy interfaces of second phases. Since all the previous suggestions involve a high energy boundary, it would appear that this is the critical requirement for sigma nucleation.

The dependency of $M_{23}C_6$ nucleation on composition

was discussed in Chapter I, part II. Lower carbon concentration or the addition of a stabilizing element was seen to retard the growth of $M_{23}C_6$. The primary nucleation sites for $M_{23}C_6$ are the austenitic grain boundaries (22-25). However, $M_{23}C_6$ also nucleates on incoherent twin boundaries, coherent twin boundaries (22), and dislocations (23). $M_{23}C_6$ is observed to undergo the following sequence of morphological changes at the grain boundary (23): small feathery dendrites change to large dendrites which in turn change to compact idiomorphic forms. High temperatures are seen to increase the rate of these changes. This is explained by the replacement of iron by chromium in the $M_{23}C_6$ crystal lattice. The rate of this transfer increases with increasing temperature.

Orientation of the precipitate with respect to the matrix is a factor determining its growth. The precipitate will grow far more rapidly in the direction in which the degree of misfit between the precipitate and the matrix is the lowest (26). Grain boundary $M_{23}C_6$ is observed to be initially coherent with one grain and to maintain its orientation relationship with this grain throughout growth.

II. GENERAL CHARACTERISTICS OF PHASE INSTABILITIES IN AUSTENITIC STAINLESS STEELS

There are numerous articles on phase stability in austenitic stainless steels of various compositions in the literature (3-5,13-37). From the consideration of the

precipitation sequences contained in these studies, it is possible to generate the following general precipitation sequence for austenitic steels:

1. Carbide phases nucleate first due to the high carbon diffusion rates and segregation of carbide forming elements to easy nucleating sites such as grain boundaries.

2. As the carbon content decreases, intermetallic phases are able to form, i.e., a certain minimum carbon concentration must be reached in the austenitic matrix before intermetallic phases can form. The chi phase which can accept some carbon often forms before sigma which evidently requires a low carbon content.

3. A depletion in the matrix of chromium and other alloying elements will increase the solubility of carbon. The complex $M_{23}C_6$ carbides which are less stable than the MC carbides may redissolve into the matrix and leave regions which are locally enriched in the slower diffusing substitutional solutes.

4. Further growth of intermetallic phases result because of new sites rich in metallic solute atoms due to carbide resolution.

5. Carbide phases of the type M_6C may be generated at long aging times by the addition of elements such as molybdenum to $M_{23}C_6$ or may result from high solute/carbon ratios existing in the matrix.

Alloy composition, solution treatment temperature,

and cold deformation effect the mechanisms and kinetics of this sequence without altering the general trend of precipitation. Alloy content determines the precipitates and their precise compositions. A change in the proportion of alloying elements also changes the growth rate of these precipitates, but the sequence of carbide formation before intermetallic phase precipitation remains unchanged. The presence of a stabilizing element delays the growth of complex $M_{23}C_6$ carbides, but at longer aging times this effect is less significant. The ratio of the solute concentration to carbon content plays a major role in the precipitation sequence (4,28).

Higher solution treatment temperatures promote the growth of complex carbides (4). This is associated with the larger grain size and smaller grain boundary surface area and with changes in solute supersaturation at the nucleation sites and perhaps also the quenched-in vacancy concentration. Higher solution treatment temperatures also result in more uniformly distributed intragranular carbide precipitates (4,35). Intermetallic phase precipitation does not seem to be appreciably effected by small changes in solution treatment. However, Yu. P. Bulanov et al. (28) show a considerable increase in sigma formation in type 321 when the solution treatment temperature is dropped from 1100°C to 900°C. This was explained by the larger amount of TiC present after the 900°C solution treatment and consequent lower carbon in solution.

In general, cold work accelerates the precipitation sequence of a stainless steel. Fast and early nucleation of precipitates in cold worked materials is due to the presence of many more dislocations and stacking faults which provide sites for precipitation. The sigma phase is found to grow at an accelerated rate in cold worked steels due to the early removal of carbon from the matrix by carbide precipitation. Normally early precipitating phases, such as chi and Laves, are retarded in growth because of early growth of sigma.

Although a review of the literature on austenitic steels suggests that each precipitation sequence can be understood in terms of thermodynamic stability, reaction kinetics, solubility effects, and matrix depletion due to precipitation, there is nothing to indicate that the kinetics of one type of austenitic stainless steel can be applied to another to give the precise knowledge of phase stability necessary for safe, efficient use of the alloy. Thus, for the present, at least, it is necessary to determine the precipitation reactions, kinetics and their effect on properties for each case of interest.

III. PHASE STABILITY OF TYPES 321 AND 316

Experimental characterization of phase stability in type 321 stainless steel has been sparsely conducted and findings are inconsistant for similar time-temperature

ranges. For instance, C. da Casa (27) has reported the presence of TiC, TiCN and Y-phase, a carbosulfide of titanium ($Ti_4S_2C_2$), while Yu P. Bulanov et al. (28) report TiC, $M_{23}C_6$, and sigma for similar aging conditions. Thus, a more systematic study of this steel is needed to resolve these inconsistencies and determine its detailed behavior.

The phase reactions of type 316 stainless steel are perhaps the best known among austenitic steels. This is due to the systematic studies of White and Le May (36,37), Weiss and Stickler (4), and Spruiell et al. (5). White and Le May characterized the phase stability of hot-rolled and annealed type 316 showing the effects of aging time and temperature.

S. Weiss and R. Stickler determined Time-Temperature-Precipitation (TTP) diagrams for type 316 stainless steel over a wide range of time and temperature. They combined the TTP diagrams with observation of the nucleation and growth of the various phases, their amount, morphology and composition to hypothesize a model for the observed phase reactions. Their data reveal the considerable effects of relatively minor compositional changes, of various thermal and thermomechanical pretreatments, and of aging conditions.

J. E. Spruiell et al. have investigated phase stability in type 316 stainless steel for a broad range of pretreatments. Large variations in both phase stability and

recrystallization behavior were observed to be effected by appropriate pretreatments. These variations are discussed as functions of dislocation density, grain size, alloying elements in solution, precipitate distribution, size, and morphology.

From these papers, the phase stability of type 316 can be outlined. The precipitation sequence for this alloy is as follows: initially, $M_{23}C_6$ precipitates below 900°C as a result of the super-saturation of the matrix by carbon. As the carbon concentration lowers, chi and Laves phases, possessing ability to dissolve some carbon, form. The solubility of carbon in the austenitic matrix increases with increasing temperature and with decreasing chromium and molybdenum content in the matrix. Sigma forms after enough carbon is absorbed by the carbides.

After precipitation of a certain amount of chi, Laves, and sigma phases, the carbon solubility of the molybdenum and chromium depleted matrix increases, resulting in a resolution of the $M_{23}C_6$ carbide. Areas rich in molybdenum and chromium result, providing sites for further sigma and chi growth.

The precipitation sequence of type 316L is found to be accelerated with respect to type 316 in terms of the intermetallic phases while the carbide phase is somewhat retarded. This can be explained in terms of carbon solubility and content. The growth of the carbide is restricted by

the lower amount of carbon in type 316L. Also, because of the low carbon content, it is possible for chi and sigma to form directly from the matrix at aging temperatures at which the carbon content is lower than the solubility limit. In type 316L, these temperatures are greater than 900°C. The growth of the intermetallic phases are retarded in type 316 due to higher carbon content in solution. This results in no sigma or chi formation at temperatures greater than 900°C and longer nucleation times for these phases at lower temperatures.

The prehistory of the steel also has an effect on phase stability. In type 316L, higher solution treatment temperatures shifted the precipitation of $M_{23}C_6$ to shorter aging times and slightly lower temperatures. The same behavior is also observed in type 321 (28). This can be explained by grain size. The larger grain size after higher solution treatment temperature implies a smaller total grain boundary surface area which results in a higher solute segregation along these grain boundaries. Thus, a shorter aging time is required for nucleation at these sites.

Cold working prior to aging accelerates the precipitation of $M_{23}C_6$ and the growth of sigma, but retards the growth of chi. The accelerated precipitation of phases is explained by an increase in nucleation sites (dislocations and faults) and enhanced diffusion in the highly dislocated matrix. The retarded growth of chi in cold worked type 316

is explained by the earlier nucleation of sigma which now competes sooner with chi for chromium and molybdenum.

The research papers discussed above have provided an understanding of the phase reactions in type 316 stainless steel that allows the microstructural stability of this alloy to be predicted with some accuracy. The observations of phase reactions have also added to the understanding of the mechanisms of phase formation. Although early studies on sigma formation (13,15) observed that cold working accelerates the rate of sigma formation, the existing mechanisms of sigma growth could not explain this effect until the work of Singhal and Martin. They stated that sigma phase nucleation requires high energy interfaces, such as high-angle grain boundaries, incoherent twin boundaries, or high-energy interfaces of second phases, such as oxide inclusions. The work of Weiss and Stickler (4) and Spruiell et al. (5) support this statement. These investigators reported that cold work enhances sigma formation by enhancing the recrystallization of the microstructure. Spruiell et al. state that the mechanism by which recrystallization enhances sigma formation is associated with providing ready nucleating sites to the unstable matrix and enhanced diffusion along the mobile boundary and in the cold-worked matrix.

The extensive study of the phase stability of type 316 provides an excellent background for the study of the phase reactions in titanium-modified type 316. Lowering the

carbon content or the addition of a stabilizing element improves resistance of alloy to intergranular corrosion by retarding the growth of the chromium-rich carbide, $M_{23}C_6$. In type 316L, the precipitation of $M_{23}C_6$ was retarded and the precipitation of intermetallic phases were accelerated by a low carbon concentration. The observation of phase stability in type 316TiM will show the effect of titanium on precipitation in the type 316 grade of stainless steels. No previous systematic work on the phase stability of titanium-modified type 316 steel exists.

CHAPTER III

EXPERIMENTAL PROCEDURE

I. MATERIALS, PRETREATMENTS, AND AGING CONDITIONS

The compositions of the two stainless steels investigated in this study are presented in Table II. The major differences between the two steels were that the titanuim-modified type 316 (316TiM) heat contained molybdenum, more nickel and less titanium than the type 321 steel. The type 316TiM heat was provided by researchers at Oak Ridge National Laboratory and was a portion of a 5000 pound, double vacuum melted heat purchased for scale-up studies. This material was received as half-inch diameter bars and given the pretreatments listed in Table III. The processing of these bars was arranged so that the final diameter of the pretreated rods was 0.125 inch. Reduction of the material was by swaging. Both intermediate and final solution treatments were carried out by heating under a purified argon atmosphere followed by quenching in water.

The type 321 material was vacuum melted material provided by investigators in the Breeder Reactor Development Division, General Electric Company, San Jose, California. This material came in the form of 0.25 inch outside diameter tubing with a wall thickness of 0.014 inch. The steel had been given the pretreatments listed in Table III (except for

TABLE II

Chemical Analysis of Titanium-Modified Type 316 and Type 321 Austenitic Stainless Steels

	316TiM	321
C	0.057	0.06
Ni	13.96	9.58
Cr	17.52	17.48
Mo	2.51	
Ti	0.29	0.50
Mn	1.41	1.69
Si	0.03	0.54
P	0.005	0.012
S	0.004	0.006
N	0.0035	0.011
B	0.0005	0.001
Co	0.018	0.02
V	0.03	—
Al	0.015	—
Nb	0.005	—
Ta	0.015	—
As	0.005	—
Cu	0.01	0.02

TABLE III

Pretreatment Conditions for the Time-Temperature-Precipitation of Titanium-Modified Type 316 and Type 321 Stainless Steels

A.	Solution Treated at 1204°C initially and during sample processing with a final grain size control anneal at 1093°C.
B.	Same as A plux 10% cold deformation.
C.	Same as A plus 20% cold deformation.
D.	Same as A plus 40% cold deformation.

D) by the process of tube drawing.

Both austenitic stainless steels were subsequently aged at the temperatures and times listed in Table IV. For times of 200 hours and less, aging treatment was performed under a purified argon atmosphere. For aging times of 2000 and 4000 hours, the samples were sealed in evacuated Inconel tubes. The samples of type 316TiM were 2.5 inches in length while samples of type 321 were 1.25 inches long for each aging condition. All samples were water quenched after each aging treatment.

II. EXPERIMENTAL TECHNIQUES

Bulk extraction of the precipitates for x-ray diffraction analysis was carried out electrolytically in a 10% HCl in methanol electrolyte with a current density of 175-225 milliamperes/cm^2. The weight fraction of precipitate was determined by weighing the bulk sample before and after partial dissolution and also weighing the extracted and dried residue. X-ray patterns of the extracted powder were made using a graphite crystal diffracted beam monochromator mounted on a Norelco diffractometer. The x-ray source was Cu K_α radiation with a wavelength equal to 1.54178Å. The powder was mounted on a single crystal of silicon in order to lessen background scattering and thereby improve peak to background ratios and peak resolution. Intensity data was collected by a digital rate meter at 5-second intervals and

TABLE IV

Aging Treatments Investigated for Each Pretreatment

Temperature, °C	Time, Hours
950	0.2, 2, 20, 200
850	0.2, 2, 20, 200 2000
750	0.2, 2, 20, 200, 2000
650	0.2, 2, 20, 200, 2000, 4000
550	2, 20, 200, 2000, 4000
450	200, 2000, 4000

simultaneously printed on paper and punched onto paper tape while scanning at 1/2 degree/minute. These data were then processed and plotted via computer. Qualitative phase identification was carried out by comparison of the diffraction pattern of the residue with standard patterns from the phases expected to occur in austenitic stainless steels. Several powder samples were analyzed by standard x-ray powder diffraction techniques using a Debye-Scherrer camera to assure the reliability of the monochromator method.

For the metallographic examination the heat treated samples were sectioned, conventionally mounted and polished. The etching solution used to reveal the microstructure consisted of 45.5% HCl, 45.5% distilled water, and 9% HNO_3. Standard light microscopy was employed to determine the nucleation sites, distribution, and morphology of the precipitates.

Thin foils for transmission electron microscopy were prepared by a jet electrochemical thinning method utilizing an electrolyte of 70.0% ethanol, 10.0% butyl cellosolve, 8.0% percholoric, and 12.0% distilled water followed by a final thinning in an electrochemical cell containing an electrolyte of 6.0% perchloric acid in ethanol. Precipitated particles in the thin foils were identified from electron diffraction patterns taken with the Philip's EM 300 transmission electron microscope. Transmission electron micrographs supplied supporting data for microstructural analysis.

Hardness measurements were performed on the samples prepared for optical metallography using a Kentron micro-hardness tester.

CHAPTER IV

RESULTS AND DISCUSSION

I. CHARACTERIZATION OF AS-PRETREATED SAMPLES

Titanium-Modified Type 316

The microstructures of type 316TiM for each pretreatment condition are presented in Figure 1. Bulk extractions carried out on these samples revealed that their extractable particle content was less than 0.04 weight percent. X-ray diffraction analysis revealed that these particles were mainly $Ti_4C_2S_2$ with traces of Ti(C,N). $Ti_4C_2S_2$ was also distinguishable under light microscopy because of its characteristic orange color (27).

The transmission electron micrographs of Figure 1 show the effect of cold work on the microstructure of type 316TiM. The solution treated sample is relatively free of dislocations but exhibits annealing twins, due to previous cold working and annealing treatments, Figure 1(a). The cold worked microstructures exhibit the greatly increased dislocation densities characteristic of cold deformation, Figures 1(b), 1(c), and 1(d). However, they also contain a substructure not observed in type 316 stainless steel. This substructure changes from a banded or acicular appearance in 10% reduced type 316TiM, Figure 1(b), to a cellular structure for 40% reduced type 316TiM, Figure 1(d). Electron diffraction patterns of these areas show that the crystallographic

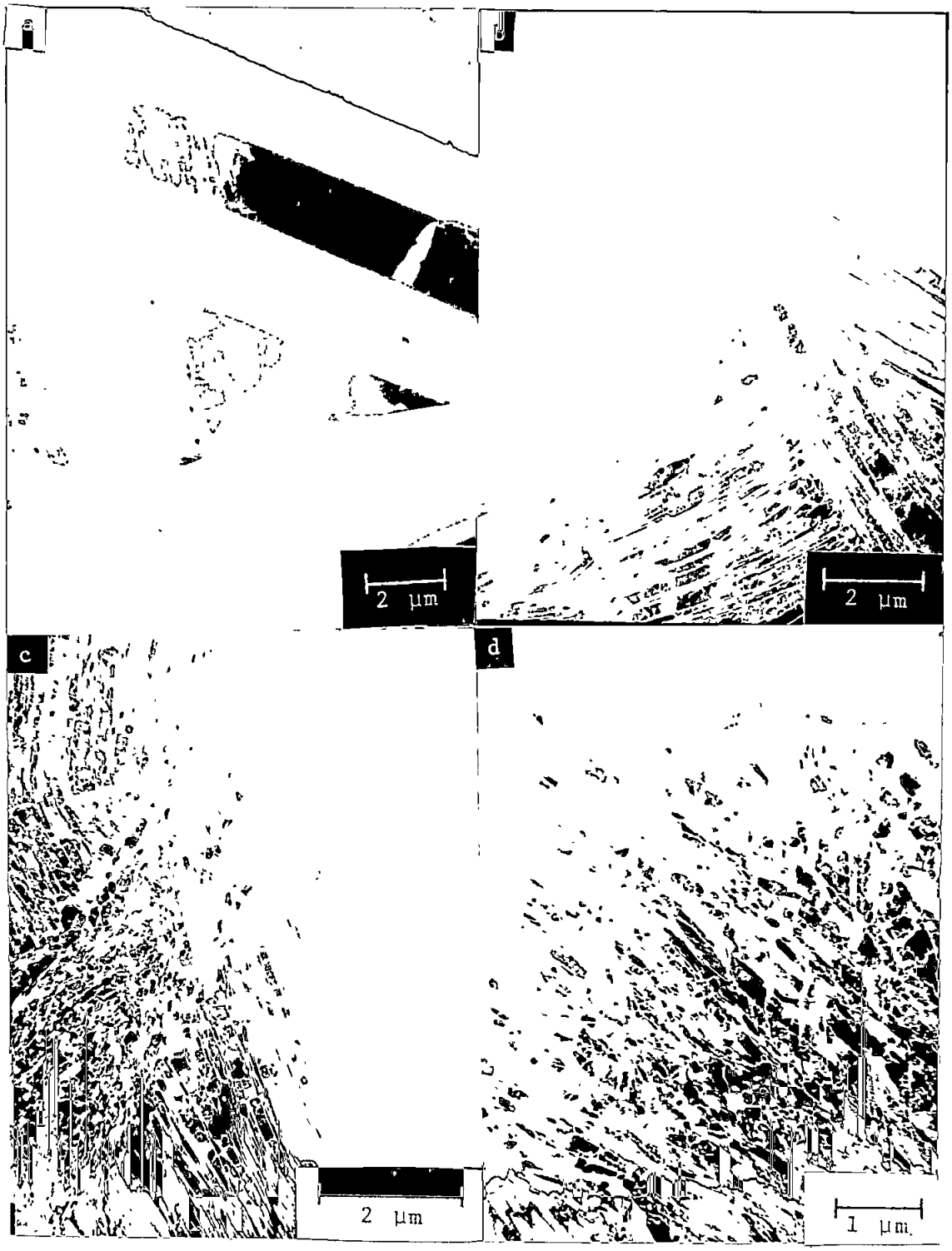


Figure 1. Microstructures of As-Pretreated Type 316TiM Stainless Steel. (a) Solution Treated, (b) 10% Reduced, (c) 20% Reduced, (d) 40% Reduced.

orientation is nearly the same throughout each region consisting of parallel bands of the acicular structure, Figure 2(a), while considerable misorientation exists among the cells of the cellular structure, Figure 2(b). The 20% reduced samples contain both the acicular and cellular structures as shown in Figure 1(c).

Analysis of the electron diffraction patterns for the cold work structure revealed only the austenitic matrix. No evidence for the formation of either ε (hexagonal) or α (bcc) martensite was observed (29,30). The substructures thus cannot be explained by the formation of these phases during deformation as has been suggested for certain substructures developed in other stainless steels due to deformation (29,30). Perhaps these substructures can be explained by the mechanism of band formation in type 316 proposed by Weiss and Stickler (4). They postulated that the bands were due to overlapping stacking faults produced by slip on closely spaced slip planes. In 316TiM the addition of titanium may change the stacking fault energy sufficiently to result in the different appearance observed as compared to the standard type 316 grade. Another cause of the different microstructures may be associated with the deformation method. The previously published microstructures for type 316 are for rolled structures observed normal to the plane of the rolled sheet. The present type 316TiM samples were swaged and are observed in Figure 1 parallel to the swaging

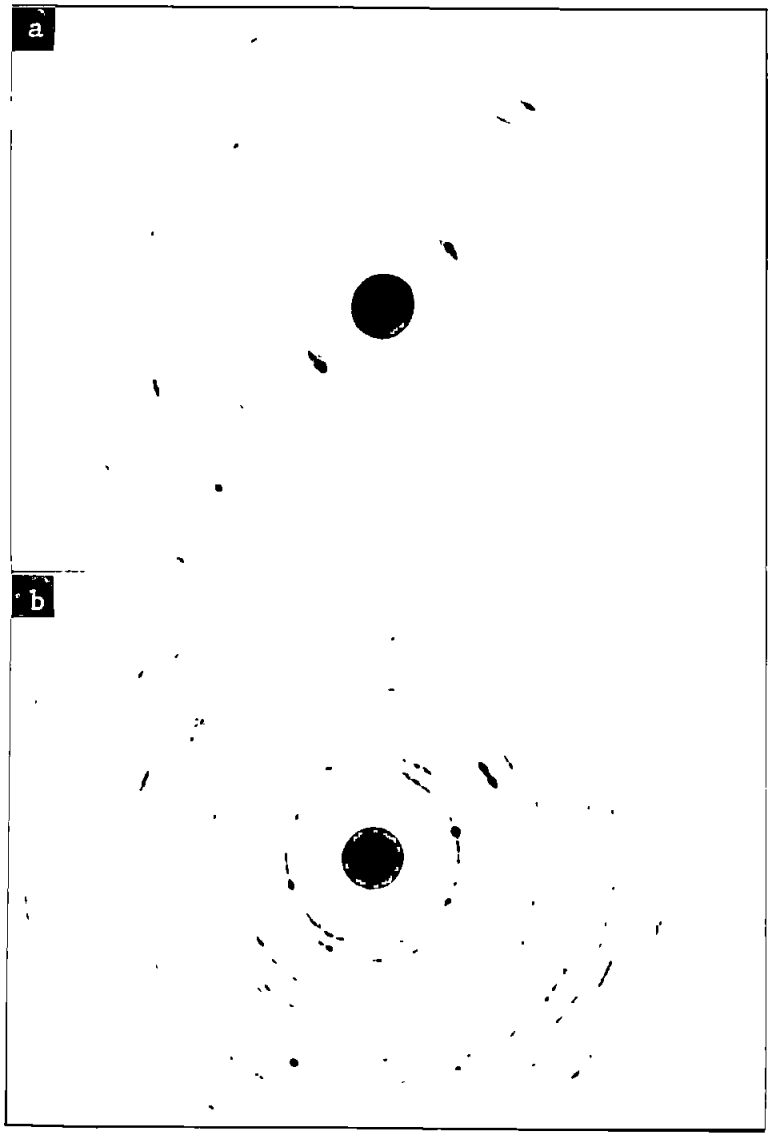


Figure 2. Electron Diffraction Patterns of As-Pretreated 20% Reduced Type 316TiM Stainless Steel in Figure 1(c). (a) Acicular Structure, (b) Cellular Structure.

direction.

Grain size measurements on these type 316TiM samples were not performed because of the large variation in grain size observed across a diameter of the samples. The variation in grain size was presumably caused by the variation of dislocation density with radial position resulting from the swaging process used in preparing the samples.

Type 321

In Figure 3 are transmission electron micrographs of the type 321 stainless steel investigated for each pretreatment. Bulk extractions carried out on the samples revealed the amount of extracted residue to be about 0.4 weight percent in each case. X-ray diffraction analysis again revealed the precipitate to be Ti(C,N) and $Ti_4C_2S_2$.

As was observed in type 316TiM, the dislocation density increases greatly with cold work. The cold worked samples of type 321 exhibit the banded appearance reported for type 316, Figures 3(b) and 3(c). These bands are also similar to the bands of the acicular structure observed in type 316TiM (compare Figure 3(c) and Figure 1(b)). As previously mentioned, the type 321 samples were cold deformed by tube drawing. Due to the thin-walled nature of the tubes, the direction of observation is parallel to a radius of the tube. It is expected that such observations would be more analogous to observation of a rolled sheet in the normal direction. This is consistent with the possibility that the

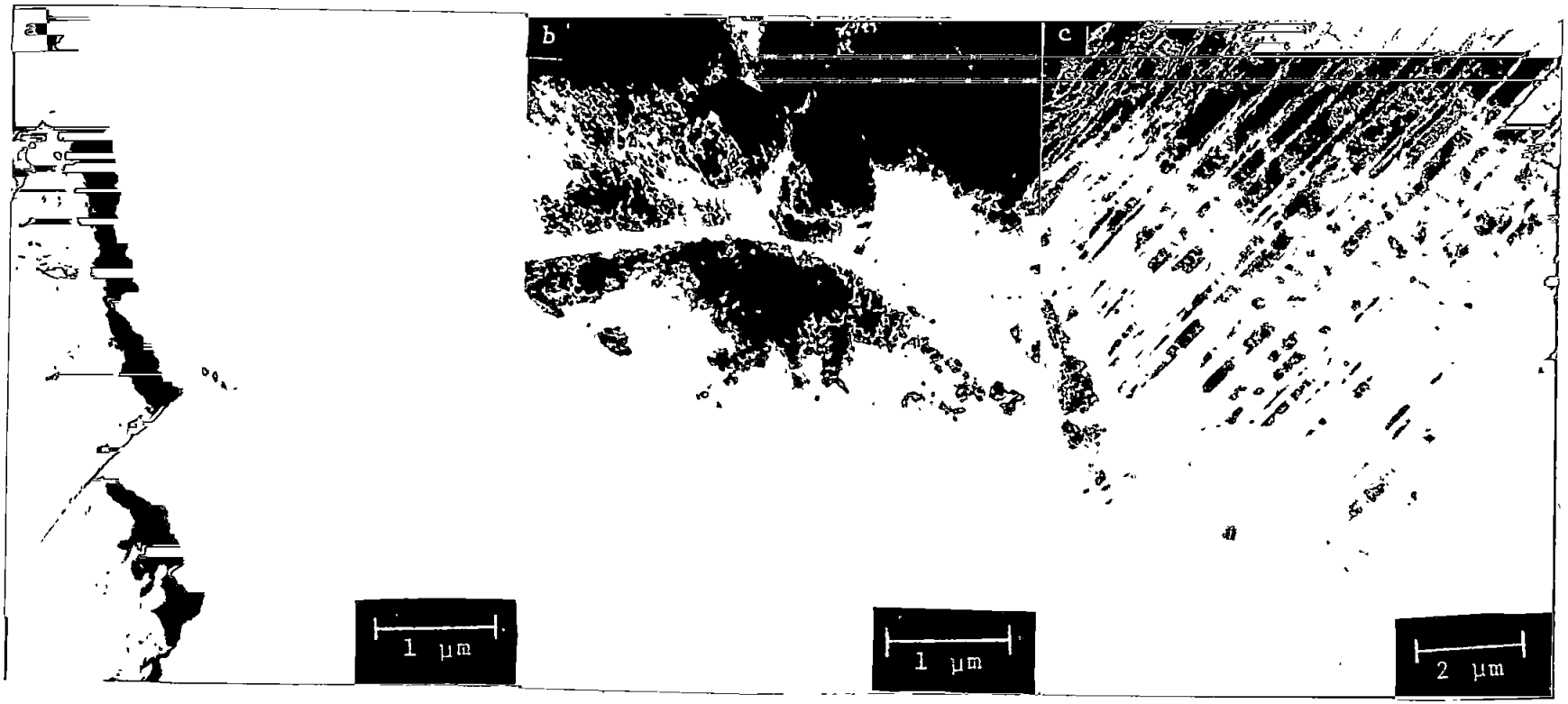


Figure 3. Microstructures of As-Pretreated Type 321 Stainless Steel. (a) Solution Treated (b) 10% Reduced, (c) 20% Reduced.

appearance of the microstructure of the type 316TiM samples result from the deformation method and direction of observation relative to the primary axis of strain.

The grain size of the type 321 samples varied from ASTM 6 to ASTM 10 in the pretreated conditions. These grain size measurements were part of the background data received from investigators at General Electric Company with the type 321 steel.

II. EFFECT OF AGING TREATMENTS-PRECIPITATION BEHAVIOR AS DETERMINED BY X-RAY DIFFRACTION OF BULK EXTRACTED RESIDUES

Titanium-Modified Type 316

The results of our bulk extraction study on type 316TiM are given in Figures 4 and 5. Figure 4 shows the weight percent extracted residue plotted against aging time. Figure 4(a) shows the effect of aging at 550°C. Figures 4(b), 4(c), and 4(d) correspond to aging temperatures of 650, 750, and 850°C, respectively. The general shape of these curves are flat, revealing only a small amount of precipitation until a certain time is reached in which there is a marked increase in the rate of precipitation. These times of increased precipitation are at 200 hours, 20 hours, 0.2 hours, and 20 hours for 40% reduced type 316TiM aged at 550, 650, 750, and 850°C, respectively. Similar trends can be seen for the other pretreatments.

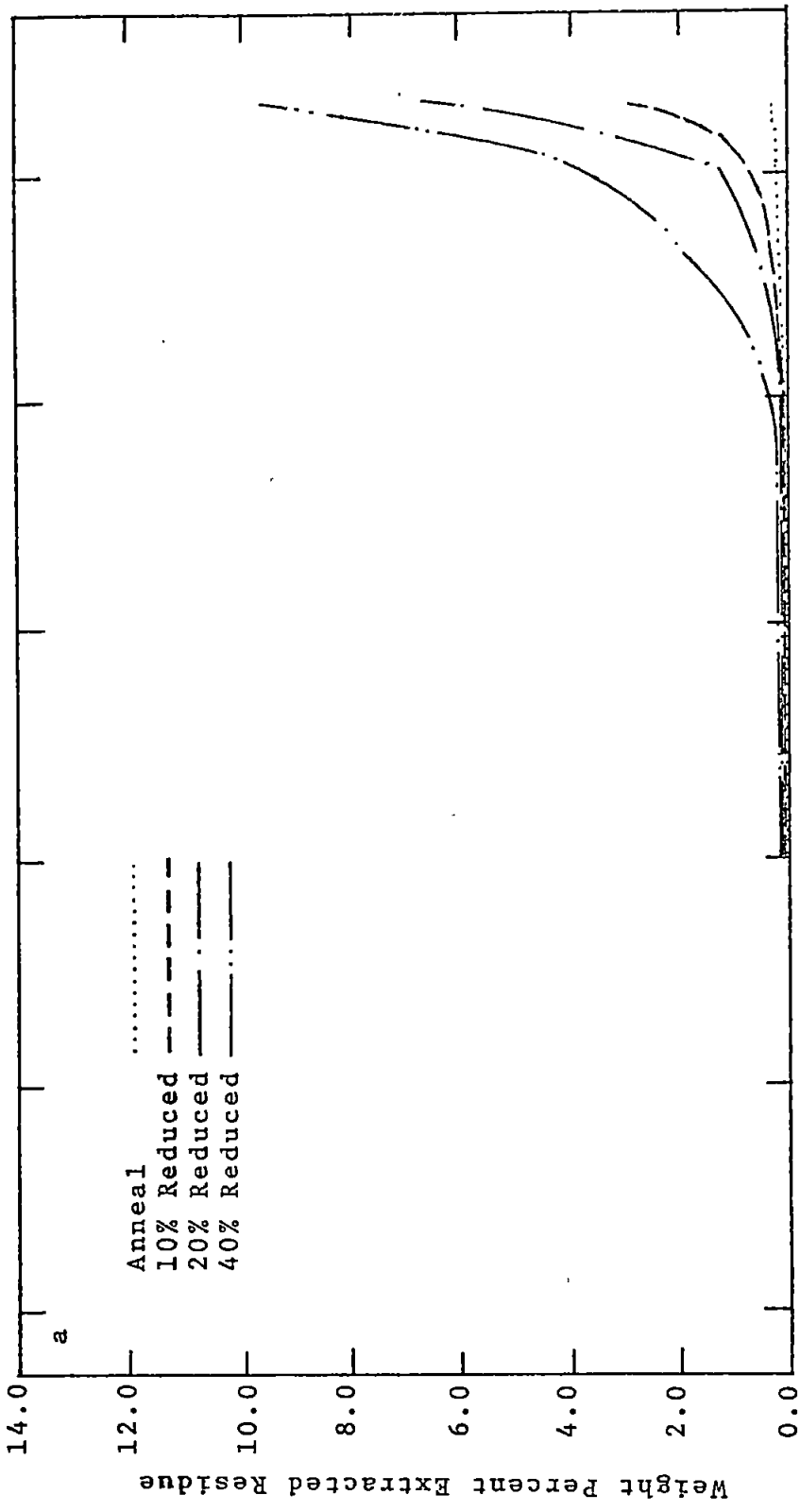


Figure 4. Weight Percent of Particles Extracted from Type 316TiM as a Function of Reduction in Area by Swaging and Aging Time. (a) Aged at 550°C, (b) Aged at 650°C, (c) Aged at 750°C, (d) Aged at 850°C

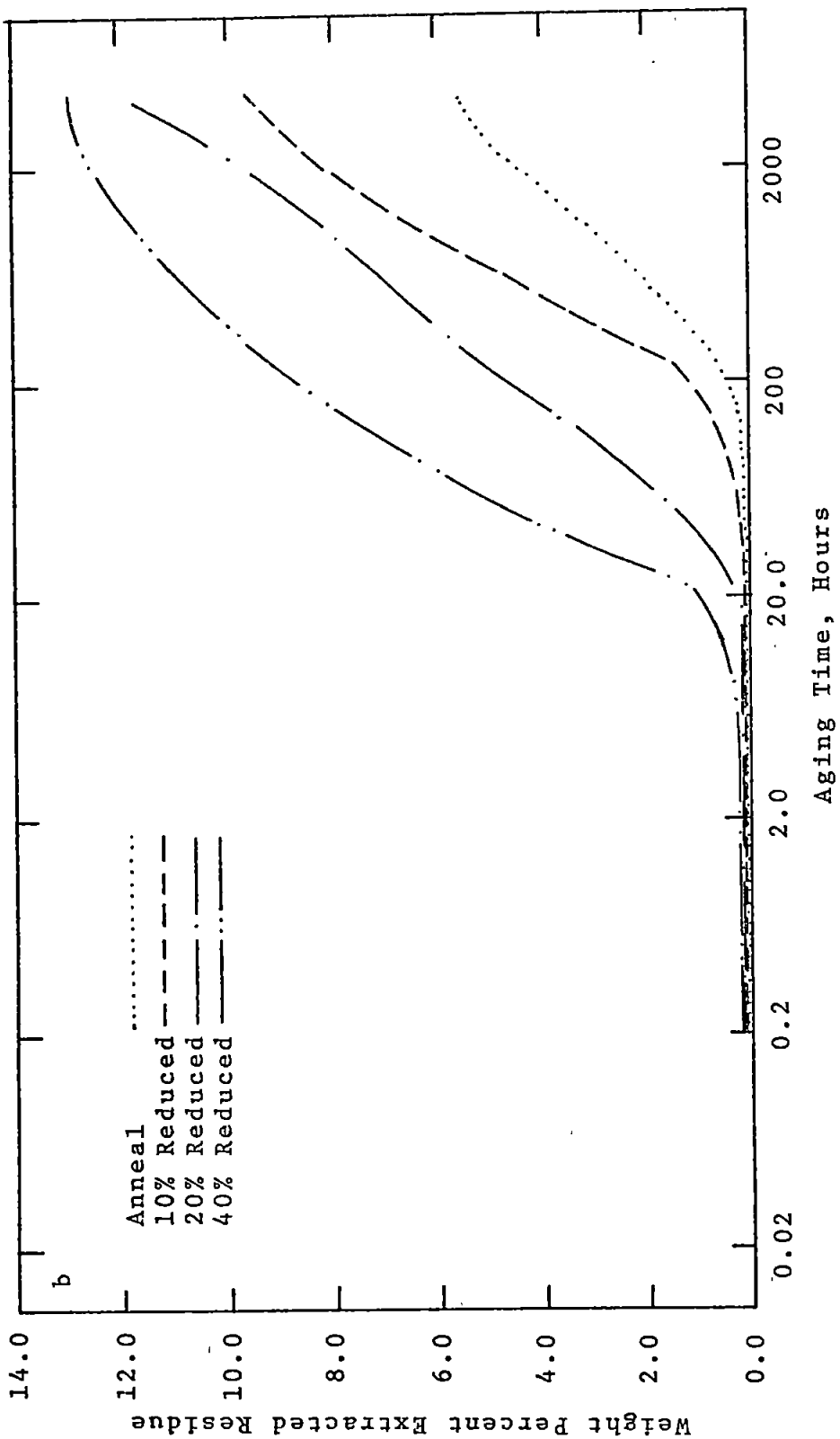


Figure 4. Continued

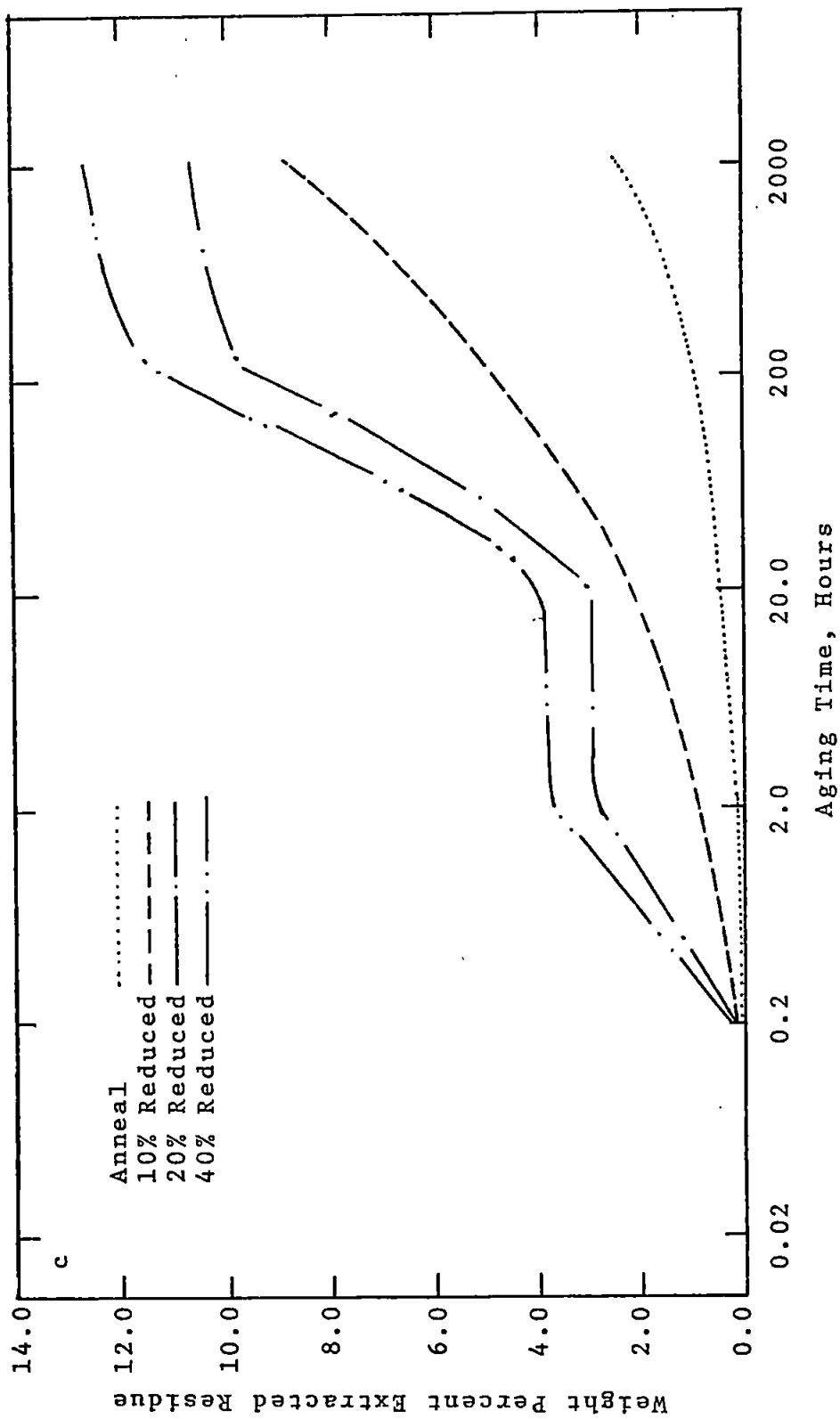


Figure 4. Continued

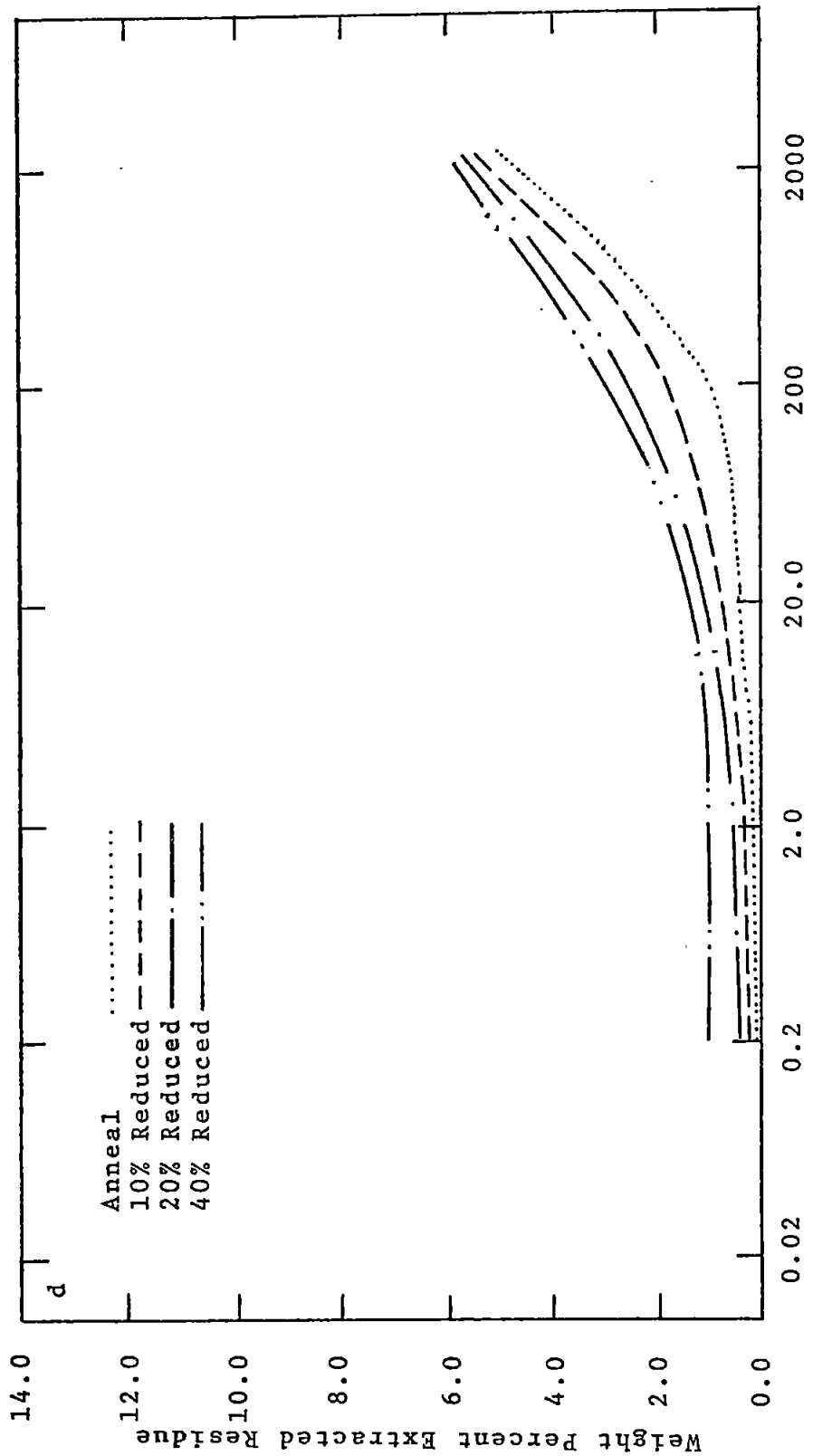
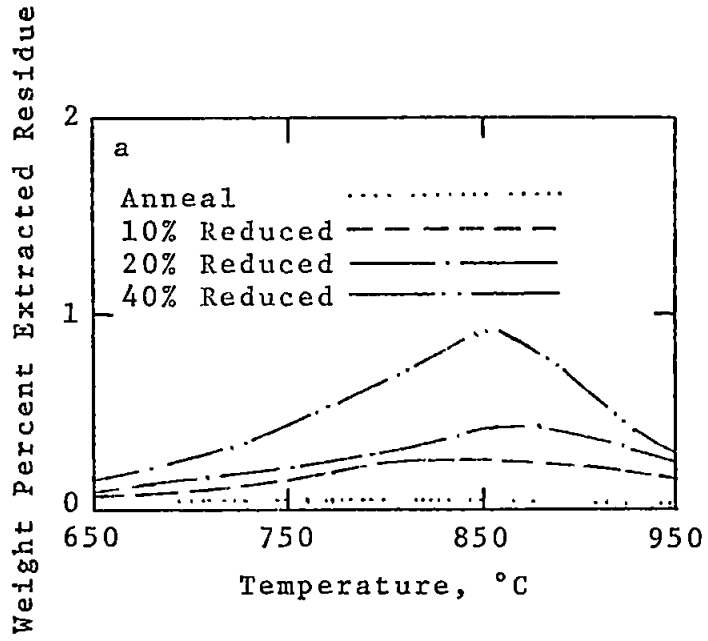


Figure 4. Continued



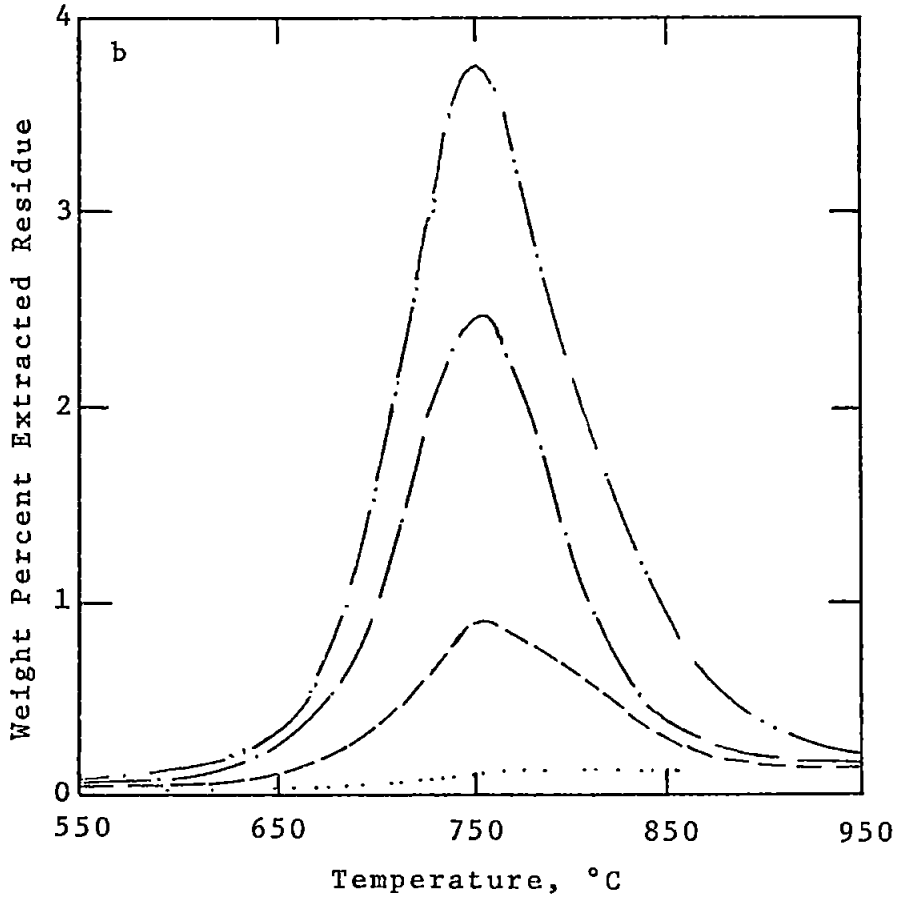


Figure 5. Weight Percent Extracted Residue Plotted Versus Aging Temperature for Aging Times of (a) 0.2 Hours, (b) 2 Hours, (c) 200 Hours.

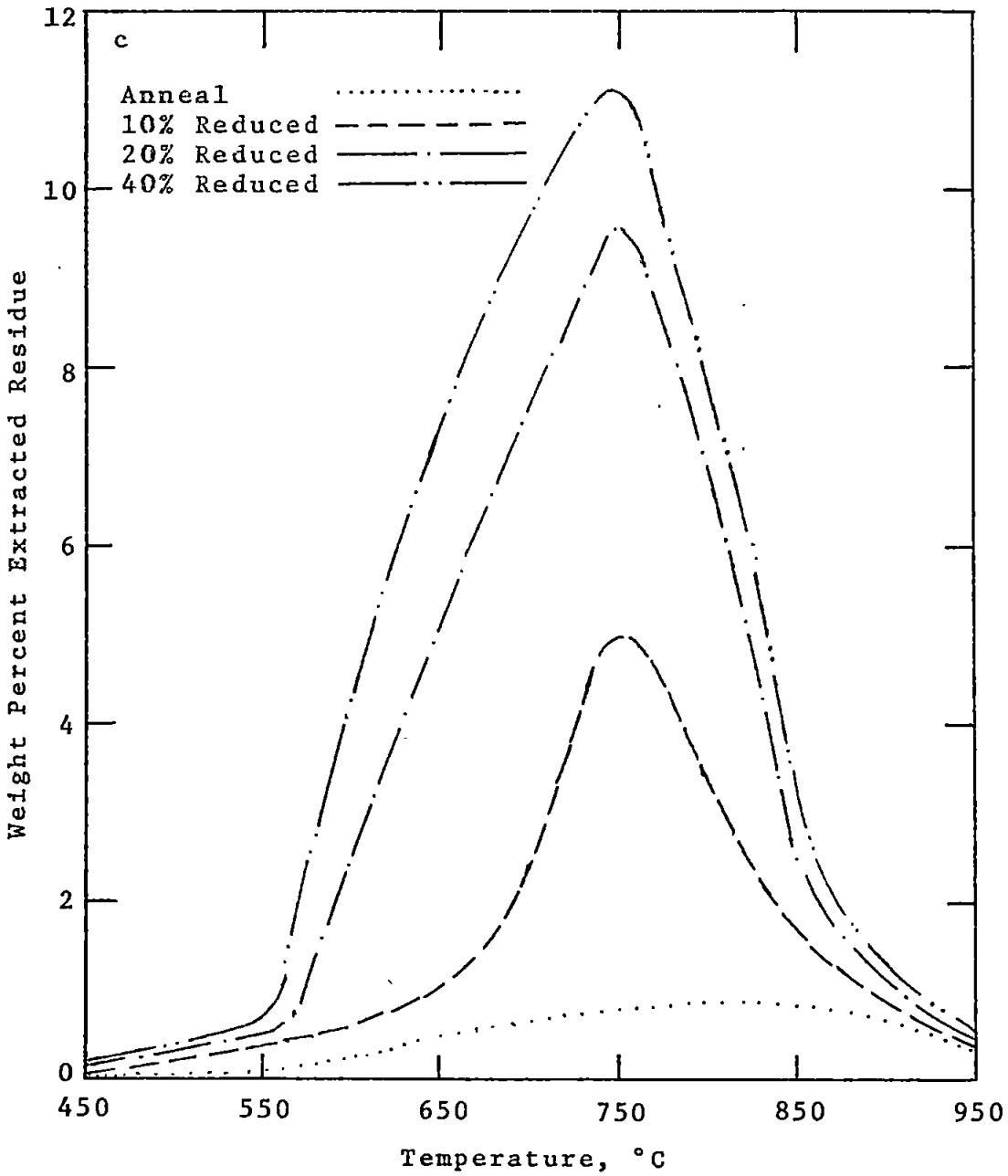


Figure 5. Continued

Precipitation activity at 450°C is not substantial. Our data indicates less than 0.2 weight percent residue extracted after 4000 hours of aging at 450°C from both 20% and 40% reduced type 316TiM. The amount of precipitate is even less in solution treated and 10% reduced 316TiM. Similarly at 950°C, only 0.5 weight percent residue was found to have precipitated after 200 hours of aging.

Figures 5(a), 5(b), and 5(c) show the bulk residue data cross plotted against aging temperature for aging times of 0.2, 2, and 200 hours respectively. These figures graphically reveal the variation in the amount of precipitation with temperature. The effect of pretreatment on the amount of precipitation is also readily noted. The shift in the peaks of the curves from 850°C for 0.2 hours of aging, Figure 5(a), to 750°C for times of 2 hours and longer, Figures 5(b) and 5(c) is of interest. This shift results from the fact that the major proportion of the precipitate present after only 0.2 hours of aging consists of carbides, while for the longer aging times the major proportion of the precipitate is either sigma or chi phase or a mixture of these two intermetallic phases.

Figure 6 presents an example of the x-ray data obtained using the bulk extracted residue from a sample of solution treated 316TiM aged at 750°C for 200 hours. The peaks for TiC, TiN, $M_{23}C_6$, sigma, and chi are marked. This example shows that the technique clearly distinguishes what

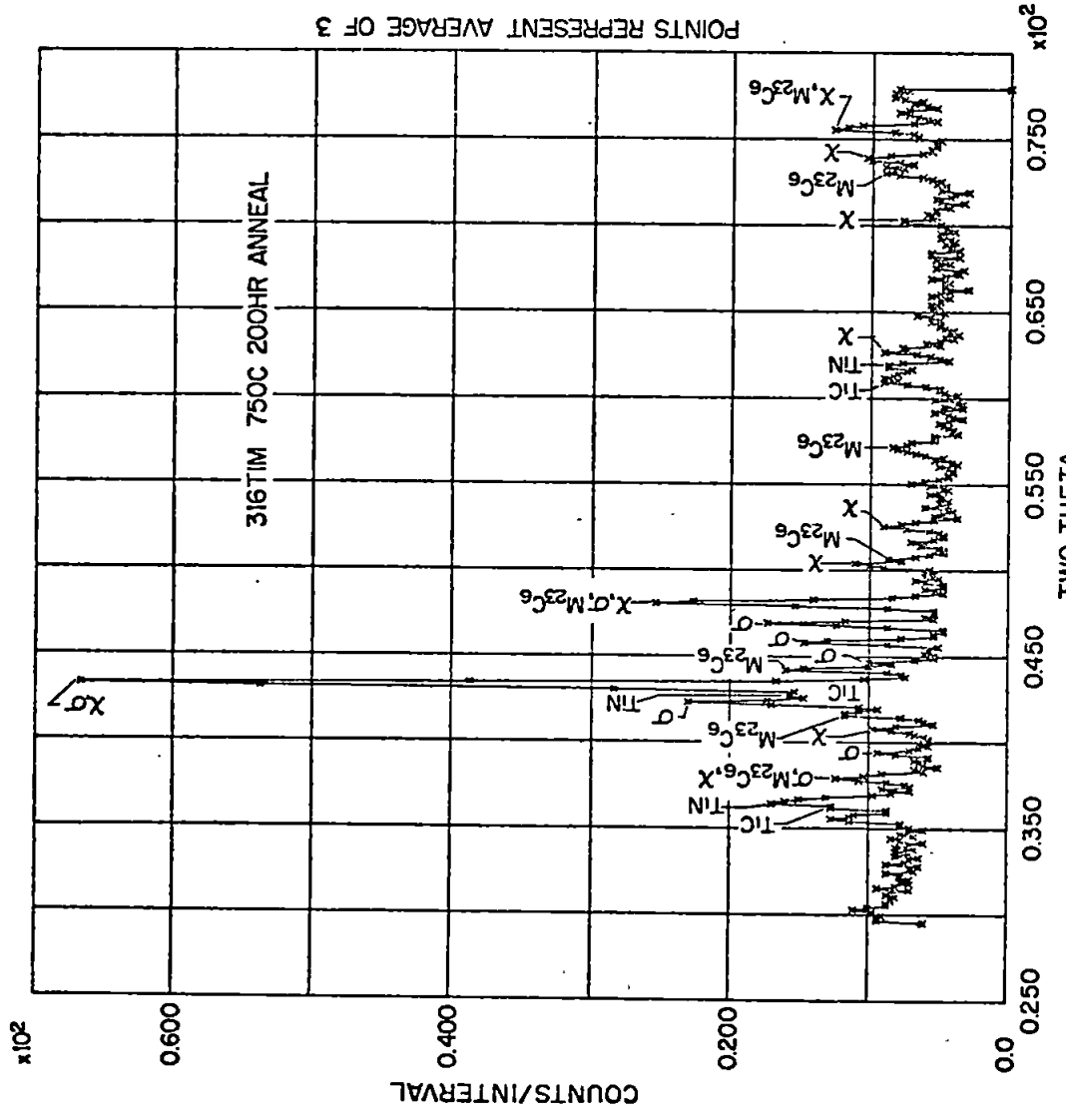


Figure 6. X-Ray Pattern From Extracted Residue Illustrating the Resolution of Diffraction Lines from Five Different Phases.

phases are present even though there may be several of them.

Comparison of the x-ray data with the weight percent residue data shows initial precipitation of small quantities of TiC and then $M_{23}C_6$. The areas of marked increase in the amount of precipitation are found to correspond to the massive precipitation of sigma. Figure 7 shows three x-ray data plots for solution treated type 316TiM aged at 650°C. Figure 7(a) shows peaks for TiC and $M_{23}C_6$ after 20 hours of aging. Figure 4(b) (page 35) reveals that the amount of precipitate is only about 0.1 weight percent. When aged for 200 hours there still is only TiC and $M_{23}C_6$ present, Figure 7(b). After 4000 hours at 650°C there is a massive precipitation of sigma, Figure 7(c), which Figure 4(b) reveals to be about 5 weight percent of the sample.

Using the x-ray data obtained with the diffracted beam monochromator time-temperature-precipitation diagrams were determined for each pretreatment of type 316TiM. These are given in Figures 8-11. It is observed that the knees of the C-curves for $M_{23}C_6$ and sigma are shifted to lesser aging times and higher temperatures for increasing amounts of cold work. The acceleration in the precipitation of $M_{23}C_6$ and sigma due to cold working has been reported for other steels in the literature (4,5).

The precipitation behavior of chi phase in cold worked type 316TiM needs to be discussed. The observance of chi and sigma nucleating simultaneously in solution treated

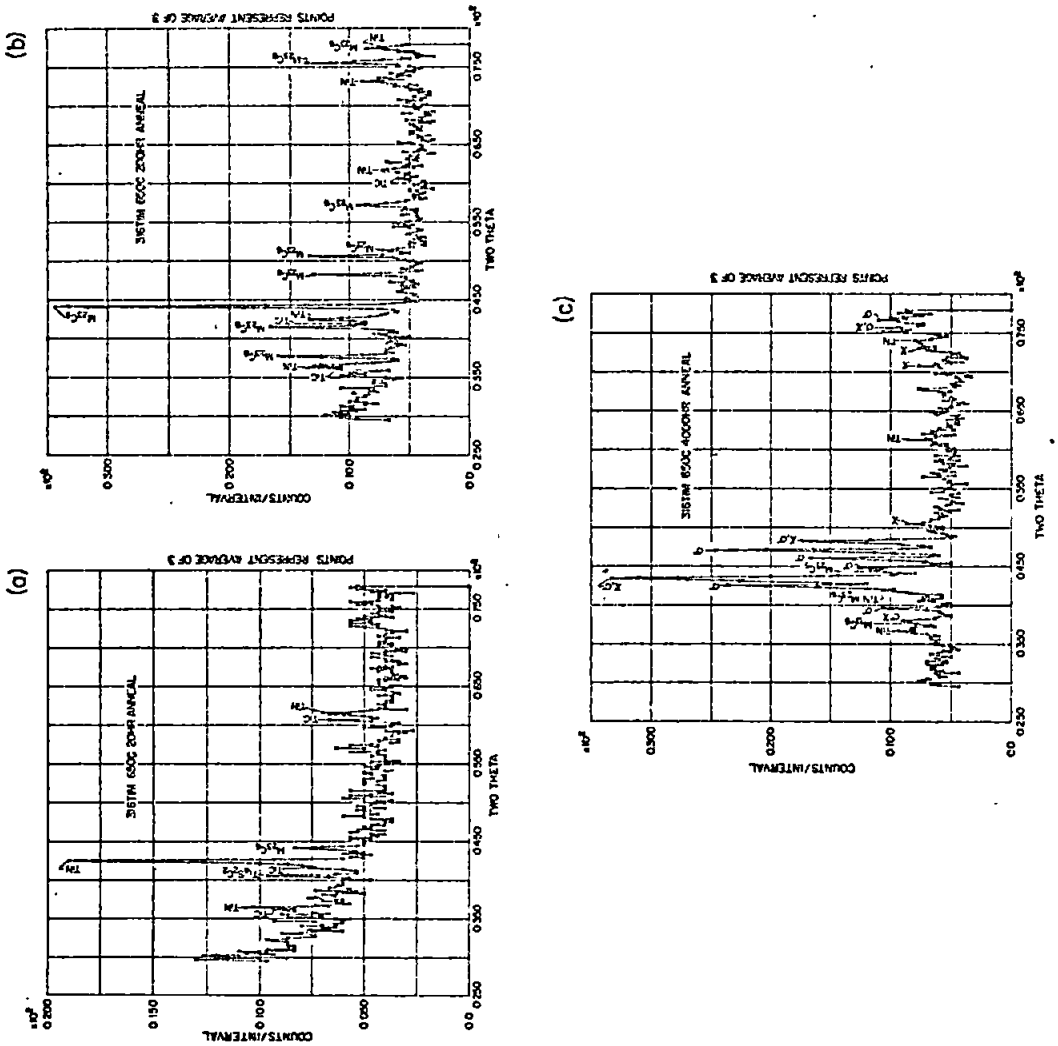


Figure 7. X-Ray Patterns from the Extracted Residue from Solution Treated Samples Aged at 650°C. (a) Aged 20 Hours, (b) Aged 2000 Hours, (c) Aged 4000 Hours.

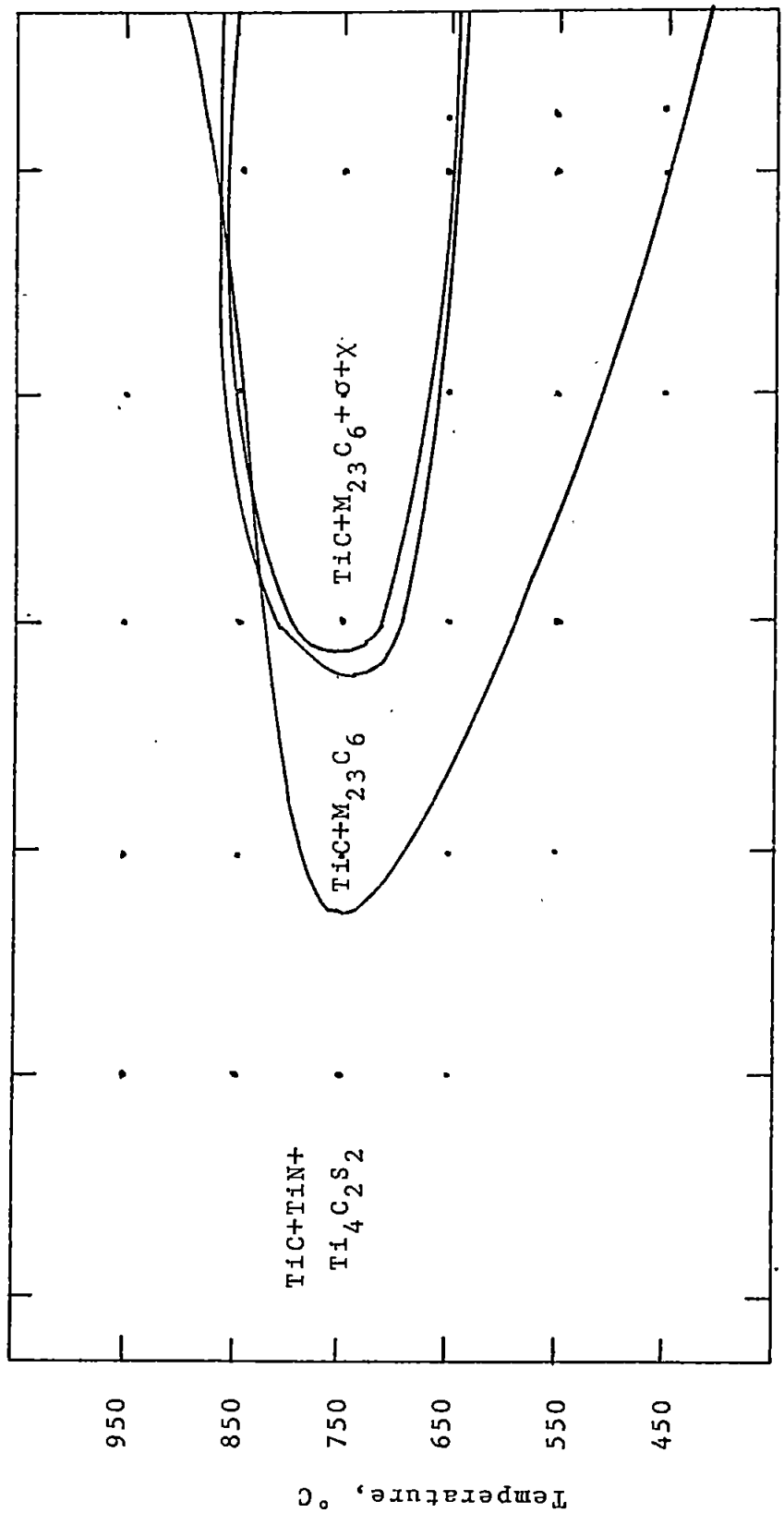


Figure 8. Time-Temperature-Precipitation Diagram for Solution Treated Type 316TiM Stainless Steel.

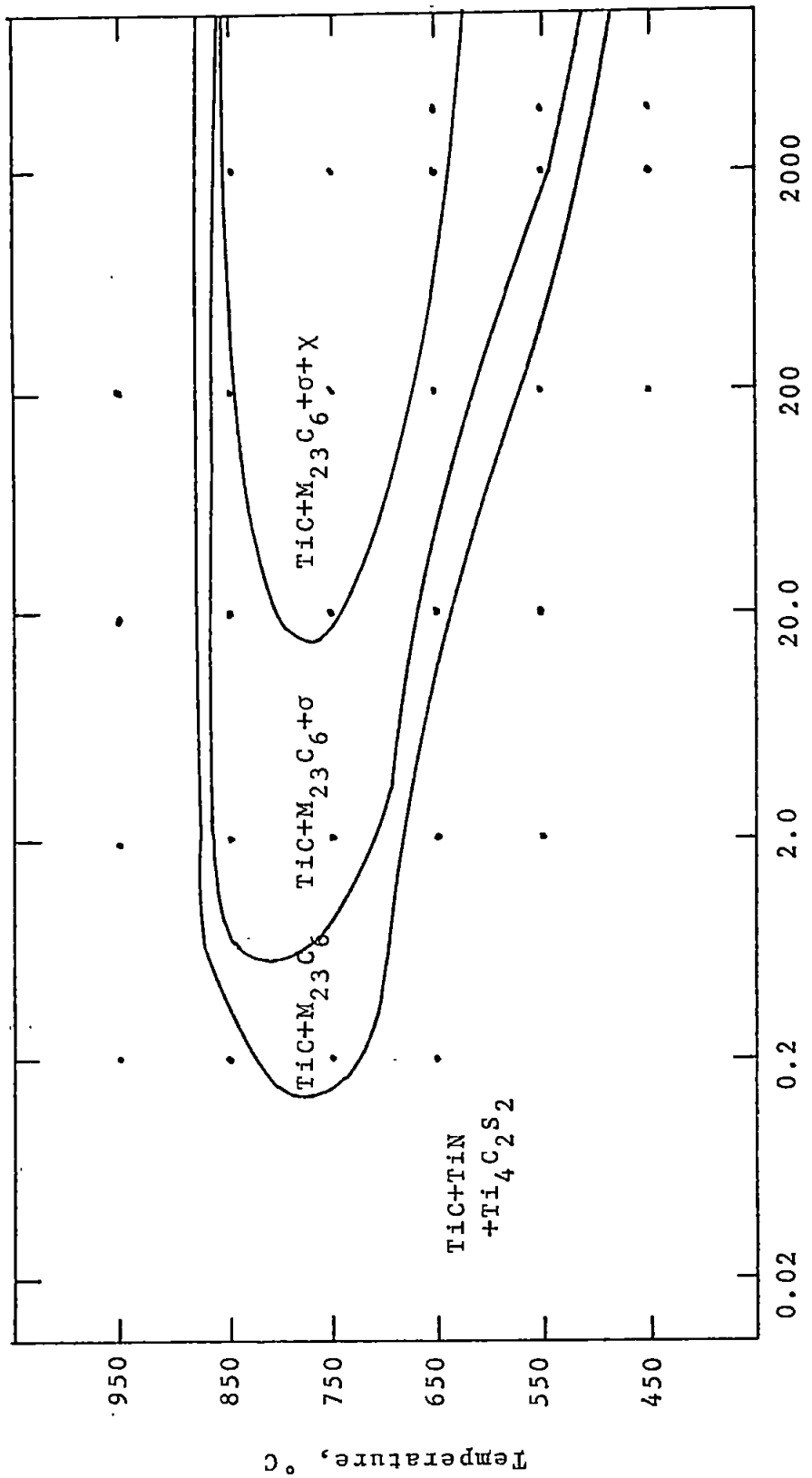


Figure 9. Time-Temperature-Precipitation Diagram for Type 316TiM Stainless Steel Given 10% Reduction in Area by Swaging Prior to Aging.

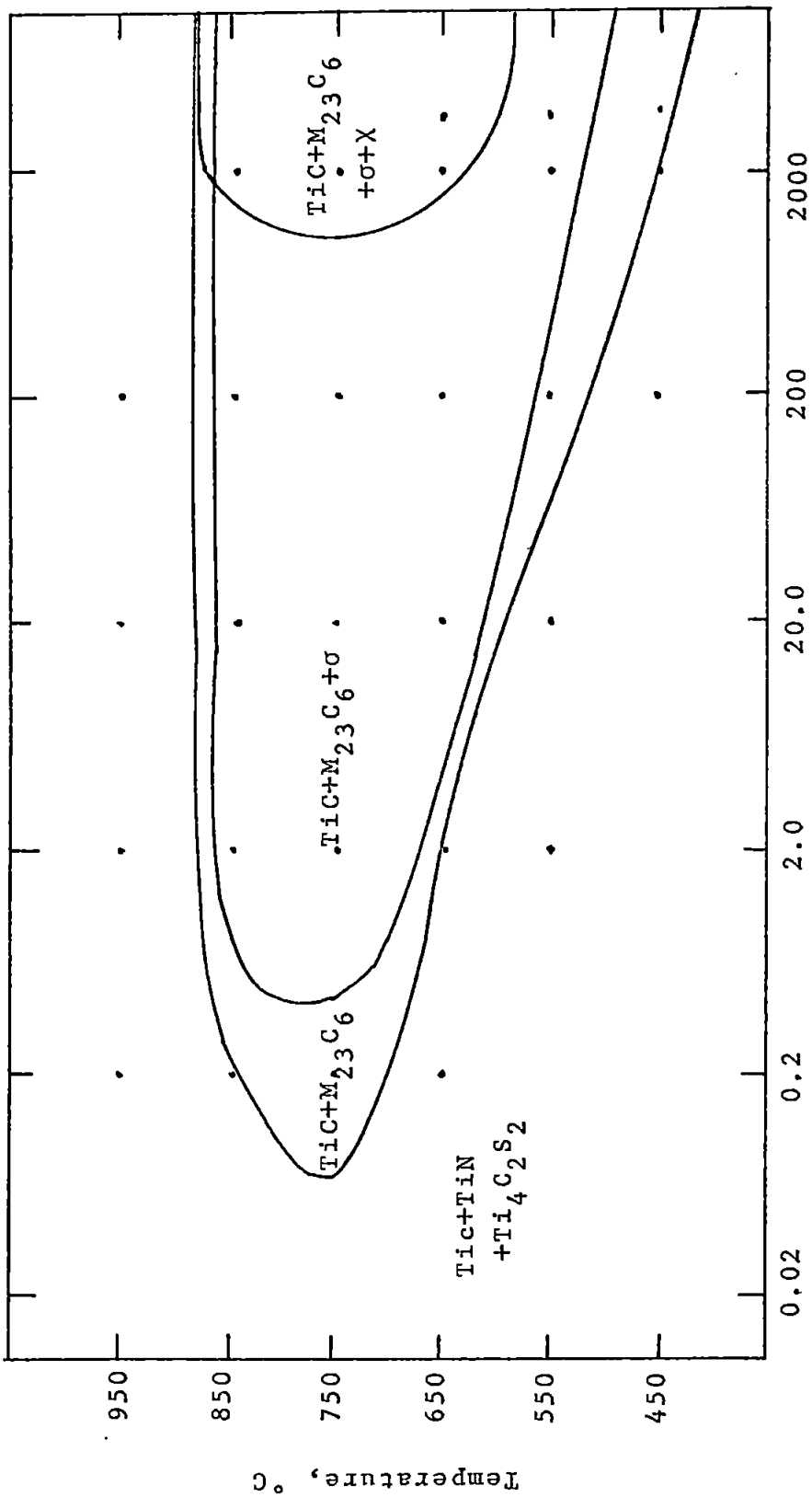


Figure 10. Time-Temperature-Precipitation Diagram for Type 316TiM Stainless Steel Given 20% Reduction in Area by Swaging Prior to Aging.

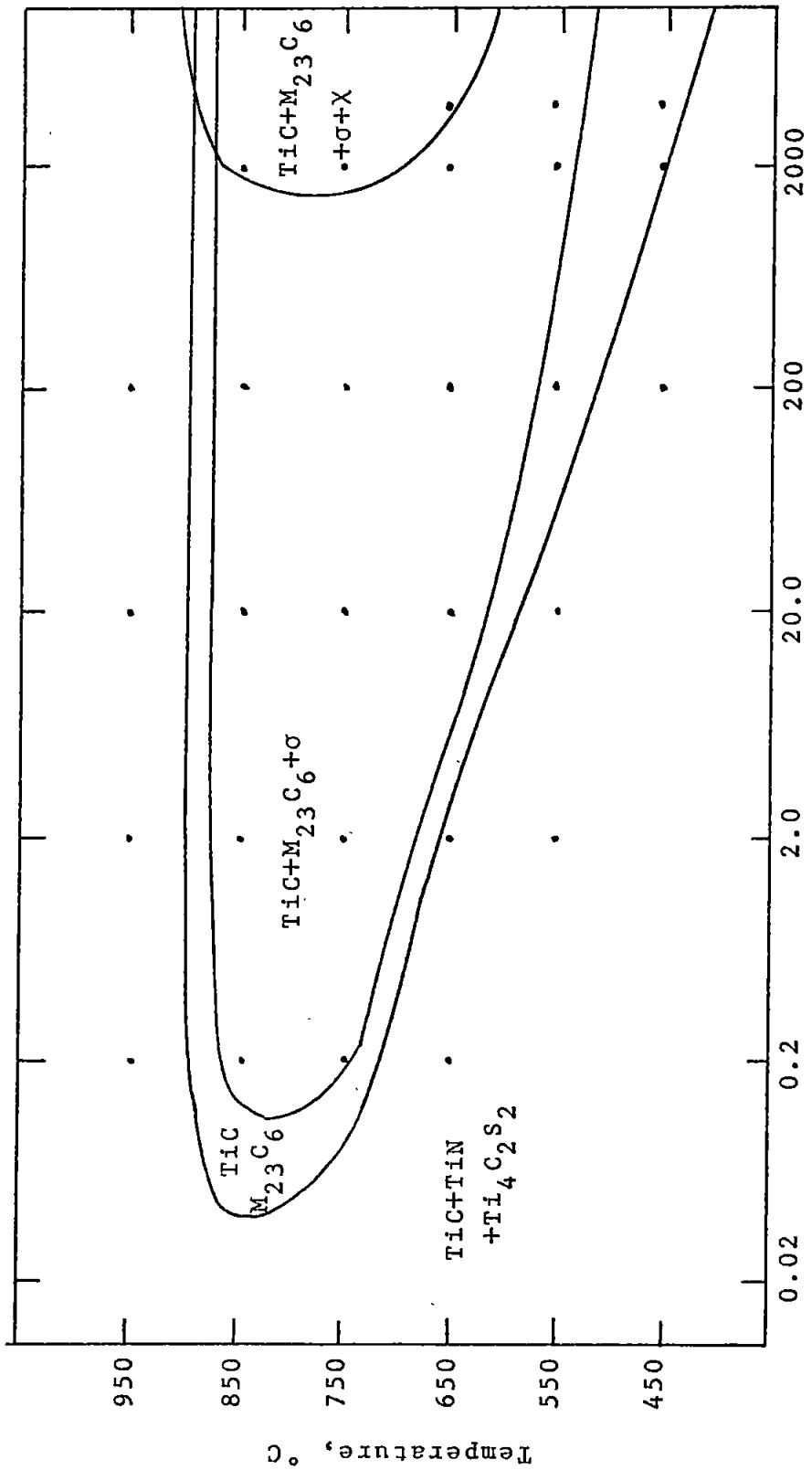


Figure 11. Time-Temperature-Precipitation Diagram for Type 316TiM Stainless Steel Given 40% Reduction in Area by Swaging Prior to Aging.

type 316TiM shows that chi does not preferentially nucleate first in this alloy as might be expected from observance of chi in other steels (4,5). In cold worked type 316TiM chi was not observable by x-ray analysis or electron diffraction techniques until after sigma had precipitated in large quantities. In 20% and 40% reduced type 316TiM chi was observed only after 2000 hours of aging at 750°C whereas sigma appeared near 0.2 hours, Figures 10 and 11. These observations appear to contradict the accepted contention that the nucleation of chi phase is accelerated by cold work (4,5). However, if the observation of Koh (15), that the amount of chi phase relative to that of sigma phase is suppressed considerably by cold work, is considered with the fact that sigma and chi form simultaneously in solution treated type 316TiM this apparent inconsistancy can be understood. In previously studied austenitic stainless steels chi nucleated first because of its ability to incorporate some carbon into it's lattice structure while sigma does not (38). This advantage does not exist in type 316TiM because of TiC formation. Rather, the early formation of sigma suppresses chi formation by competing for chromium and molybdenum. Chi is further suppressed in cold worked type 316TiM by the acceleration of sigma nucleation.

Type 321

The present investigation of type 321 austenitic

stainless steel shows that this steel is much more stable than type 316TiM. Bulk extraction data reveals that the amount of residue increases very slowly at all temperatures except at 850°C; at 450°C, 550°C, and 650°C the quantity of residue precipitated is less than 1 weight percent for all pretreatments. Aging at 750°C for 2000 hours gives precipitation of little over 1 weight percent. The behavior of type 321 at 850°C is similar to type 316TiM in the amount of residue precipitated.

The x-ray data for type 321 reveals that most of the precipitate formed is TiC. At longer aging times, $M_{23}C_6$ and chi are evident in the steel. No sigma was found in any sample studied. Within the limited range studied here, cold working had little affect on the precipitation in type 321. That is, solution treated and 20% reduced type 321 reacted similarly in the amount of precipitation activity. For this reason, 10% reduced 321 was not extensively studied. Figures 12 and 13 are the time-temperature-precipitation diagrams determined for type 321.

III. EFFECT OF AGING TREATMENT-PHASE MORPHOLOGY AND RECRYSTALLIZATION BEHAVIOR

Titanium-Modified Type 316

Comparison of optical metallography and bulk extraction data reveals that recrystallization in type 316TiM is concurrent with a marked increase in the amount of

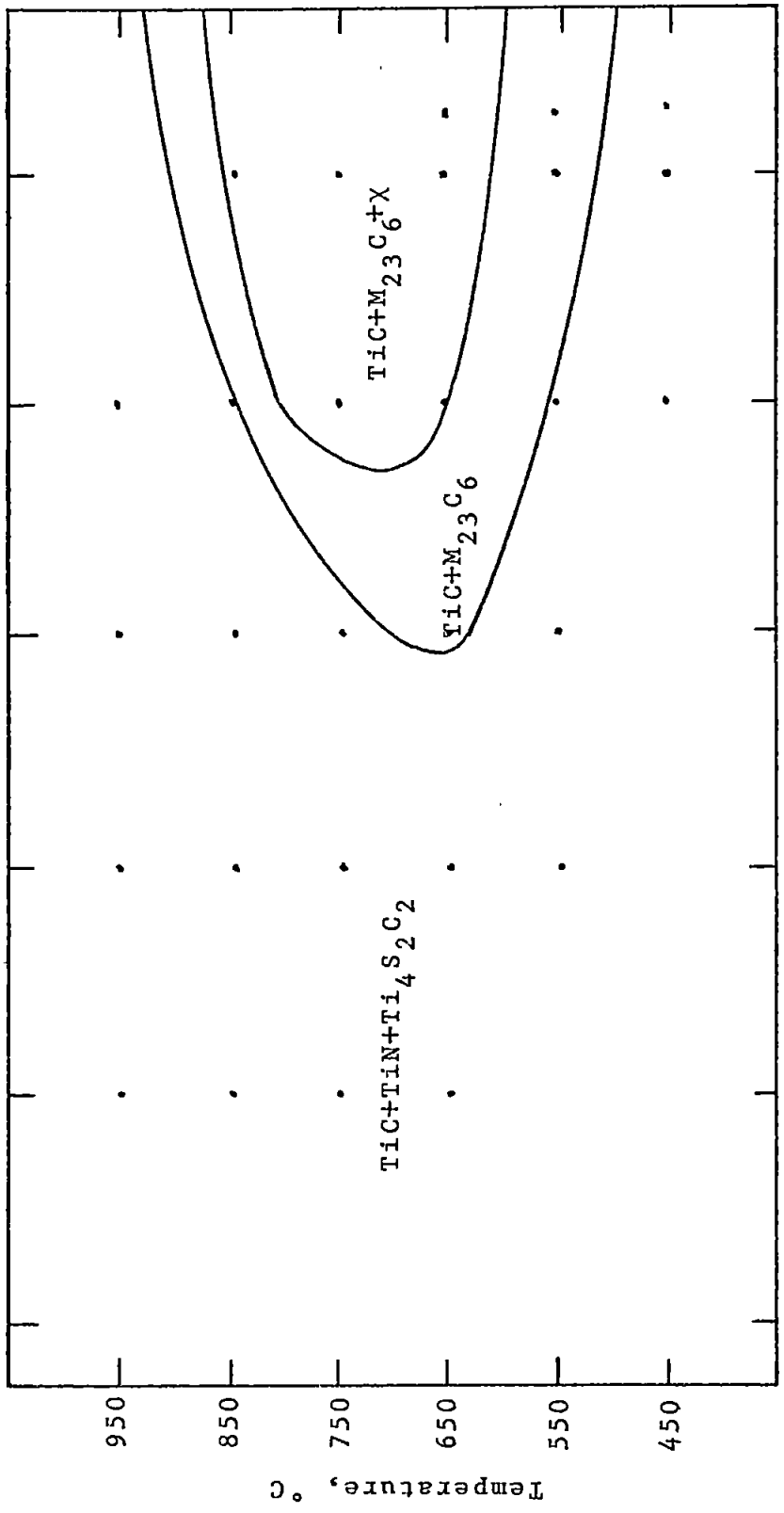


Figure 12. Time-Temperature-Precipitation Diagram for Solution Treated Type 321 Stainless Steel.

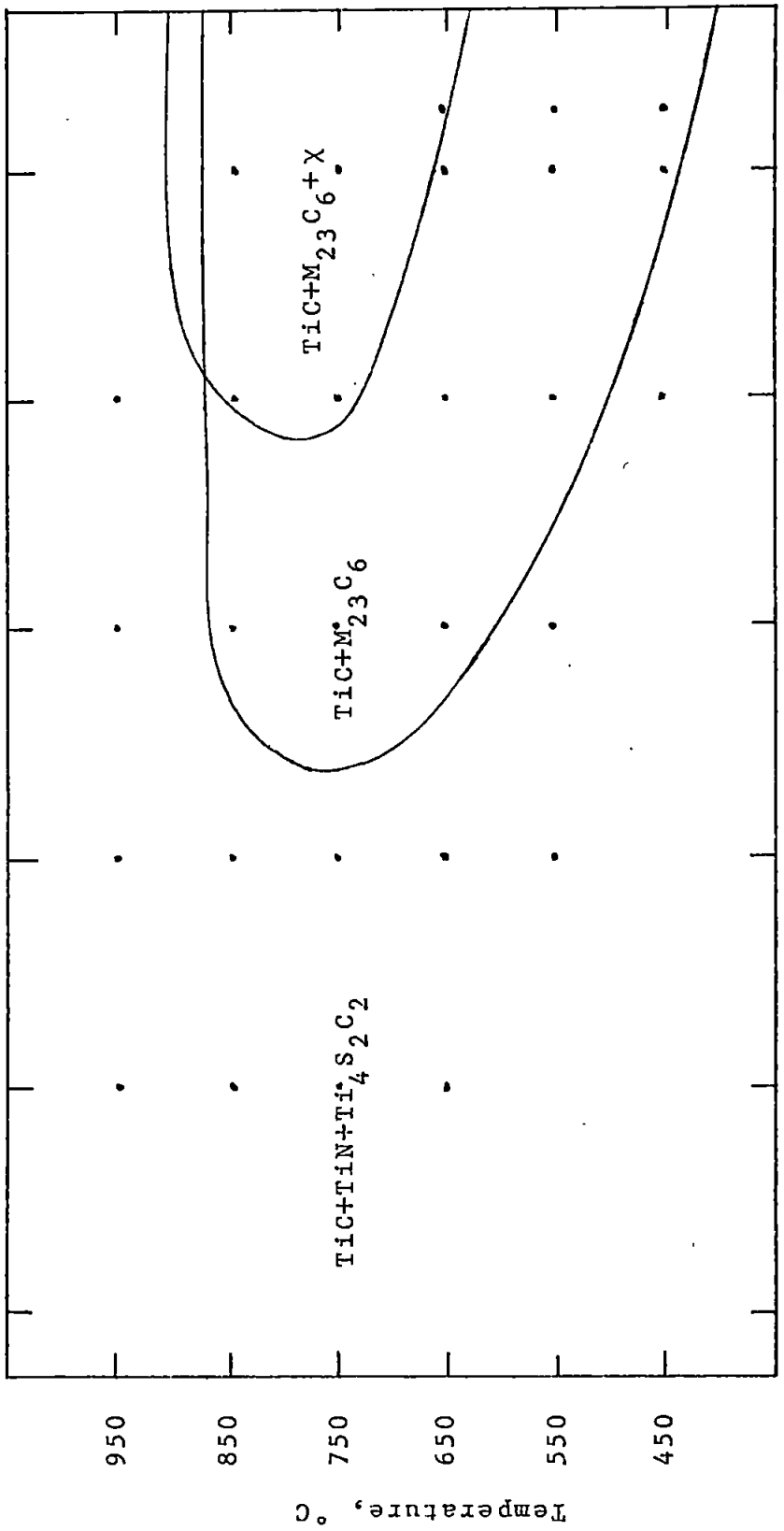


Figure 13. Time-Temperature-Precipitation Diagram for Type 321 Stainless Steel Given 20% Reduction in Area by Tube Drawing Prior to Aging.

precipitate. Both optical metallography and the x-ray data show that the increase of precipitation is due to the formation of sigma. Because recrystallization is concurrent with the increase in precipitation rate, Figures 4(a), 4(b), 4(c), and 4(d) (pages 34-37) give an indication of the recrystallization behavior of type 316TiM. Comparing Figure 14 with Figure 4(b) illustrates this relation. For 20% reduced material recrystallization has just begun after 20 hours of aging at 650°C, Figure 14(a). Figure 4(a) shows little precipitation. By 200 hours, Figure 14(b), recrystallization has progressed to about 60% completion. The amount of precipitation is 5.25%. After 2000 hours, Figure 14(c), when recrystallization is complete the microstructure contains many sigma particles. Figure 14(d) shows the coarsened sigma particles present after 4000 hours at 650°C.

The recrystallization behavior of 10% and 40% reduced type 316TiM at 750°C are illustrated in Figures 15 and 16, respectively. Figure 15 shows that recrystallization in 10% reduced type 316TiM begins before 2 hours of aging and is completed by 20 hours. In Figure 16, it is seen that recrystallization of 40% reduced type 316TiM begins by 0.2 hours and is completed before 2 hours of aging at 750°C.

The recrystallization behavior of type 316TiM is summarized in Figures 17 and 18. In Figure 17, the recrystallization behavior of 40% reduced type 316TiM is compared to the recrystallization behavior of 50% reduced type 316 as

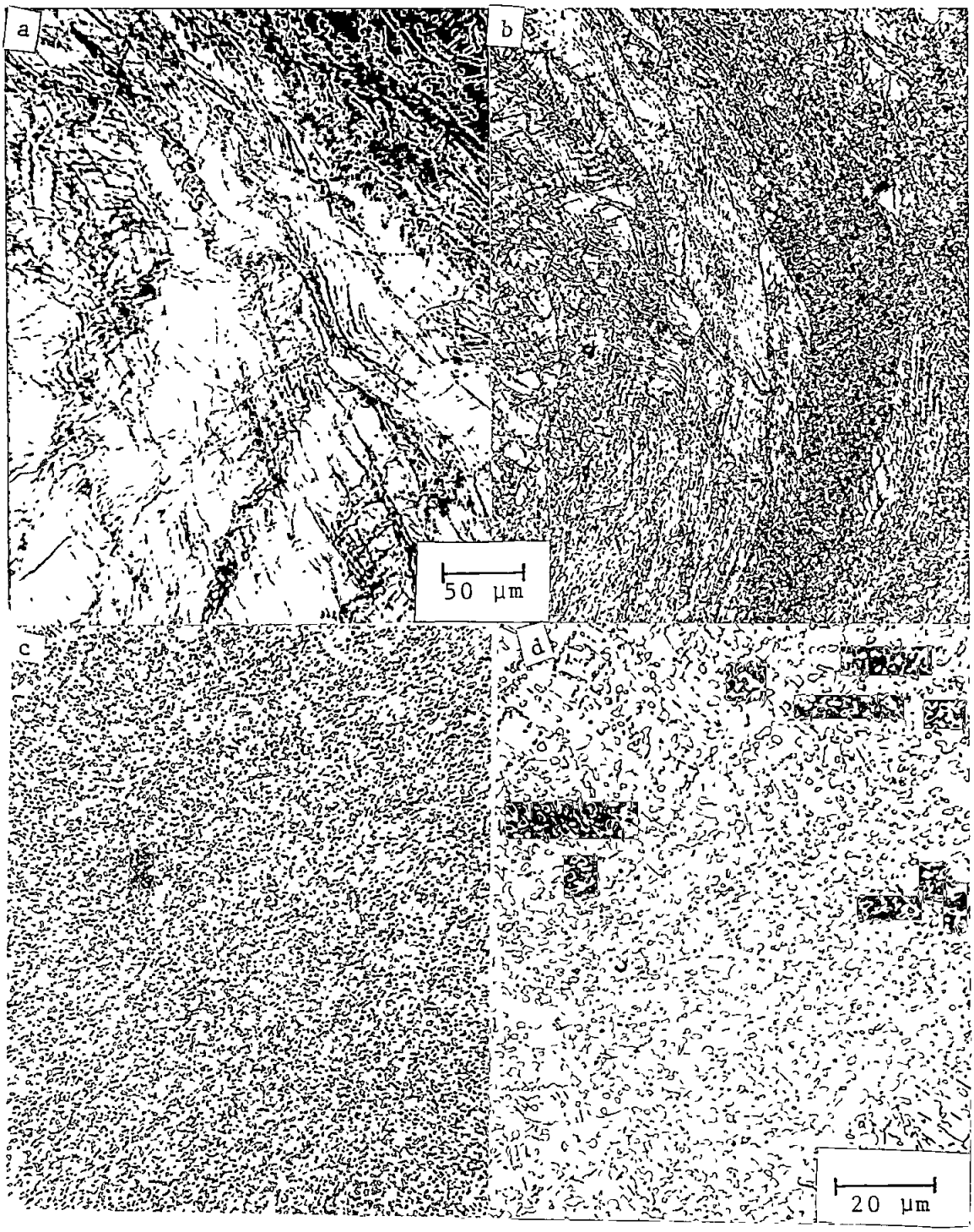


Figure 14. Type 316TiM Stainless Steel Reduced 20% and Aged at 650°C for (a) 20 Hours, (b) 200 Hours, (c) 2000 Hours, and (d) 4000 Hours.

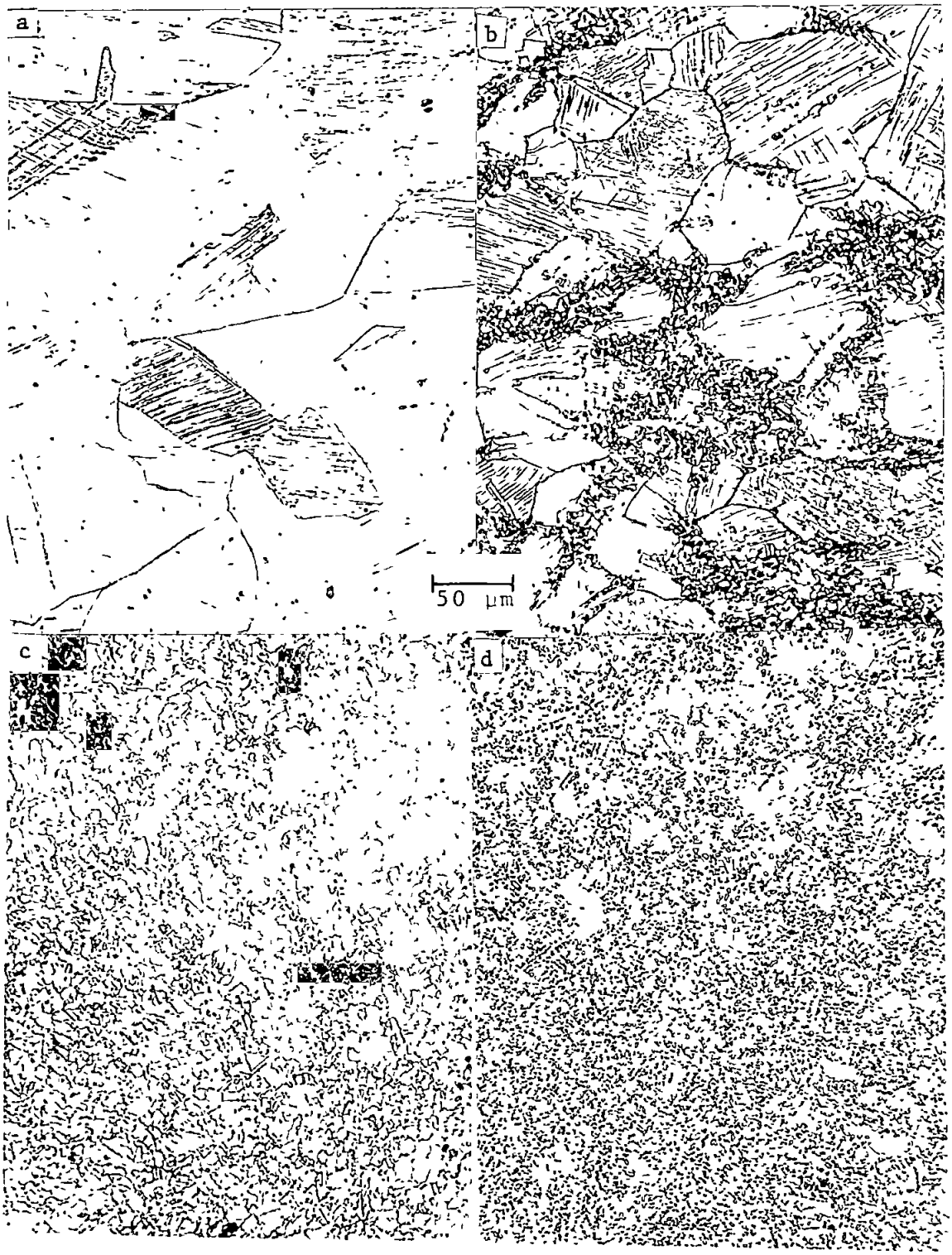


Figure 15. Type 316TiM Stainless Steel Reduced 10% and Aged at 750°C for (a) 0.2 Hours, (b) 2 hours, (c) 20 Hours, and (d) 200 Hours.

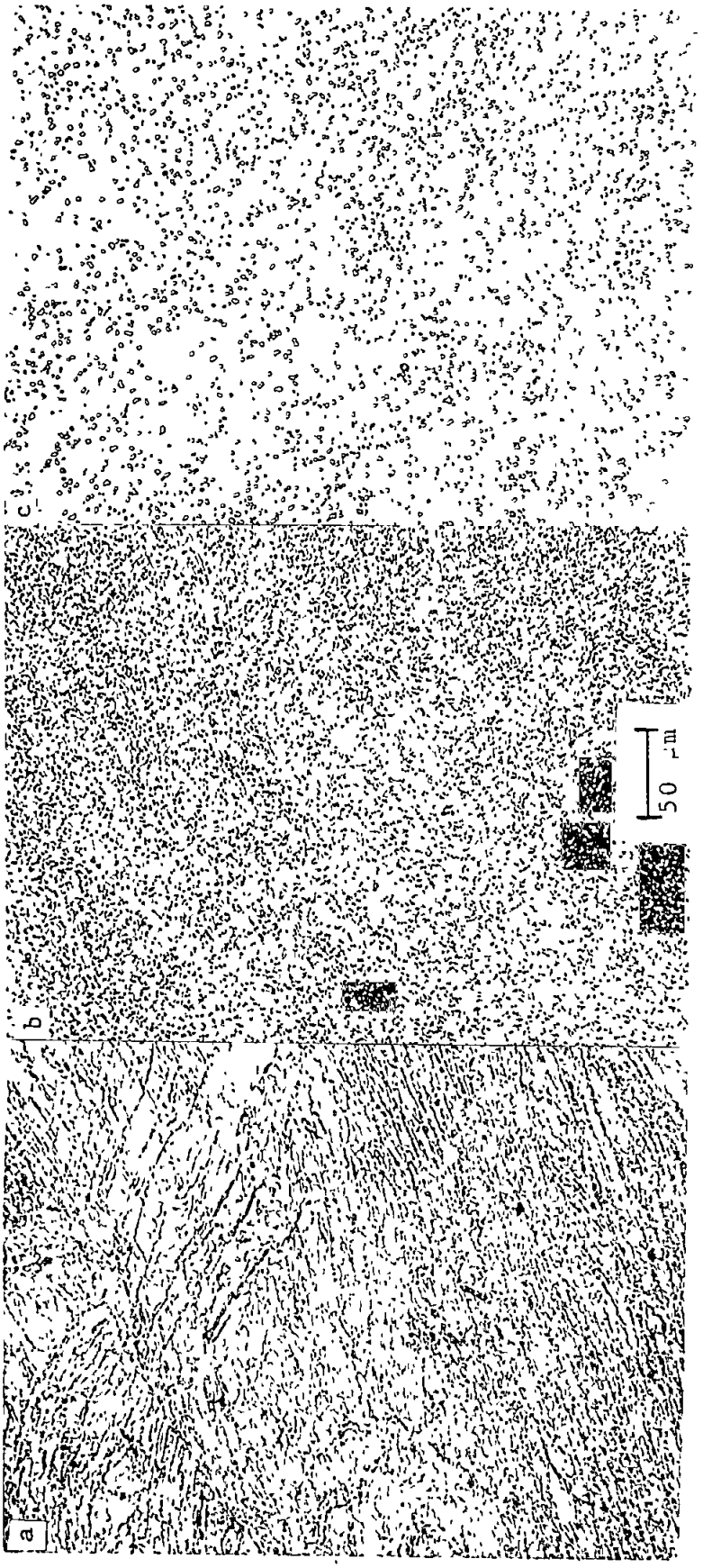


Figure 16. Type 316TiM Stainless Steel Reduced 40% and Aged at 750°C for (a) 0.2 Hours, (b) 2 Hours, and (c) 20 Hours.

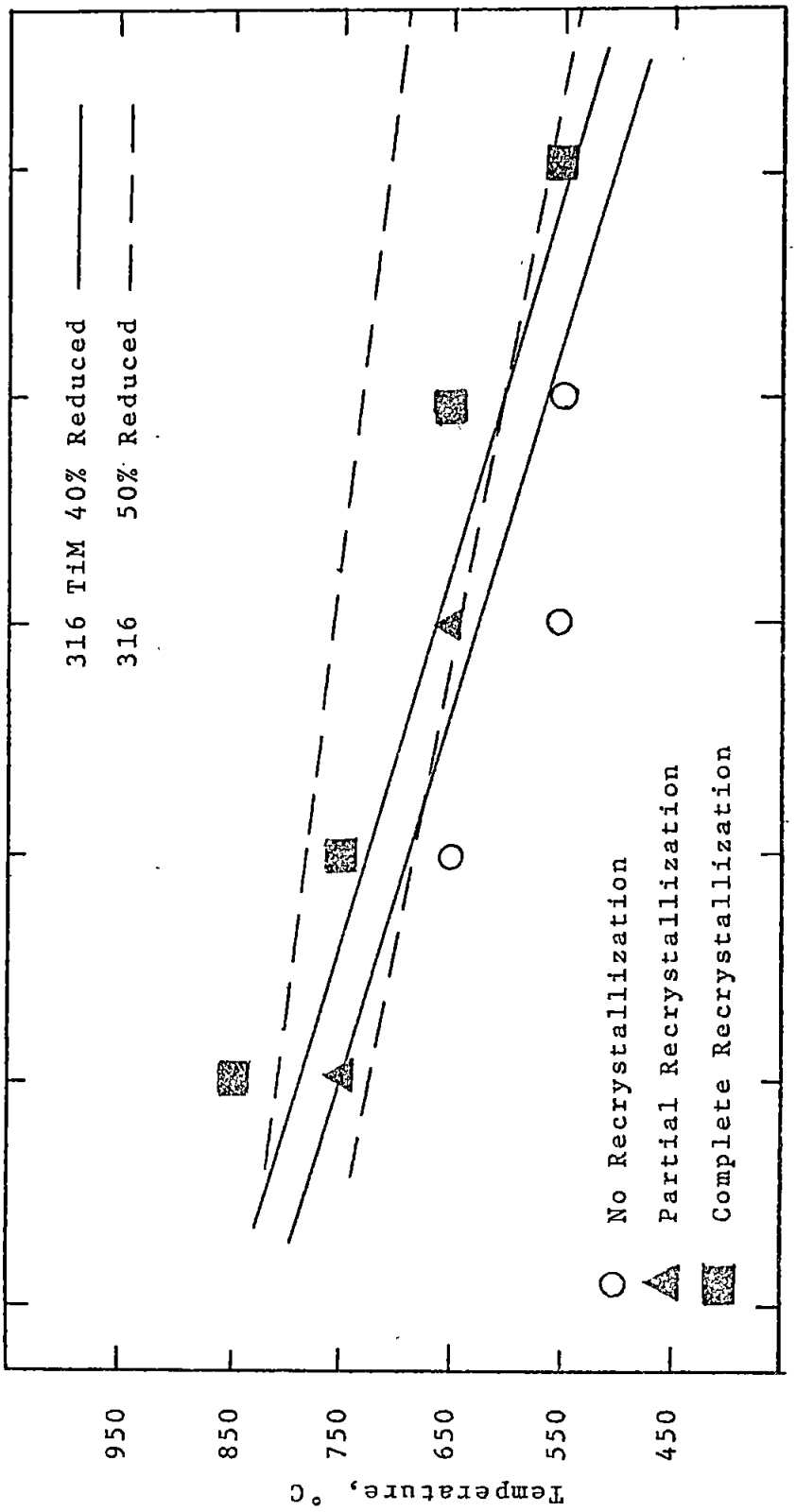


Figure 17. Recrystallization Behavior of Type 316TiM Reduced 40% by Swaging Compared with Type 316 Reduced 50% by Rolling.

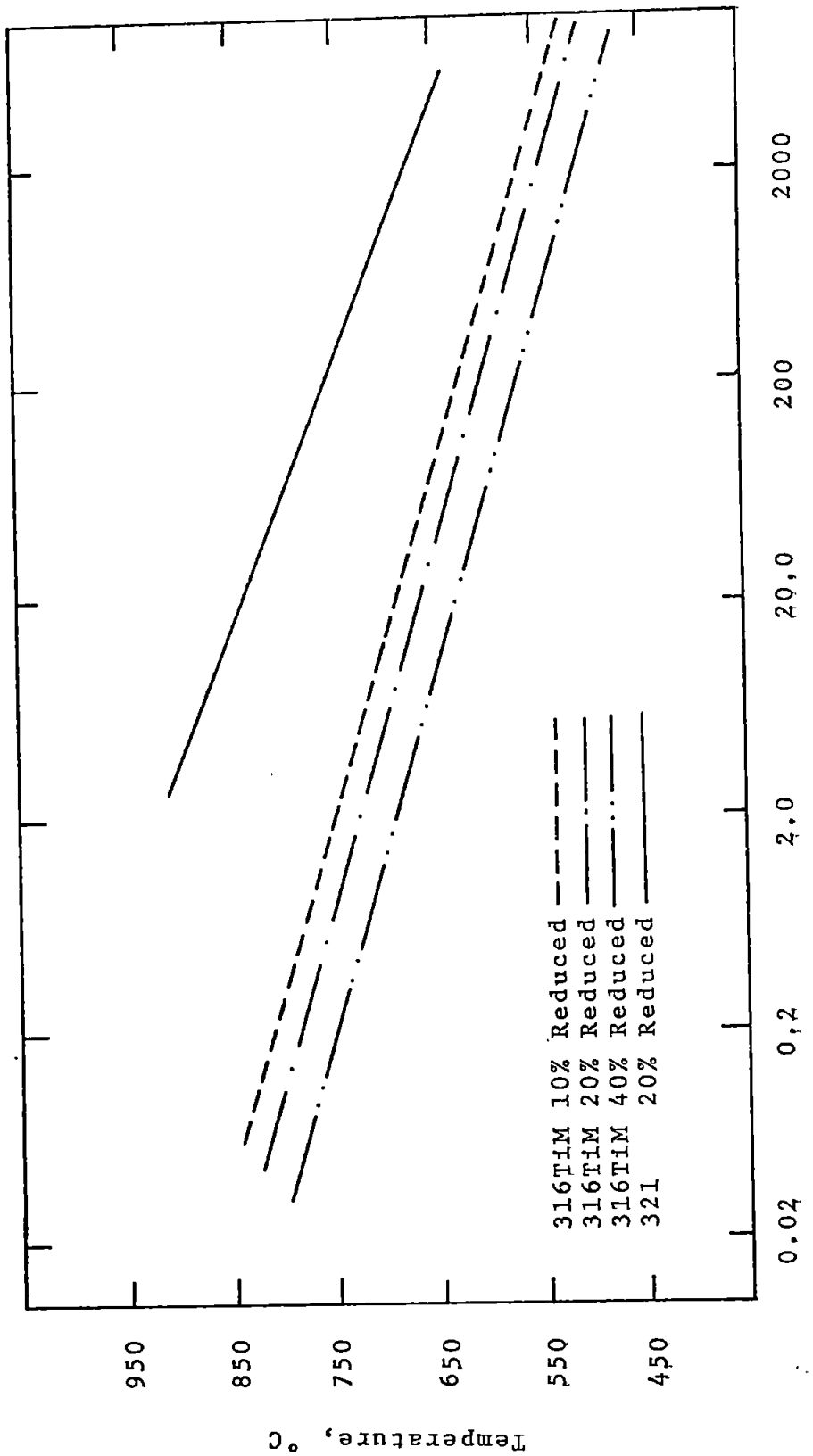


Figure 18. Recrystallization Starting Times for Type 316TiM Reduced by Swaging and Type 321 Reduced by Tube Drawing.

determined by Spruiell et al. (5). The type 316 steel was reduced by rolling and the type 316TiM was reduced by swaging. This difference in applying cold work implies that the data is not exactly comparable. However, it is believed that this difference is insufficient to account for the large difference in observed recrystallization behavior. The data indicate that recrystallization occurs earlier and more rapidly in the present heat of type 316TiM than in the standard type 316 stainless steel. Spruiell et al. observed no recrystallization in type 316 solution treated and reduced 10 or 20% even after 3250 hours at 710°C. It was found that 10 and 20% reduced type 316TiM recrystallizes after 0.2 hours at 750°C (Figure 15 page 54). Also, recrystallization in 20% reduced type 316TiM aged at 650°C begins before 20 hours (Figure 14, page 53). Figure 18 graphically presents the start of recrystallization for 10, 20, and 40% reduced type 316TiM.

The growth in the sigma particles with time is seen in Figures 14 and 16. In particular, the comparison of Figures 16(b) and 16(c) illustrate the large diameter of the sigma particle after 20 hours of aging at 750°C as compared to 2 hours.

The difference in the microstructure due to cold work and aging at 850°C is illustrated in Figure 19. Solution treated, 10, 20, and 40% reduced type 316TiM aged 200 hours at 850°C are shown in Figure 19(a), 19(b), 19(c), and



Figure 19. Type 316TiM Stainless Steel Aged 200 Hours at 850°C. (a) Initially Solution Treated, (b) 10% Reduced, (c) Reduced 20%, (d) Reduced 40%.

19(d), respectively. The large grain size and lack of much sigma are clearly seen in the solution treated type 316TiM. The reduced samples have a small grain size caused by recrystallization and large numbers of sigma particles.

Transmission electron microscopy allowed the determination of phase morphology and distribution. Figures 20 and 21 contain electron micrographs and selected area diffraction patterns of type 316TiM for various pretreatments and aging conditions. In solution treated type 316TiM, $M_{23}C_6$ precipitated on the grain boundaries and was identified by electron diffraction patterns, Figure 20(a). (The procedure followed in identifying a precipitate from a selected area diffraction pattern is illustrated by an example in Appendix A.) TiC precipitated intragranularly. Cold work accelerated the precipitation of $M_{23}C_6$. The alignment of the carbide particles in the recrystallized grains of Figure 20(b) parallel to the acicular features of the adjacent cold worked substructure suggests the nucleation of intergranular carbides along these features. At aging times after complete recrystallization only TiC was identified by selected area diffraction patterns within the grains, Figure 20(c). Thus if $M_{23}C_6$ had formed intergranularly on the cold worked substructure, it had redissolved by this time. For short aging times or low aging temperatures, the $M_{23}C_6$ precipitate consists of small blocky particles, Figure 20(a). However, at 850°C, $M_{23}C_6$ forms massive ribbons at the grain boundaries,

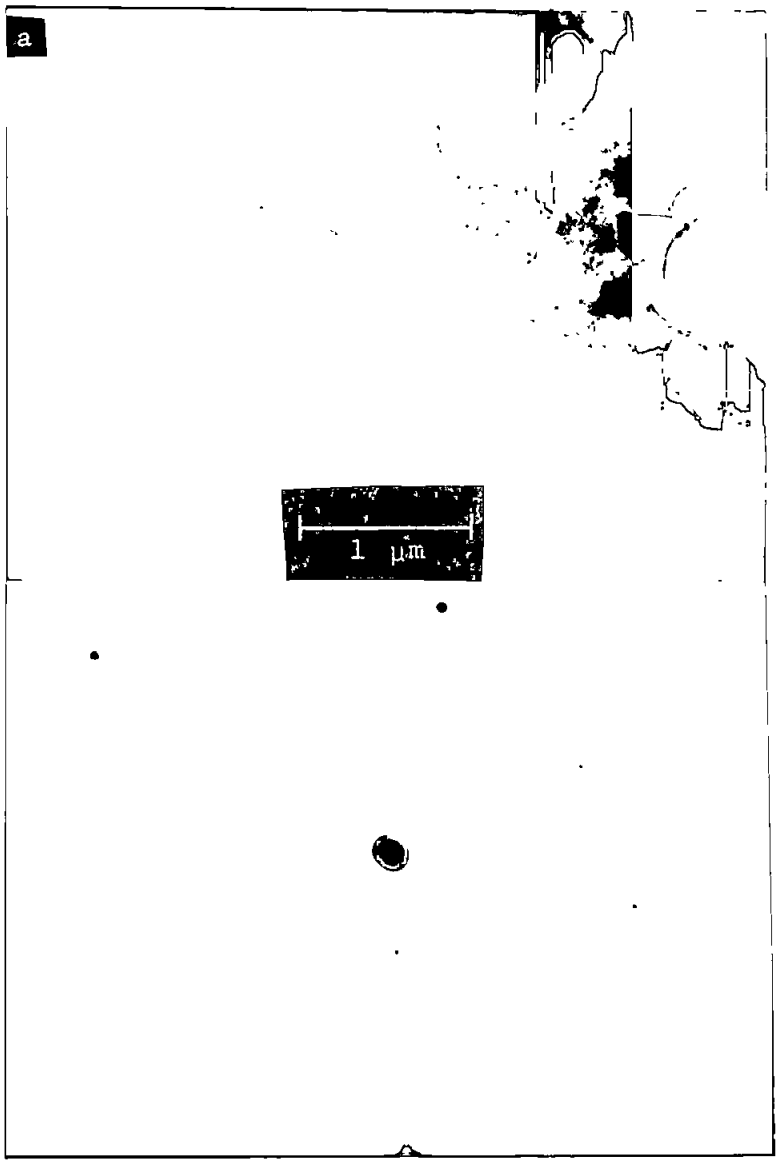


Figure 20. Transmission Electron Micrographs of Type 316TiM. (a) Solution Treated and Aged 4000 Hours at 550°C, (b) 10% Reduced and Aged 2 Hours at 750°C, (c) 20% Reduced and Aged 20 Hours at 750°C, (d) Solution Treated and Aged 2000 Hours at 850°C.



Figure 20. Continued

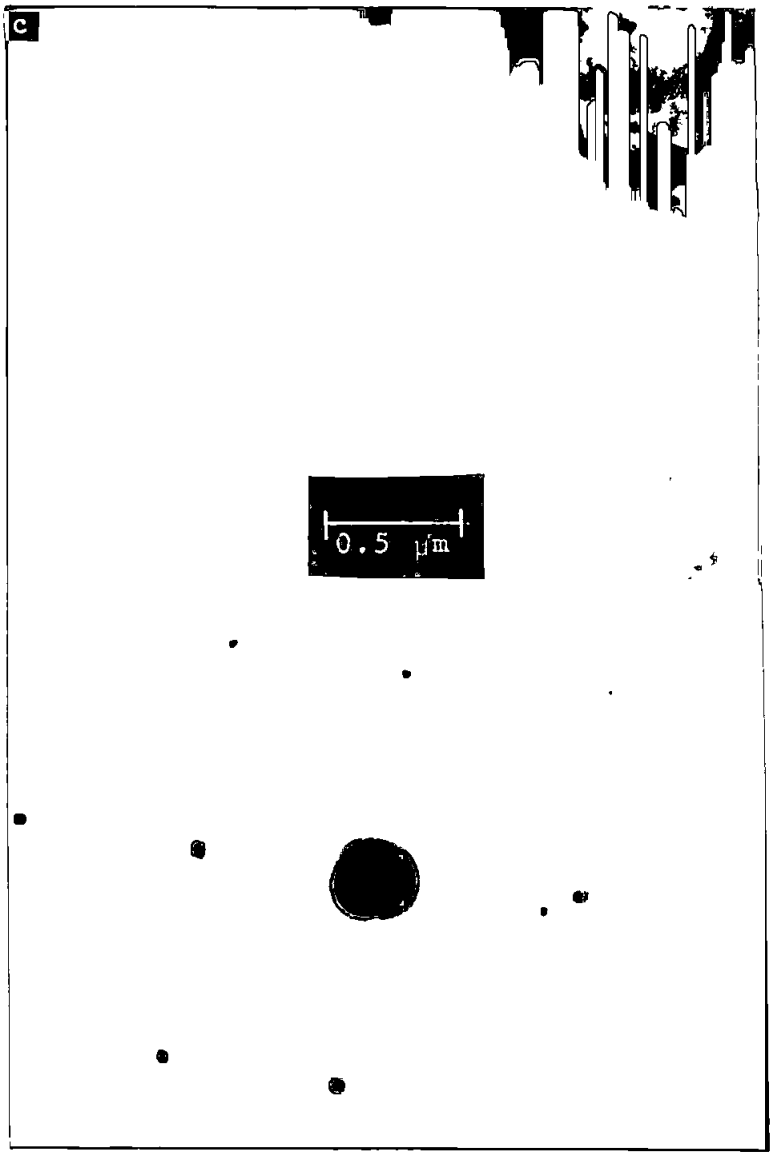


Figure 20. Continued

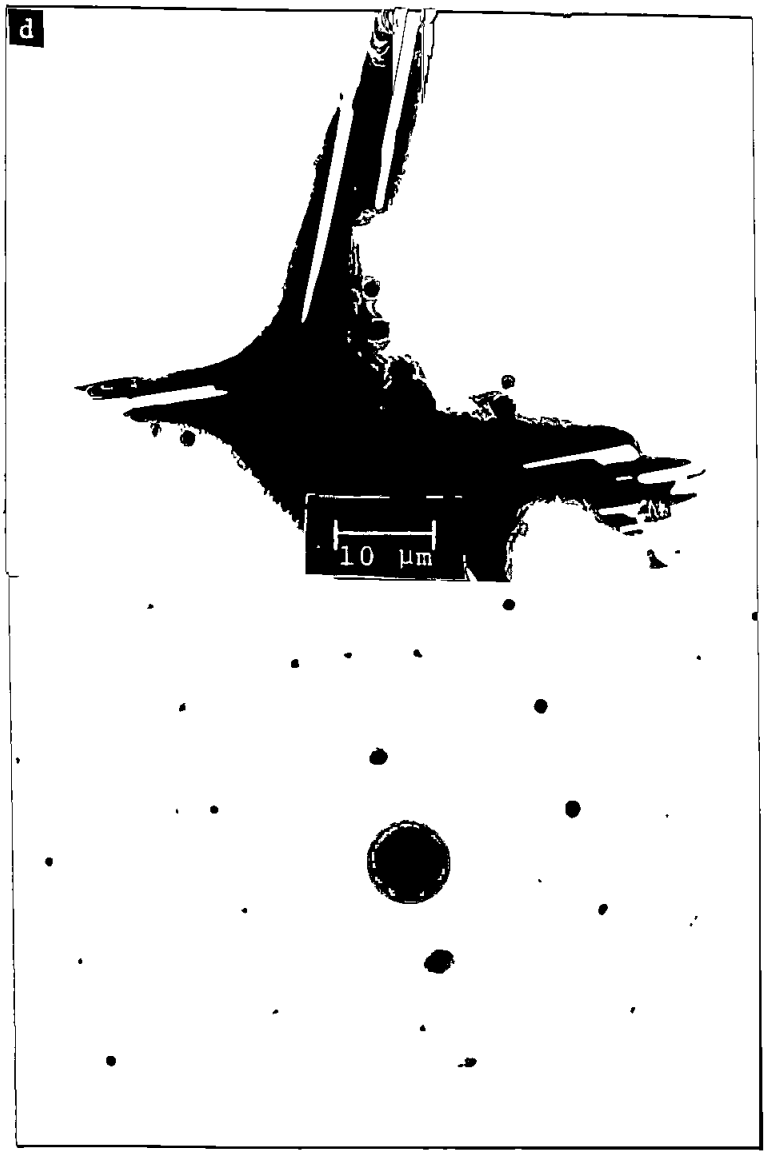


Figure 20. Continued

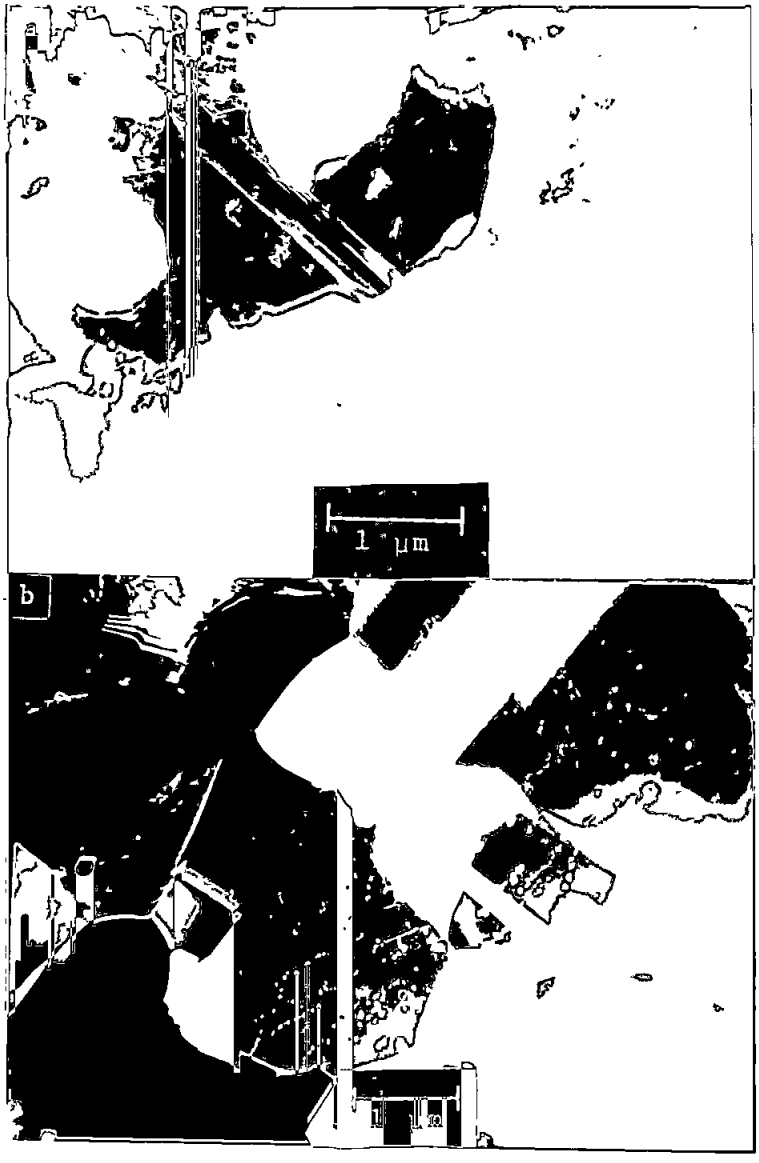


Figure 21. Transmission Electron Micrographs of Type 316TiM. (a) 10% Reduced and Aged 4000 Hours at 550°C, (b) 10% Reduced and Aged 20 Hours at 750°C, (c) 20% Reduced and Aged 2000 Hours at 750°C, (d) Solution Treated and Aged 2000 Hours at 750°C.

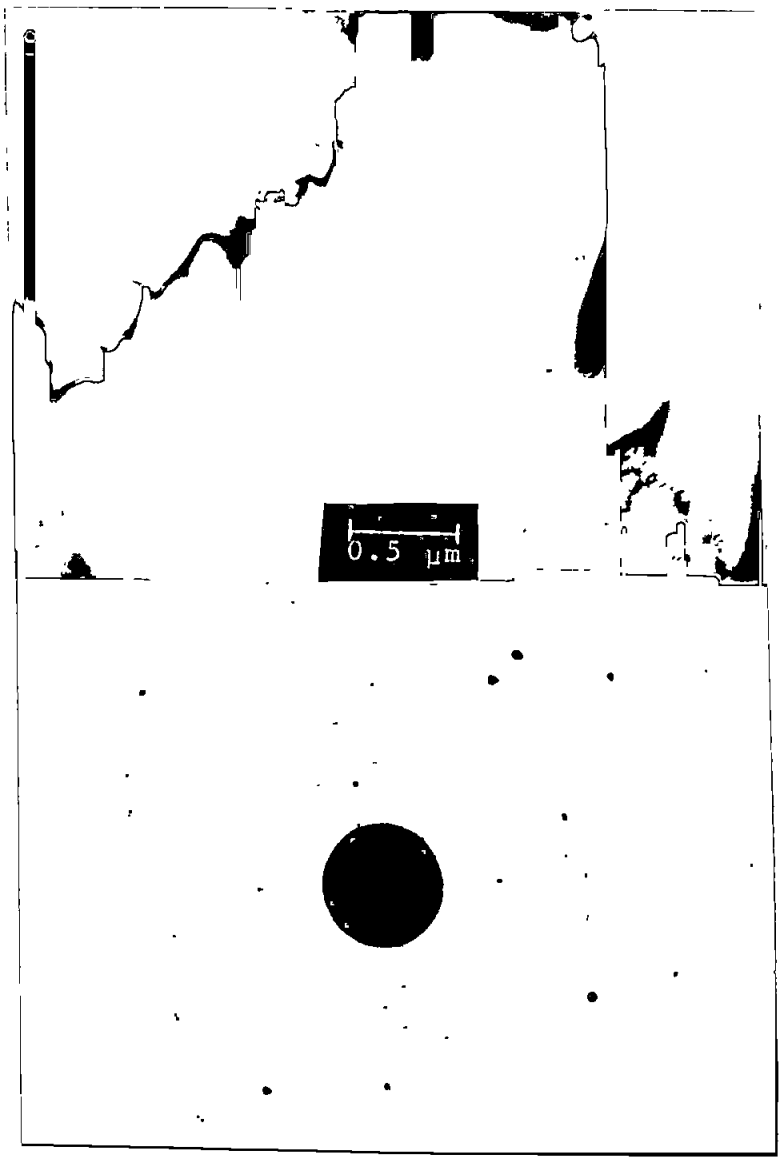


Figure 21. Continued

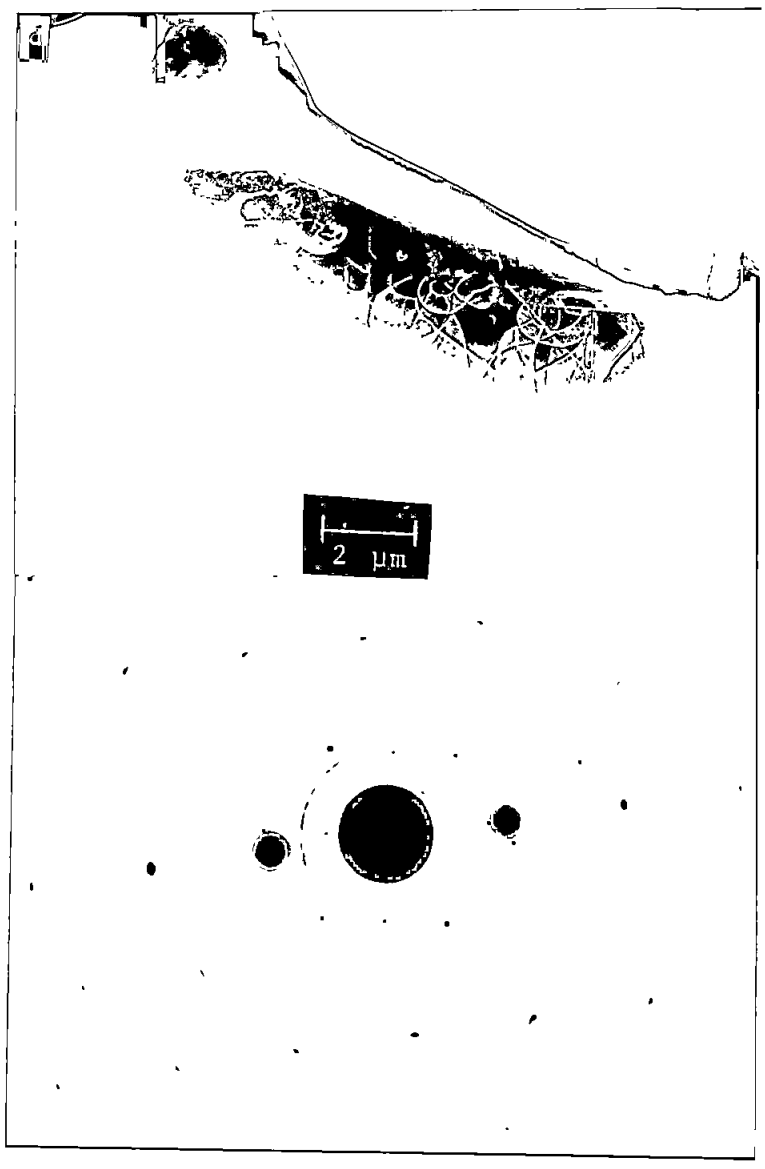


Figure 21. Continued

Figure 20(d), after aging for 2000 hours. The selected area diffraction pattern in Figure 20(d) is of one of these particles. Due to early recrystallization, cold work does not seem to affect this behavior.

Sigma particles are observed to nucleate during recrystallization of type 316TiM. Figure 21(a) shows sigma particles forming at the grain boundaries between cold worked grains and recrystallized grains. Triple points between grains are also ideal sites for sigma growth, Figure 21(b). In this study, sigma was always observed as the large blocky particles as seen in Figure 21(b). Also at longer aging times sigma was observed to form on twin boundaries and intragranularly on included particles.

Chi phase behaved similarly to sigma in solution treated type 316TiM. This phase first formed at the grain boundaries and then intragranularly, Figure 21(c). However, in the reduced samples, chi did not nucleate during recrystallization and was not observed until appreciably later times. Thus, the early recrystallization in cold worked type 316TiM appeared to change the order in which sigma and chi formed. The only way chi phase could be distinguished from sigma was by selected area diffraction patterns. At long aging times chi phase was seen to form long smooth continuous particles, Figure 21(d), while sigma formed short strings of particles by impingement.

Type 321

The micrographs in Figures 22, 23, and 24 illustrate the behavior of type 321 stainless steel. Figures 22(a) and 22(b) show the microstructure of solution treated and 20% reduced type 321, respectively, after 4000 hours of aging at 650°C. A similar amount of precipitate is observed in both samples. However, the reduced sample has an elongated grain structure which displays a mixture of cold worked and recrystallized grains.

The micrographs of Figures 22(c) and 22(d) show a marked change in the morphology of the precipitate between 200 hours and 2000 hours of aging at 850°C for the as-solution treated type 321 steel. Cold reduced type 321 shows the same behavior. X-ray diffraction reveals the precipitate is mostly $M_{23}C_6$ with traces of chi phase. Optically these phases are indistinguishable. Selected area diffraction patterns reveal $M_{23}C_6$ and chi to exist as both globular and elongated particles on the grain boundaries in alternating clusters. That $M_{23}C_6$ and chi exists in close contact with each other is consistant with the literature (4).

In Figure 23 is illustrated the behavior of type 321 on aging at 750°C. Optically, it is difficult to distinguish the recrystallization behavior. However, transmission electron microscopy allows easy determination of recrystallization. Figure 24(a) shows the growth of a chi particle at the boundary between a recrystallized grain and

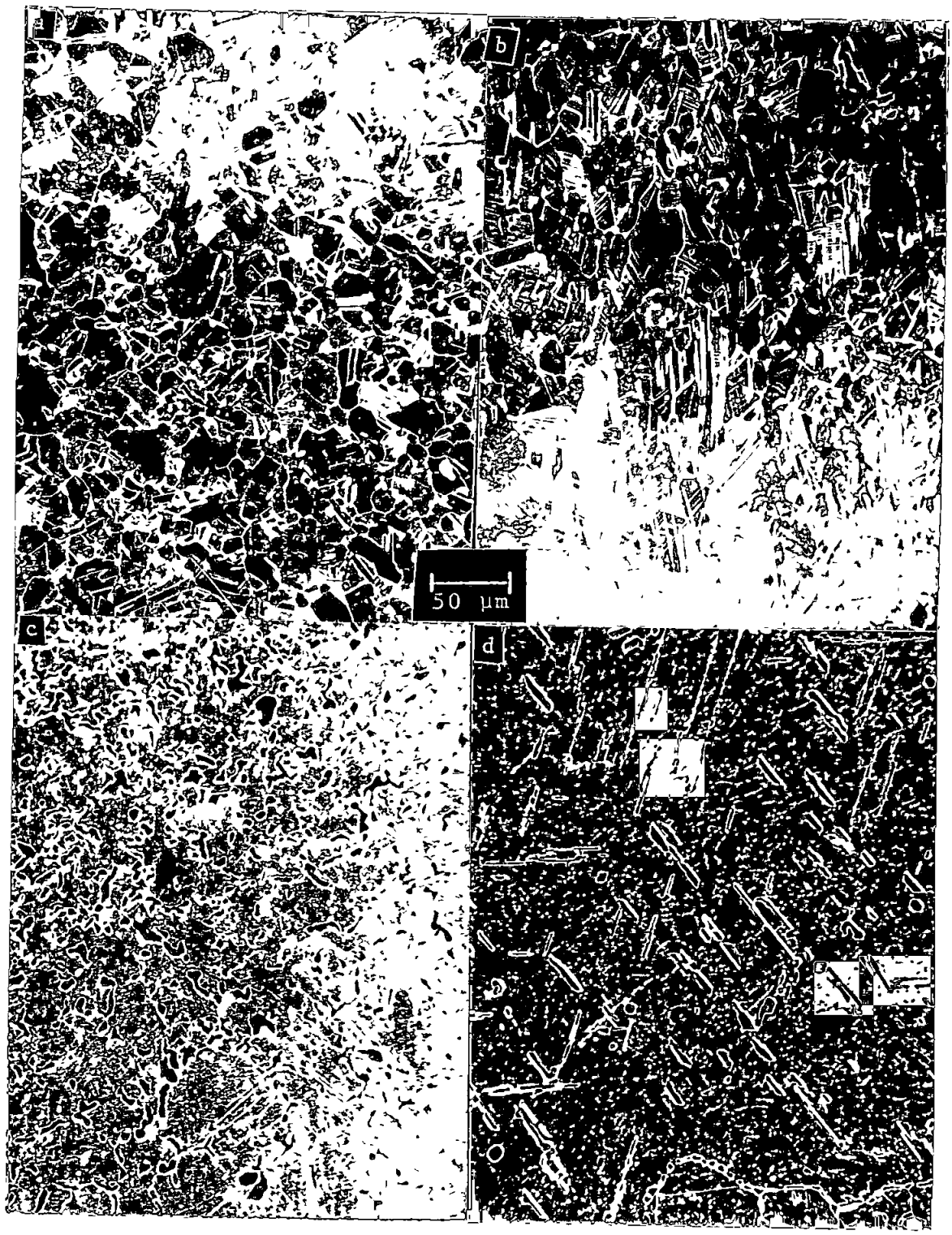


Figure 22. Type 321 Stainless Steel. (a) Solution Treated and Aged 4000 Hours at 650°C, (b) Reduced 20% and Aged 4000 Hours at 650°C, (c) Solution Treated and Aged 200 Hours at 850°C, (d) Solution Treated and Aged 2000 Hours at 850°C.

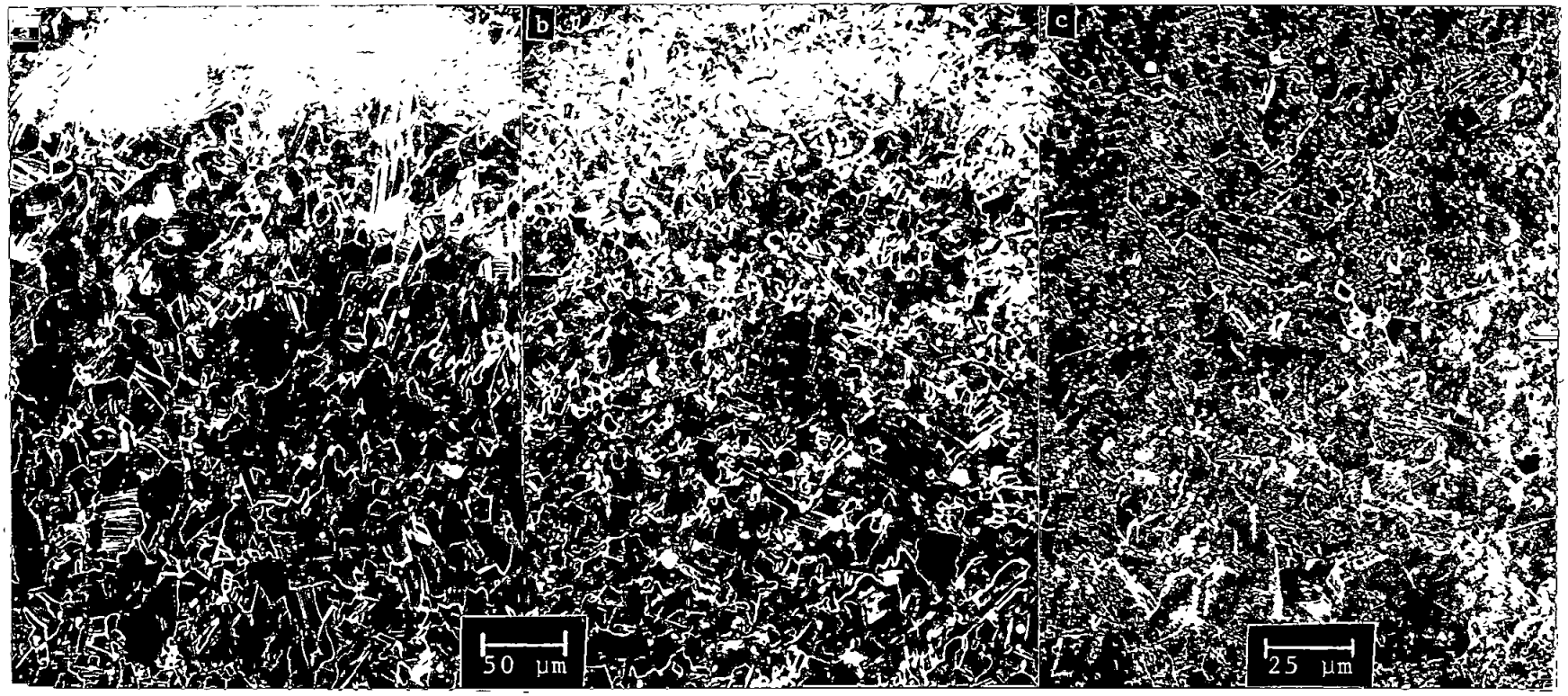


Figure 23. Type 321 Stainless Steel Reduced 20% and Aged at 750°C for (a) 2 Hours, (b) 200 Hours, and (c) 2000 Hours.

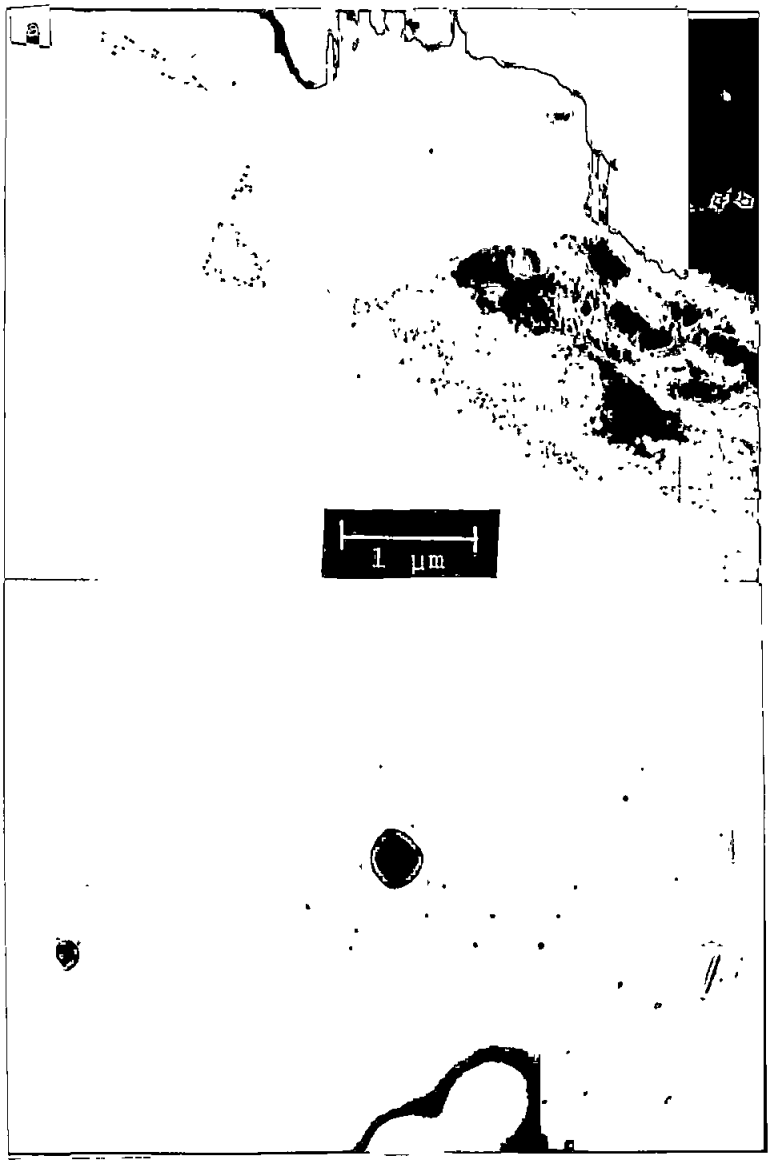


Figure 24. Transmission Electron Micrographs of Type 321. (a) Reduced 20% and Aged 200 Hours at 750°C, (b) Solution Treated and Aged 200 Hours at 650°C.

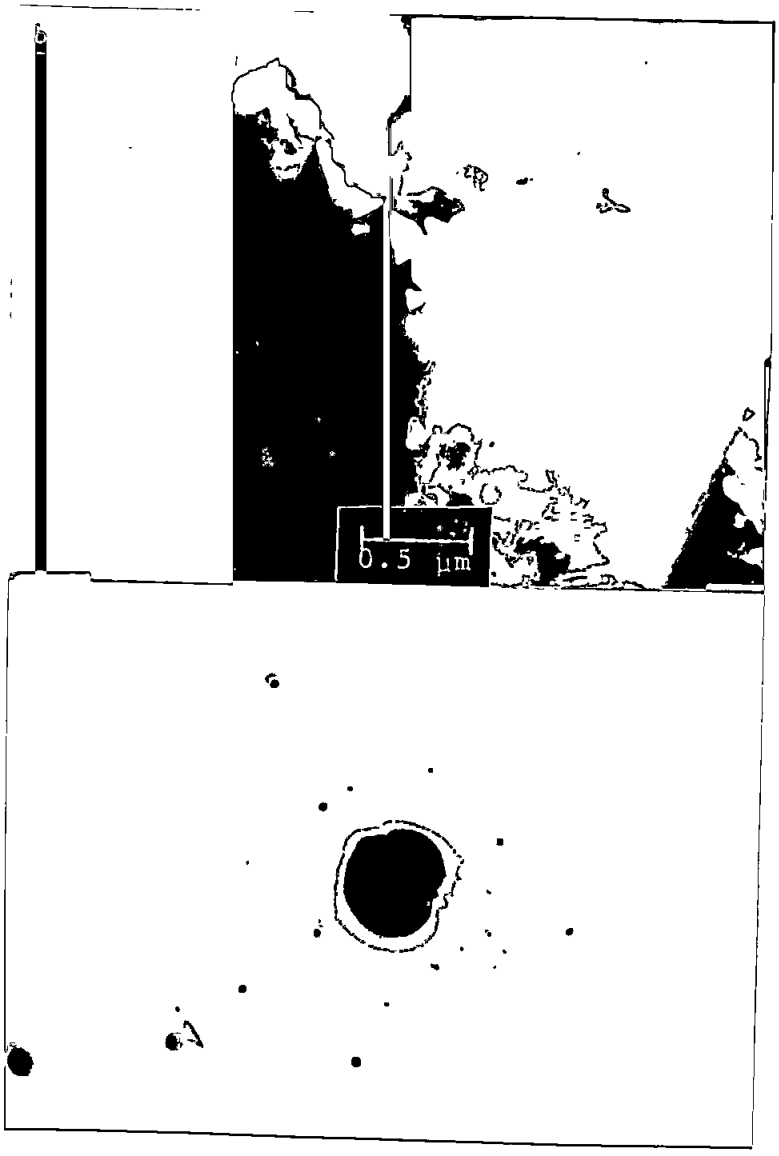


Figure 24. Continued

a cold worked grain in 20% reduced type 321 aged for 200 hours at 750°C. The recrystallization behavior of 20% reduced type 321 is given in Figure 18 (page 57).

Figure 24(b) shows chi and $M_{23}C_6$ particles growing on the grain boundary in solution treated type 321 aged at 650°C for 200 hours. Initially $M_{23}C_6$ forms at the grain boundaries as small blocky particles at short aging times and temperatures of 750°C and below. Chi nucleated after some $M_{23}C_6$ had formed. Both phases grow into large globular particles on aging at 850°C.

IV. HARDNESS MEASUREMENTS

It is clear that the various pretreatments and aging behavior exhibited by types 316TiM and 321 will have marked effects upon the properties of these austenitic stainless steels. Therefore, the determination of the changes in hardness as a function of pretreatment and aging condition have been measured. The results of the hardness measurements for type 316TiM aged at 550, 650, 750, and 850°C are given in Figures 25(a), 25(b), 25(c), and 25(d), respectively. Examination of this data reveals that cold working increases the hardness as expected, but recrystallization does not return the hardness to the level of the solution treated samples. This is apparently caused by the precipitation of sigma associated with recrystallization. Since recrystallization is rapid in type 316TiM, there was little opportunity

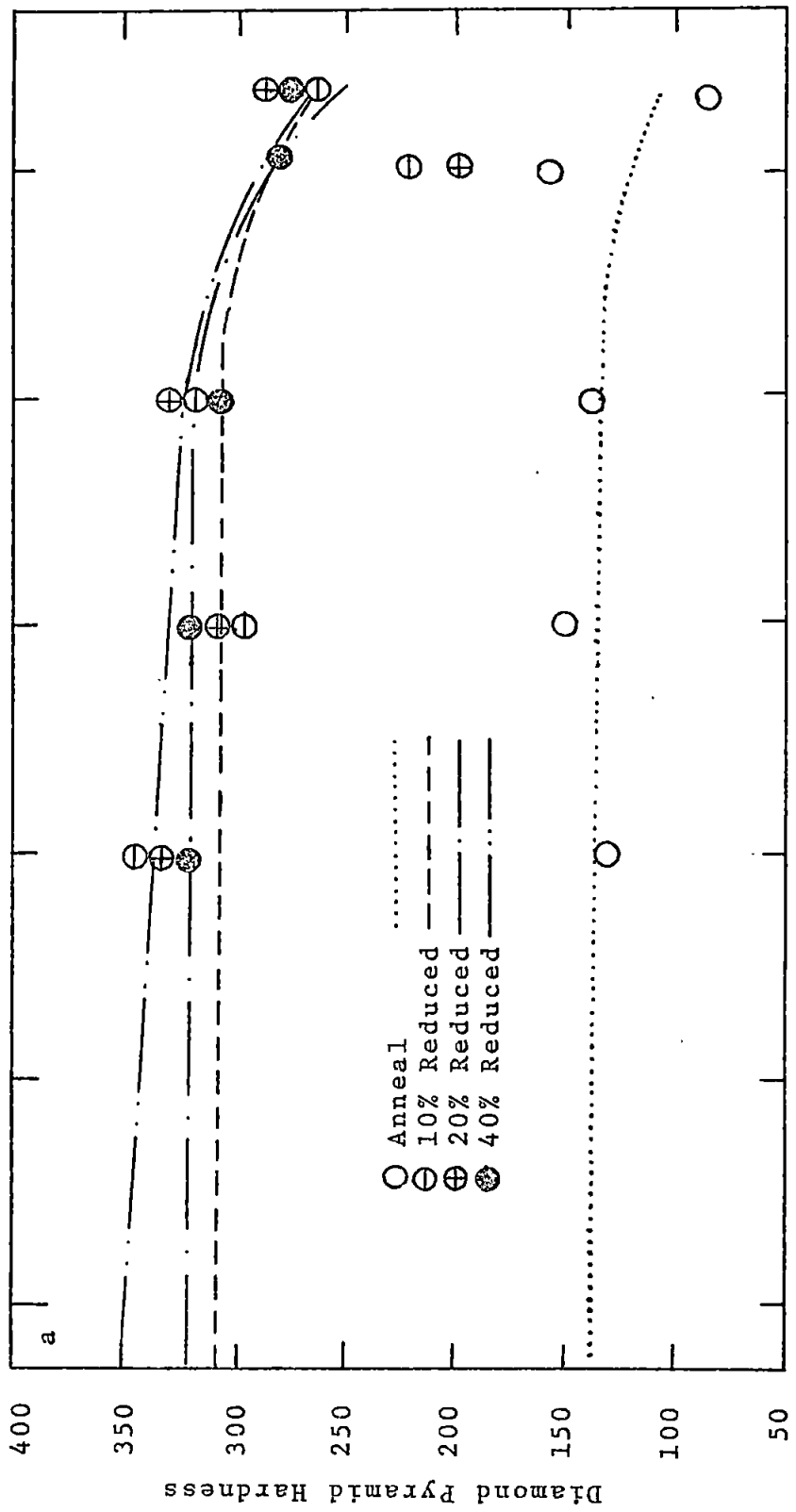


Figure 25. Diamond Pyramid Hardness of Type 316TiM as a Function of Reduction in Area and Aging Time. (a) Aged at 550°C, (b) Aged at 650°C, (c) Aged at 750°C, (d) Aged at 850°C.

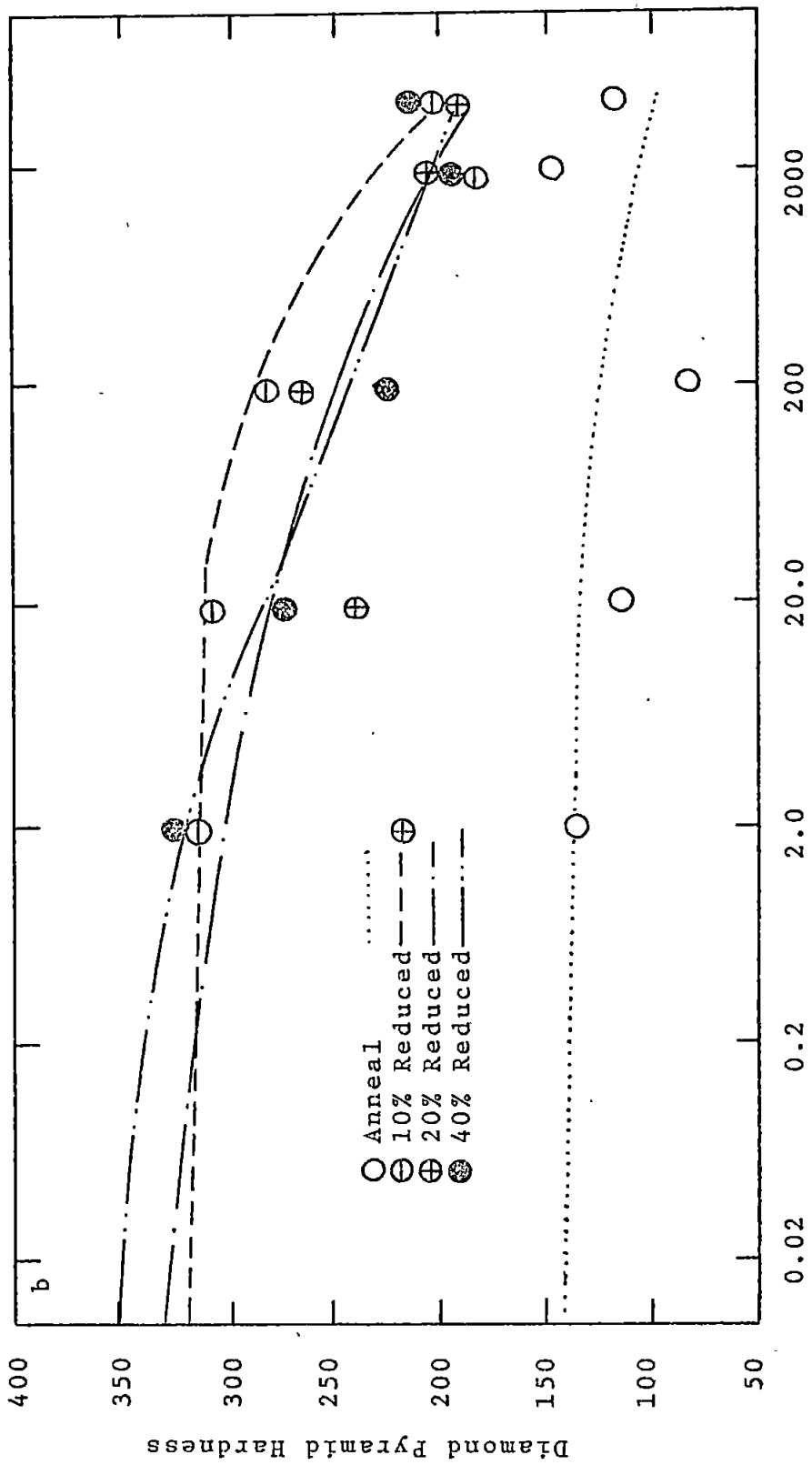


Figure 25. Continued

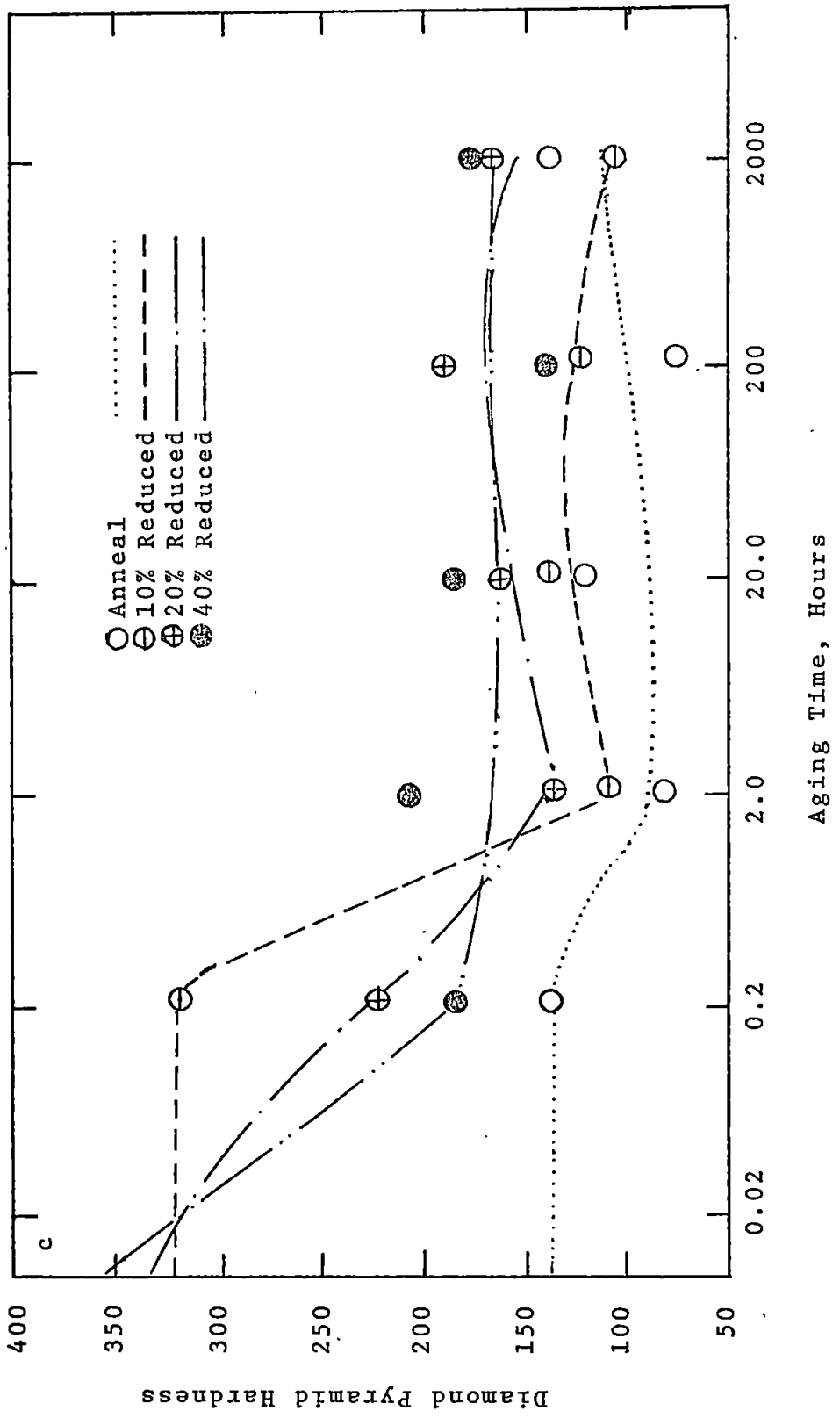


Figure 25. Continued

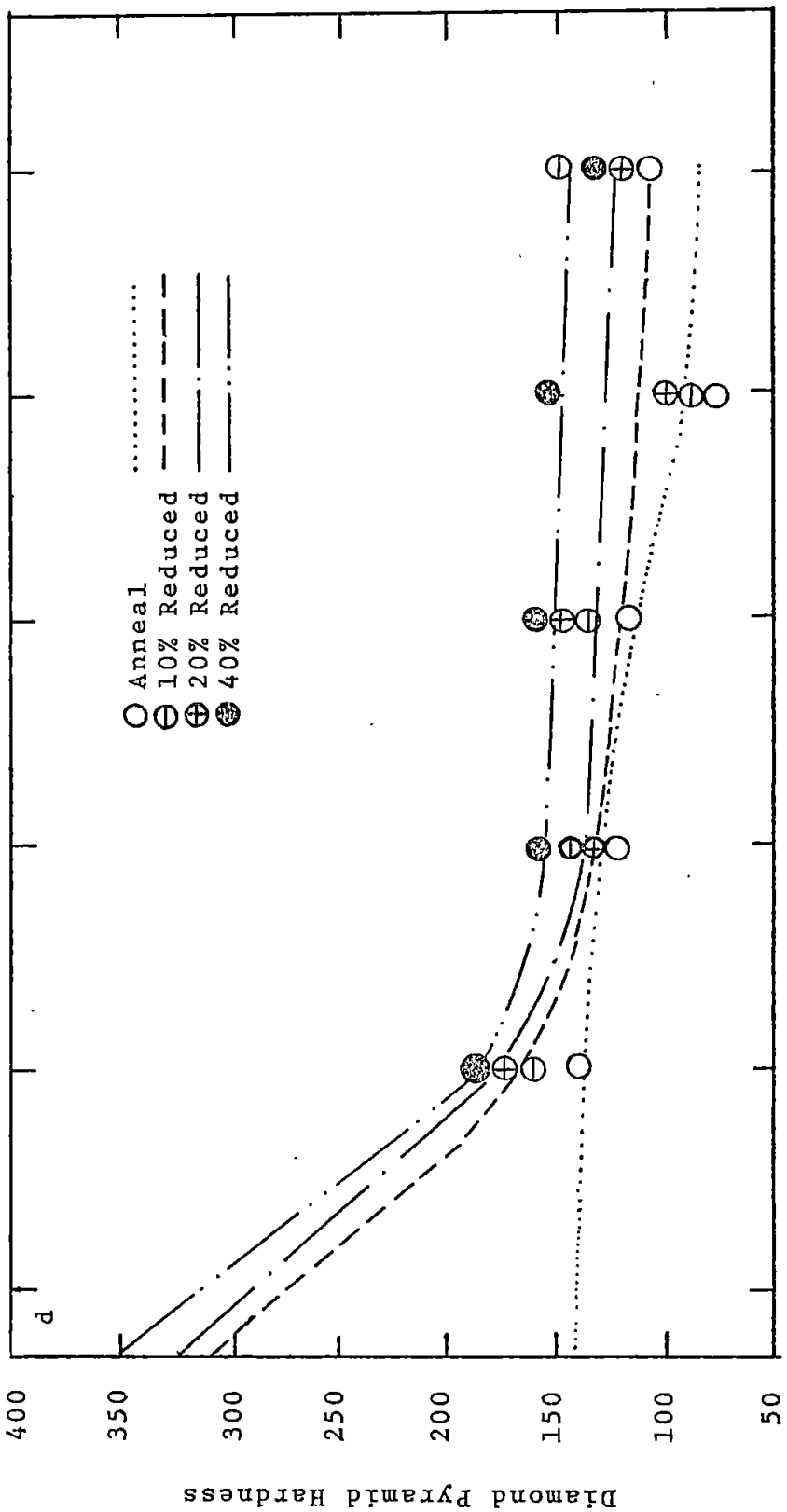


Figure 25. Continued

to observe the effect of recovery alone. It would appear that hardness changes associated with recovery per se were small in any case.

The effect of temperature on the change in hardness is revealed by comparing Figures 25(a), 25(b), 25(c), and 25(d). At 550°C there is little difference in the behavior of the reduced samples, Figure 25(a), while at 650°C and 750°C, Figures 25(b) and 25(c), respectively, there is a difference in the behavior of the reduced samples. This difference is due to the difference in recrystallization behavior of the reduced samples. Earlier recrystallization drops the hardness sooner. That the change in hardness at 850°C, Figure 25(d), is similar for all samples reflects the similarity in precipitation activity at this temperature. Hardness measurements at 450 and 950°C reveal changes similar to those at 550 and 850°C, respectively.

Figures 26(a), 26(b), and 26(c) present the hardness changes in type 321 aged at 650, 750, and 850°C, respectively. Comparison of these figures shows that aging conditions had a minor effect on the hardness of solution treated type 321. As was observed in type 316TiM, cold work increased the hardness of type 321. At each aging temperature the hardness level is observed to decrease. At 750 and 850°C the hardness decreases to a level just above that of the solution treated samples. This is consistant with the observation that these samples had completely recrystallized.

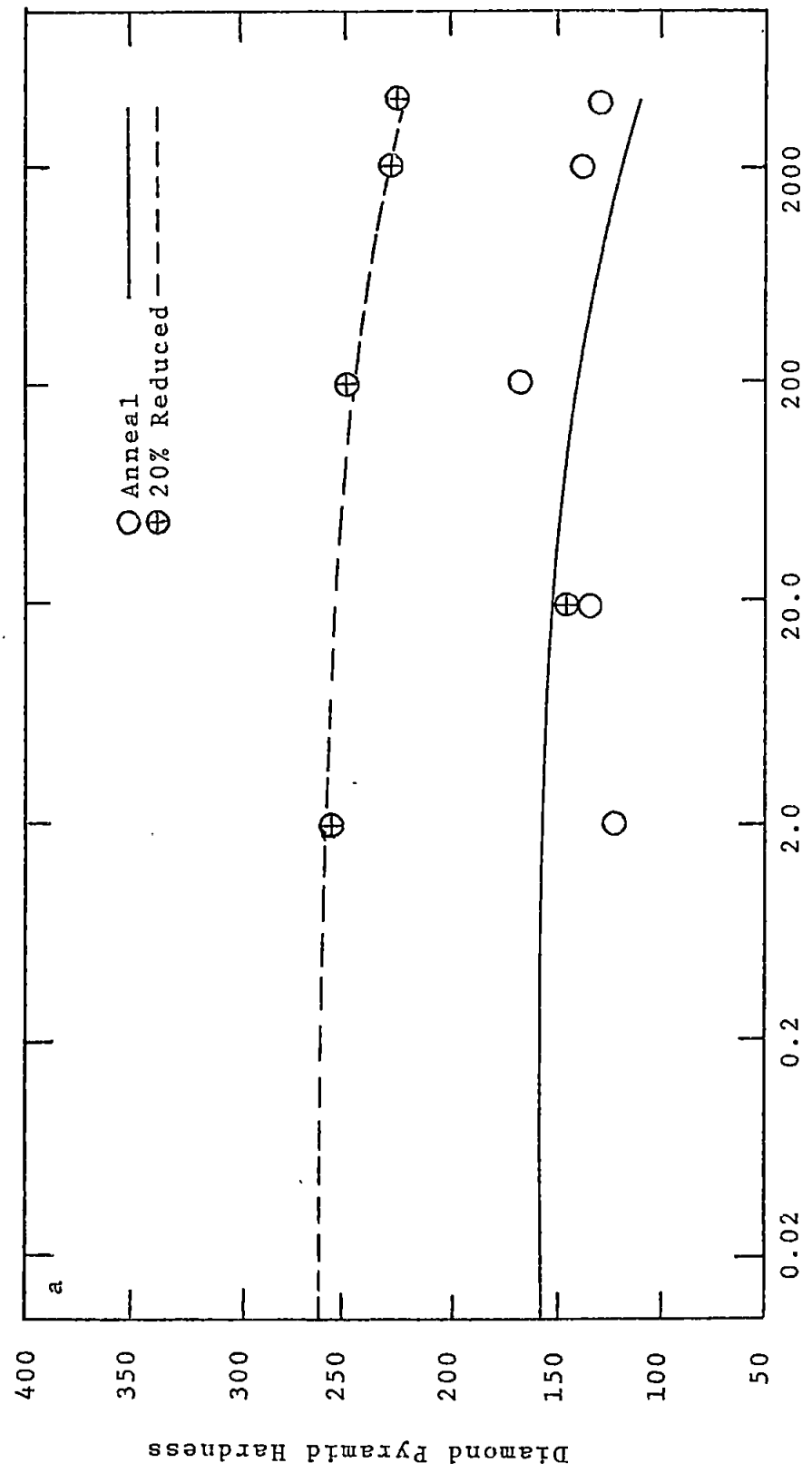


Figure 26. Diamond Pyramid Hardness of Type 321 as a Function of Reduction in Area and Aging Time. (a) Aged at 650°C, (b) Aged at 750°C, (c) Aged at 850°C.

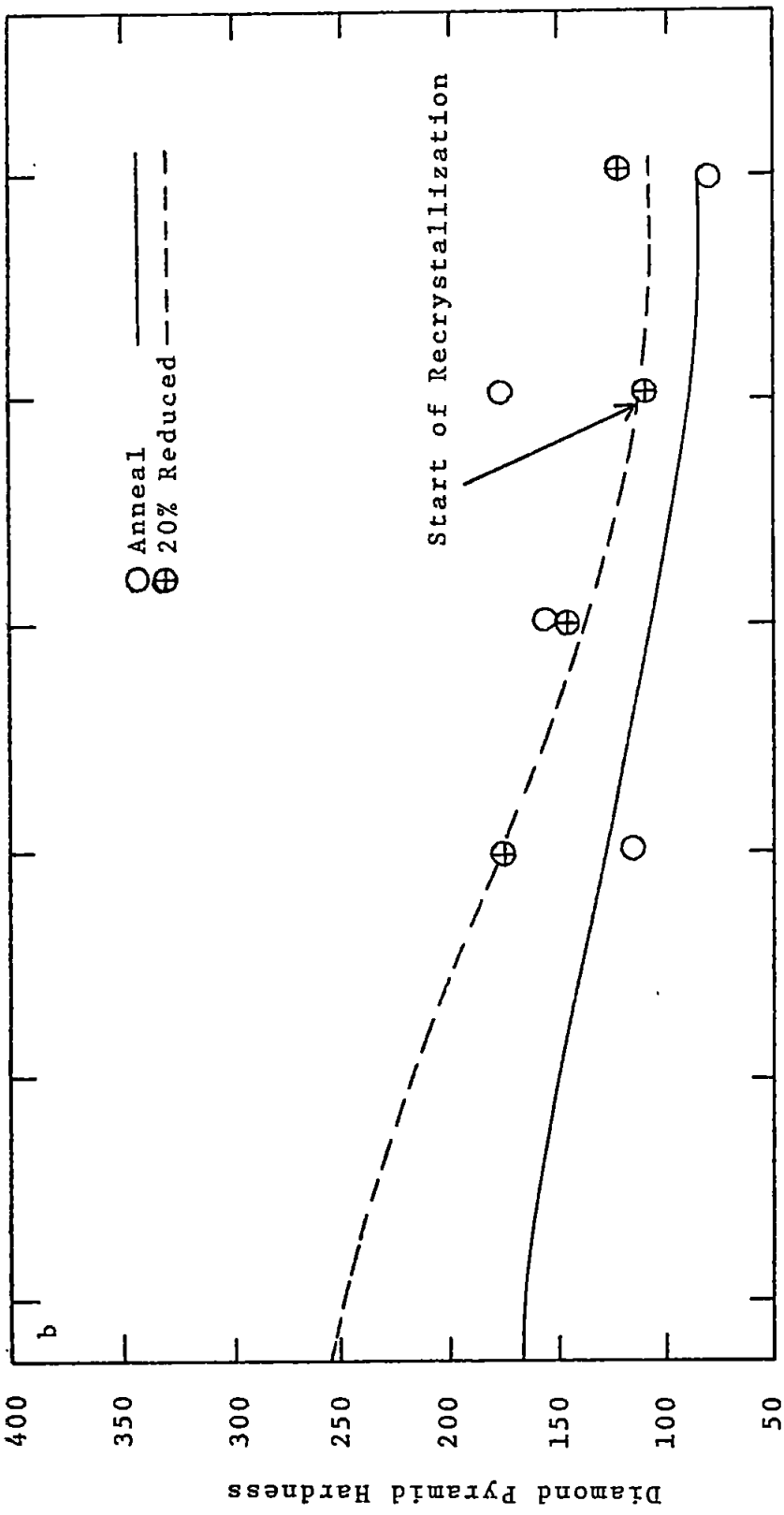


Figure 26. Continued

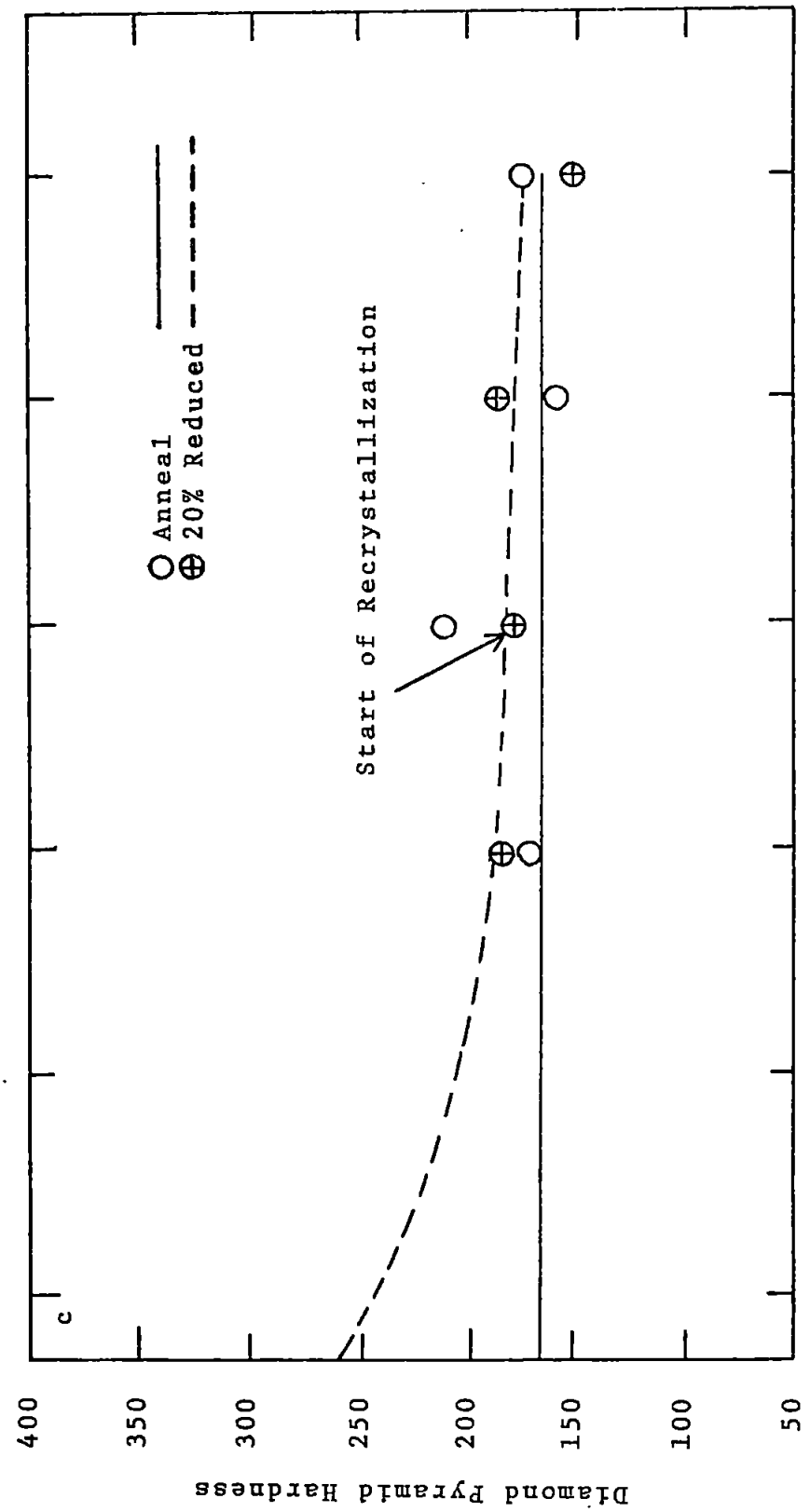


Figure 26. Continued

Some hardness decrease is observed prior to the onset of recrystallization. This is presumably associated with recovery processes and the depletion of the matrix of solid solution hardening elements due to carbide precipitation. Hardness measurements at 450 and 550°C revealed changes similar to those at 650°C. Changes in hardness at 950°C were similar to those at 850°C.

V. FURTHER DISCUSSION

The results of this study on the microstructural stability of types 316TiM and 321 austenitic steels when compared with existing knowledge of phase instability of types 316, 316L, 304, and 304L allow a qualitative analysis of the effect of titanium on precipitation processes in austentic stainless steels. The addition of titanium is seen to change the nucleation rates of the various phases as well as their absolute and relative amounts.

These changes are directly related to the early precipitation of TiC and $Ti_4S_2C_2$, both of which are controlling factors in the carbon content of the austenitic matrix. The latter phase also controls the amount of sulfur in the matrix which may be a factor in the post irradiation ductility of these alloys, a major concern in nuclear application. The carbon content plays an important part in the precipitation of $M_{23}C_6$ and the intermetallic phases.

In type 316TiM, the nucleation of $M_{23}C_6$ is seen to be retarded as compared to type 316. The degree of retardation is similar to that resulting from the low carbon content of type 316L. Weiss and Stickler (4) reported the minimum incubation time for $M_{23}C_6$ in type 316L, solution treated at 1090°C, to be about 1 hour. Figure 8 (page 44) shows that the minimum incubation time for $M_{23}C_6$ in solution treated type 316TiM is also about 1 hour. Both these times are longer than is required to nucleate $M_{23}C_6$ in type 316. Comparison of samples given the same amount of cold work reveals the same trend.

This same behavior is repeated for types 304, 304L, and 321 stainless steels (39,40). The nucleation of $M_{23}C_6$ in solution treated type 321 begins before 20 hours of aging. The difference between types 316TiM and 321 for the nucleation time of $M_{23}C_6$ can be explained in terms of the lower nickel content, the absence of molybdenum, and the higher titanium content in type 321. Kregg and Silcock (41) have observed that the $M_{23}C_6$ precipitation rate decreases with decreasing nickel content. Weiss and Stickler determined that decreasing the molybdenum content increases carbon solubility and therefore decreases the rate of formation of $M_{23}C_6$. A higher titanium content promotes TiC precipitation which results in less carbon for $M_{23}C_6$. Therefore, the longer incubation time of $M_{23}C_6$ in type 321 than in type 316TiM is consistent with previous observations.

The effect of TiC on the precipitation behavior of the intermetallic phases in type 316TiM is prodigious. As was observed in type 316L, the nucleation of sigma in type 316TiM was accelerated with respect to type 316. However, the shift of sigma stability to higher temperatures exhibited by type 316L was not observed in type 316TiM. This is the result of the lower stability of TiC at higher temperatures. The consequence is that a higher carbon concentration is maintained at temperatures greater than 900°C in the austenitic matrix of type 316TiM than in type 316L. Also, the formation of TiC maintains a lower carbon concentration at temperatures less than 900°C leading to earlier and more massive sigma nucleation at these temperatures in type 316TiM than in both type 316L and type 316.

The nucleation of chi and Laves phases is also affected by the lower concentration of carbon at lower temperatures. Within the experimental sensitivity of the techniques used in this investigation the latter phase was not observed in either type 316TiM or in type 321. Chi and sigma phases are seen to nucleate simultaneously in solution treated type 316TiM. Initial precipitation of sigma is greater than chi. At longer aging times the relative amount of chi increased. Aging temperature also affected the amount of chi relative to sigma. The formation of chi in type 316TiM was earlier than what has been reported in type 316, but later than in type 316L (4). In type 316, chi formed before sigma,

while in type 316L chi and sigma formed at the same time as was observed in type 316TiM. The similarity of the minimum inclubation time for sigma and chi in types 316L and 316TiM reflects the low carbon content of the austenitic matrices of these stainless steels. In type 316, sigma nucleation was deferred because of the higher carbon content existing in its matrix.

The effect of cold work illustrates the interdependence of sigma and chi nucleation. By comparing Figures 8 and 9, pages 44-5, it is seen that the nucleation of chi is unchanged by 10% reduction in area while sigma nucleates by about a factor of ten earlier. As the amount of cold work is increased, the nucleation of sigma occurs still earlier. Chi formation occurs well after sigma formation and at times greater than those required for its formation in the solution treated case, see Figures 10 and 11, pages 46-47. Thus, cold work, by causing earlier nucleation of sigma, suppresses the growth of chi.

The mechanism by which cold work accelerates sigma formation is reported to be due to recrystallization (4,5,19). Where recrystallization is rapid, its main effect on sigma formation is providing more sites for subsequent nucleation during aging, provided that the grain size is refined by recrystallization. The observations on recrystallization in type 316TiM on aging at 750°C support this, i.e., recrystallization refined the grain size creating more grain

boundary surface area, triple points and twin boundaries which acted as nucleating sites for the growth of sigma. When recrystallization proceeds slowly, sigma formation at the interface between cold worked and recrystallized grains may be expected due to enhanced diffussion along the moble boundary and in the cold worked matrix. The formation of sigma at the interface between cold worked and recrystallized grains was observed in 10% reduced type 316TiM aged at 550°C for 4000 hours as shown in Figure 21(a), page 65. When aged at 750°C for 2 hours, sigma was not observed at the interface between cold worked and recrystallized grains in 10% reduced type 316TiM as shown in Figure 20(b), page 62. However, sigma was observed in the recrystallized regions of this sample located mainly at triple grain junctions.

In a like manner, the similarity observed in the precipitation behavior of cold worked and solution treated type 321 can be related to their grain size. Initially, the grain size of these samples were in the range of ASTM 6 to 10. Recrystallization in 20% reduced type 321 did not change the grain size of these samples appreciably. Figure 23, page 71, shows that the grain size after recrystallization, Figure 23(c), was about the same as before, Figure 23(b). Also this grain size is the same as in solution treated type 321, Figure 22(a), page 70.

This study shows that type 321 is much more stable than type 316TiM. This has been explained in terms of

austenitic composition for the case of $M_{23}C_6$ nucleation. Austenitic stainless steels of varying composition are known to exhibit different behavior upon exposure to elevated temperatures. The literature reports that type 321 is more susceptible to sigma formation than type 304 (1), that type 316 is more susceptible than types 304 (1,13) and 321 (1), and that type 316L is more susceptible than type 316 (4). The data of this study confirms that type 321 is more stable than type 316 and shows that type 316TiM is less stable than type 316.

It is possible to explain the relative stabilities of these steels on the basis of composition. Nicholson et al. (14) state that a minimum chromium content of about 18% is needed to induce sigma formation in Fe-Cr-Ni alloys. Sticka (1) and Hull (2) in the manner of Schaeffler (42) have shown that the affect of other alloying elements on the precipitation of sigma can be expressed in terms of chromium equivalents. In this manner, a minimum equivalent chromium content is needed for sigma formation and a higher equivalent chromium content makes a steel more susceptible to sigma nucleation. Hull has investigated the chromium equivalents of many elements for exposure at 816°C and determined the following equation for equivalent chromium in weight percent;

$$\text{Equivalent Chromium} = \%Cr + 0.31 \times \%Mn + 1.76 \times \%Mo + 0.97 \times \%W + 2.02 \times$$

$$\%V + 1.58 \times \%Si + 2.44 \times \%Ti + 1.70 \times \%Nb + 1.22 \times \%Ta - 0.226 \times \%Ni - 0.177 \times \%Co$$

By using this equation, the equivalent chromium content of 316TiM is 20.1 weight percent and that of type 321 is 17.6 weight percent. For types 316L and 316 (4), the equivalent chromium contents are 20.2 and 18.6 weight percent, respectively. These calculations imply that types 316L and 316TiM are more susceptible to sigma than type 316 which in turn is more susceptible than type 321. This is consistant with observation.

Besides composition, pretreatment and aging conditions effect the stability of a steel. The equivalent chromium approach can accurately predict the relative stabilities of different alloys only if they are solution treated and aged at 816°C. There is no means to evaluate pretreatment and aging condition effects with the equivalent chromium approach as it now exists. However, if pretreatment and aging conditions could be converted to "effective equivalent chromium contents," this approach to predicting relative stability of different alloys under varying conditions would be extremely valuable.

Until that time when the equivalent chromium approach or a similar relationship is expanded to include the effects of pretreatment and aging conditions as well as composition, the approach used in this study of observing

phase stability is the best way of evaluating these effects.

CHAPTER V

CONCLUSIONS

This study of the microstructural stability of types 316TiM and 321 austenitic stainless steels allows the following conclusions:

1. The early nucleation of TiC and $Ti_4S_2C_2$ is an important factor in the phase stability of types 316TiM and 321. This can be related to the carbon content in the matrix.

2. Type 321 is more stable than type 316TiM. This is explained in terms of the lower nickel content, the absence of molybdenum, and the higher titanium content in type 321.

3. The precipitation of $M_{23}C_6$ is delayed and its growth retarded by the formation of TiC. This delay in precipitation of $M_{23}C_6$ is similar to that in low carbon content austenitic stainless steels of the same grade.

4. Of the intermetallic phases, sigma is preferentially precipitated in type 316TiM due to the low carbon content in the matrix.

5. Chi formation is retarded by early nucleation of sigma.

6. Cold work enhances sigma growth if recrystallization refines the grain size and provides numerous nucleation sites as in type 316TiM. At low aging temperatures

where recrystallization is slow, the grain boundaries between cold worked and recrystallized grains act as nucleation sites for sigma.

7. Cold work suppresses chi nucleation and growth if sigma growth is accelerated as in type 316TiM.

8. Cold work accelerates $M_{23}C_6$ precipitation.

9. Recrystallization in type 316TiM occurs earlier and proceeds more rapidly than in types 316 and 321.

LIST OF REFERENCES

LIST OF REFERENCES

1. E. A. Sticka: Proc., American Power Conference, Vol. XXII, IIT, Chicago, IL, 1960, pp. 285-301.

2. F. C. Hull: Welding Journal, Vol. 52, 1973, pp. 104s-113s.

3. S. M. Box and F. G. Wilson: JISI, Vol. 210, 1972, pp. 718-723.

4. B. Weiss and R. Stickler: Met. Trans., Vol. 3, 1972, pp. 851-866.

5. J. E. Spruiell, J. A. Scott, C. S. Ary, and R. L. Hardin: Met. Trans., Vol. 4, 1973, pp. 1533-1544.

6. "Liquid Metal Fast Breeder Program Plan," Vol. 7, Fuels and Materials, Washington - 1107, AEC Res. & Der. Report, August 1968.

7. P. R. Huclotter, T. R. Bump, W. T. Sha, D. T. Eggen, and P. J. Fulford: ANL-7786, Argonne National Laboratory, Argonne, IL, April 1971.

8. E. E. Bloom, Proceedings of Conference on "Irradiation Embrittlement and Creep in Fuel Cladding and Core Components," organized by the British Nuclear Energy Society, 1973.

9. D. Fahr, E. E. Bloom, and J. O. Stiegler: "Postirradiation Tensile Properties of Annealed and Cold Worked 316," to be published.

10. E. E. Bloom and J. O. Stiegler: Nucl. Tech., 1973,Vol. 17, pp. 24-37.

11. E. E. Bloom and J. O. Stiegler: Trans.,ANS, Vol. 15.1, 1972, pp. 253-254.

12. E. E. Bloom, Private Communication, 1973.

13. G. F. Tisinai, J. K. Stanley, and C. H. Samans: AIME Trans., Vol. 206, 1956, pp. 600-604.

14. M. E. Nicholson, C. H. Samans, F. J. Shortsleeve: Trans. ASM, Vol. 44, 1952, pp. 601-619.

15. P. K. Koh: J. Metals, Vol. 5, 1953, p. 339.

16. Goldschmidt: JISI, Vol. 162, 1949, p. 249.

17. R. E. Lismer, L. Price, and K. W. Andrews: JISI, Vol. 171, 1952, p. 49.

18. L. K. Singhal and J. W. Martin: Acta Met., Vol. 16, 1968, pp. 1441-1451.

19. P. Duhaj et al.: JISI, Vol. 206, 1968, pp. 1245-1251.

20. M. H. Lewis: Acta Met., Vol. 14, 1966, pp. 1421-1428.

21. L. K. Singhal and H. W. Martin: JISI, Vol. 207, 1969, p. 1382.

22. F. R. Beckitt and B. R. Clark, Acta Met., Vol. 15, 1967, pp. 113-129.

23. C. Da Casa, V. B. Nileshwar and D. A. Melford: JISI, Vol. 207, 1969, pp. 1325-1331.

24. L. K. Singhal and J. W. Martin: Trans. AIME, Vol. 242, 1968, pp. 814-819.

25. E. F. Kock and K. T. Aust: Acta Met., Vol. 15, 1967, p. 404.

26. P. Duhaj and J. Ivan: JISI, Vol. 206, 1968, pp. 1014-1016.

27. C. Da Casa: JISI, Vol. 207, 1969, P. 1003.

28. Yu P. Bulanov, M. A. Smirnow, A. M. Tolstov, and G. M. Shteinberg: Met. Sci. and Heat Treat., Vol. 13(1-2), 1972, pp. 27-31.

29. P. Duhaj: JISI, Vol. 206, 1968, p. 125.

30. P. N. Blinkinsop and J. Nutting: JISI, Vol. 205, 1967, p. 953.

31. L. K. Singhal and J. W. Martin: JISI, Vol. 205, 1967, p. 947.

32. H. J. Beattie and J. Hagel: Trans. AIME, Vol. 209, p. 911.

33. V. Ramascvany, A. E. Summer and P. R. F. West: JISI, Vol. 206, 1968, pp. 85-88.

34. R. Sumerling and J. Nutling: JISI, Vol. 203, 1965, p. 398-405.

35. M. A. P. Dewey, G. Summer, and I. S. Brammar: JISI, Vol. 203, 1965, p. 938.

36. W. E. White and J. Le May: Metallography, Vol. 3, 1970, pp. 51-60.

37. W. E. White and J. Le May: Metallography, Vol. 5, 1972, pp. 333-345.

38. H. Wiegand and M. Dorok: Arch. Eisenhuttenw., Vol. 8, 1962, p. 559.

39. S. J. Rosenberg and J. H. Darr: Trans. ASM, Vol. 41, 1949, pp. 1261-1288.

40. W. O. Binder, C. M. Brown and R. Franks: Trans. ASM, Vol. 41, 1949, pp. 1301-1345.

41. G. R. Kegg and J. M. Silcock: Met. Sci. J., Vol. 6, 1972, pp. 47-56.

42. A. L. Schaeffler: Welding Journal, Vol. 20, 1947, pp. 601s-620s.

APPENDIXES

APPENDIX A

ANALYSIS OF SELECTED AREA ELECTRON DIFFRACTION PATTERNS FOR PHASE IDENTIFICATION IN AUSTENITIC STAINLESS STEELS

I. Geometrical Nature of Electron Diffraction Patterns

The character of an electron diffraction pattern depends on the crystal structure of the sample, and for a single crystal, on its orientation and size. In crystalline materials, diffraction patterns reflect the geometric arrangement of atoms with similar regularity. Thus, the relationship between the geometry of a crystal and its diffraction pattern recorded on a photographic plate can be established. Consider the simple electron diffraction camera illustrated in Figure 27. From the geometry of the camera

$$\tan 2\theta = \frac{R}{L}$$

and as the angle, θ, is small

$$2\theta = \frac{R}{L} \qquad (1)$$

From Bragg's Law:

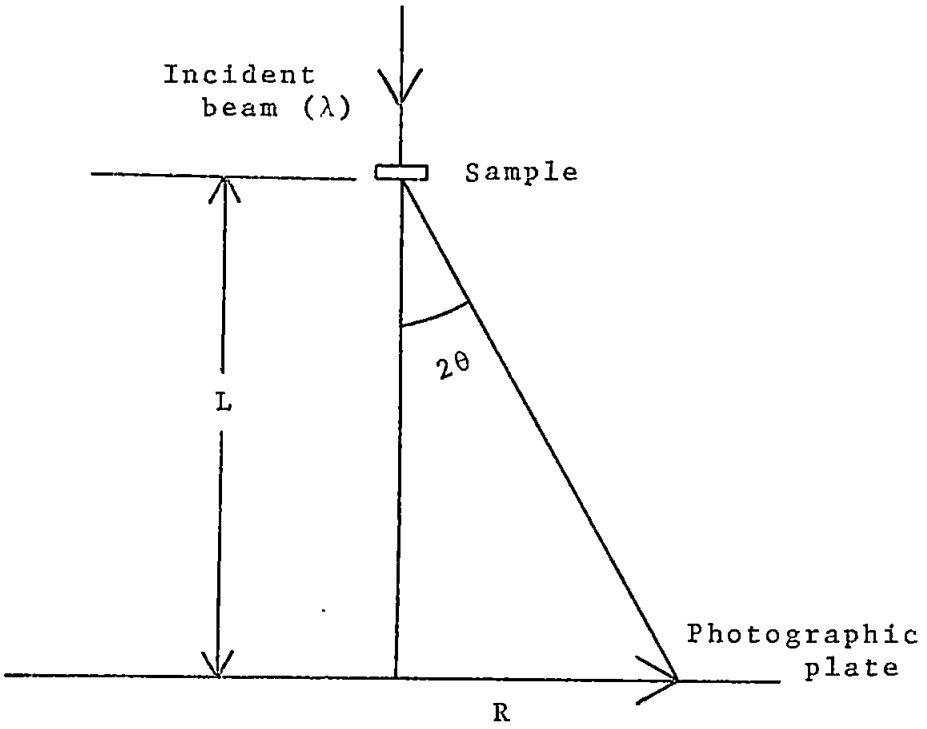
$$\lambda = 2d \sin\theta \simeq 2d\theta$$

$$\theta = \frac{\lambda}{2d} \qquad (2)$$

where d = the interplanar spacing of the reflecting planes.

by substituting equation (2) into equation (1), the following relationship is derived:

$$d = \frac{\lambda L}{R} \qquad (3)$$



L = distance from diffracting sample to photographic plate
R = distance from incident beam to diffraction spot
λ = wavelength of incident beam

Figure 27. A Simple Electron Diffraction Camera

It is seen from equation (3) that inverses of the distances measured in an electron diffraction pattern are related to the magnitudes of the interplanar spacings of the diffracting crystal multiplied by a scale factor. This constant of proportionality, λL, is called the camera constant. For each diffraction pattern there is only one camera constant. The different values of R measured on the diffraction pattern reflects the various different interplanar spacings in a crystal. Thus, once the camera constant is known, the interplanar spacings can be calculated from distances measured on the diffraction pattern by using equation (3).

II. Measurement of the Camera Constant of Electron Diffraction Patterns in Austenitic Stainless Steels

The matrix of austenitic steels has a face-centered cubic crystal structure. Therefore, the interplanar spacing for any particular reflecting planes (hkl) is given by

$$d_{hkl} = \frac{a}{(h^2+k^2+l^2)^{1/2}} \qquad (4)$$

where a is the lattice parameter listed in Table I, page 9. Equation (3) can now be rewriten as

$$(h^2+k^2+l^2)^{1/2} = \frac{a}{\lambda L} R \qquad (5)$$

If the ratio of two R values measured from the electron diffraction pattern is taken, the constant $a/\lambda L$ can be

eleminated. It is observed that the ratio of R values in cubic systems is related to the (hkl) values of the interplanar spacings. That is,

$$\frac{R_1}{R_2} = \frac{(h_1^2+k_1^2+l_1^2)^{1/2}}{(h_2^2+k_2^2+l_2^2)^{1/2}} \qquad (6) .$$

These ratios for face centered cubic systems are given in Appendix B.

The (hkl) values of the interplanar spacings of different reflection planes can be determined by fitting the ratio of the measured R values to the ratios of Appendix B. These (hkl) values can be verified by measuring the angle between the R vectors on the diffraction pattern and comparing them with the values of the angle between crystal planes with these (hkl) values. In cubic systems, the angle between two crystal planes is given by

$$\cos\theta = \frac{h_1h_2+k_1k_2+l_1l_2}{(h_1^2+k_1^2+l_1^2)^{1/2}(h_2^2+k_2^2+l_2^2)^{1/2}} \qquad (7).$$

These angles for the cubic system are given in most reference books on electron or x-ray diffraction.

Once the (hkl) values of interplanar spacings for the austenitic matrix are known, the camera constant, λL, can be determined using equation (3) with R measured from the diffraction pattern and d_{hkl} values for austenitic.

III. Phase Identification

With the camera constant calculated, the d-spacings of the unknown phase can be calculated using equation (3) once the R spacings are measured from the diffraction pattern. The d-spacings determined in this manner are then compared to the known interplanar spacings of the phases expected to precipitate in austenitic stainless steels. When a reasonable fit is made, the angles between the R vectors are measured from the diffraction pattern and compared with those expected between the crystallographic planes with the (hkl) values of the d-spacings for that phase. If both the d-spacings and the angles match the phase has been identified. Otherwise, this procedure is repeated until a reasonable fit between measured d-spacings and angles and known d-spacings and angles is obtained.

For cubic phases, the known d-spacings and the angles between them can be calculated from equations (4) and (7), respectively. For tetragonal systems, the d_{hkl} values are calculated from

$$d_{hkl} = \frac{1}{((h^2+k^2)/a^2(1/c)^2)^{1/2}} \qquad (8)$$

and the angles from

$$\cos\theta = \frac{(h_1h_2+k_1k_2)/a^2 + l_1l_2/c^2}{((h_1^2+k_1^2)2/a^2+(l_1/c)^2)^{1/2}((h_2^2+k_2^2)/a^2+(l_2/c)^2)^{1/2}} \qquad (9)$$

For hexagonal systems, the d_{hkl} values are calculated from

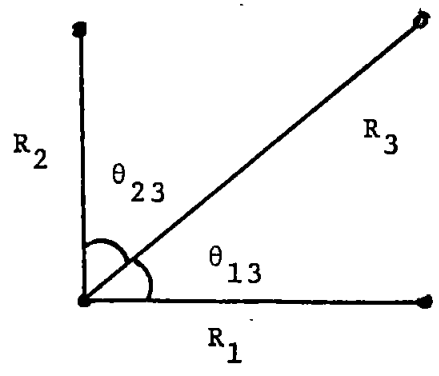
$$d_{hkl} = \frac{1}{\left(\frac{4}{3a^2}\left(h^2+hk+k^2\right)+\frac{1}{c^2}\left(l^2\right)\right)^{1/2}} \qquad (10)$$

and the angles from

$$\cos\theta = \frac{h_1h_2+k_1k_2+1/2(h_1k_2+k_1k_2)+3/4\frac{a^2}{c^2}\,l_1l_2}{\left(h_1^2+k_1^2+h_1k_1+3/4\frac{a^2}{c^2}\,l_1^2\right)^{1/2}\left(h_2^2+k_2^2+h_2k_2+3/4\frac{a^2}{c^2}\,l_2^2\right)^{1/2}} \qquad (11)$$

IV. An Example Analysis of an Electron Diffraction Pattern

Consider the selected area diffraction pattern shown in Figure 20(c), page 63. The matrix diffraction pattern consists of the larger and brighter spots in the photograph while the unknown phase diffracts the smaller spots. This is due to the greater area of the matrix in the diffraction zone and to the greater thickness of the unknown phase. This is seen in the transmission micrograph of Figure 20(c). Taking one section of the matrix diffraction pattern illustrated below,



it was measured that

$$R_1 = 2.20 \text{ cm}$$

$$R_2 = 2.55 \text{ cm}$$

$$R_3 = 3.35 \text{ cm}$$

$$\theta_{13} = 49°$$

$$\theta_{23} = 41°$$

$$\theta_{12} = 90°$$

the ratios of these R values are

$$R_1/R_2 = 0.864$$

$$R_1/R_3 = 0.655$$

$$R_2/R_3 = 0.761$$

From Appendix B, the ratio

R_1/R_2 implies (220)/(311)

R_1/R_3 implies (220)/(331)

R_2/R_3 implies (311)/331)

therefore, the (hkl) values for the d-spacings of the three measured R values would be:

$$R_1 = (220) = 022$$

$$R_2 = (311) = 31\bar{1}$$

$$R_3 = (331) = 331$$

It is seen that

$$h_1 + h_2 = h_3$$

$$k_1 + k_2 = k_3$$

$$1_1 + 1_2 = 1_3$$

which is consistant with vector addition. From

"Interpretation of Electron Diffraction Patterns" by Andrews, Dyson, and Klown, published by Plenum Press, New York, 1967, the angles between these planes are

$$\theta_{13} = 49.54°$$

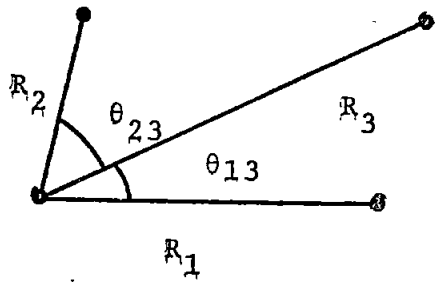
$$\theta_{23} = 40.46°$$

$$\theta_{12} = 90°$$

these angles are in good agreement with the measured angles and therefore this section of the matrix diffraction patterned has been indexed.

From Appendix C, $d_{311} = 1.082\text{Å}$. Using equation (3), and $R_2 = 2.55$ cm, the camera constant, λL, is 2.77 cm-Å.

Now a section of the phase diffraction pattern is measured as below



where

$$R_1 = 2.18 \text{ cm}$$

$$R_2 = 1.20 \text{ cm}$$

$$R_3 = 2.50 \text{ cm}$$

$$\theta_{13} = 56°$$

$$\theta_{23} = 26°$$

Using equation (3), with $\lambda L = 2.77$ cm-Å,

$$R_1: d_1 = 1.27 \text{ Å}$$

$$R_2: d_2 = 2.31 \text{ Å}$$

$$R_3: d_3 = 1.11 \text{ Å}$$

From comparing these d-spacings with those of the phases expected in type 316TiM stainless steel, the best fit is with the d-spacings of TiC. These imply that

$$d_1 = d_{\bar{1}3\bar{1}}$$

$$d_2 = d_{111}$$

$$d_3 = d_{040}$$

On this basis, the angles are calculated to be

$$\theta_{13} = 54.7°$$

$$\theta_{23} = 25.2°$$

$$\theta_{13} = 80°$$

These angles are in agreement with the measured angles. Thus, the unknown phase has been identified from the selected area diffraction pattern as TiC.

APPENDIX B

TABLE V

The Ratios of d-Spacings in Face-Centred Cubic Systems

hkl	111	200	220	311	222	400	311	420	422	511 333	440	531	442 600
111	1	1.15	1.64	1.92	2.00	2.31	2.52	2.58	2.83	3.00	3.266	3.416	3.464
200	0.866	1	1.41	1.66	1.73	2.00	2.18	2.24	2.449	2.598	2.828	2.958	3.000
220	0.612	0.707	1	1.17	1.22	1.41	1.54	1.58	1.732	1.837	2.000	2.092	2.121
311	0.522	0.604	0.854	1	1.05	1.21	1.31	1.35	1.477	1.567	1.706	1.784	1.809
222	0.500	0.578	0.817	0.957	1	1.15	1.26	1.29	1.414	1.500	1.633	1.708	1.732
400	0.433	0.500	0.707	0.830	0.866	1	1.09	1.12	1.225	1.299	1.414	1.479	1.500
311	0.397	0.459	0.649	0.760	0.795	0.917	1	1.03	1.124	1.192	1.298	1.357	1.376
420	0.387	0.446	0.632	0.740	0.774	0.894	0.975	1	1.095	1.162	1.265	1.323	1.342
422	0.354	0.408	0.577	0.677	0.707	0.816	0.890	0.913	1	1.061	1.155	1.208	1.225
511,333	0.333	0.385	0.544	0.638	0.667	0.770	0.839	0.861	0.943	1	1.089	1.339	1.155
440	0.306	0.354	0.500	0.586	0.612	0.707	0.771	0.791	0.866	0.919	1	1.046	1.061
531	0.293	0.338	0.478	0.561	0.586	0.679	0.737	0.756	0.828	0.878	0.956	1	1.014
442,600	0.289	0.333	0.471	0.553	0.577	0.667	0.726	0.745	0.816	0.866	0.943	0.986	1

APPENDIX C

TABLE VI

Interplanar Spacings of Austenite

Crystal Structure: Face-Centred Cubic

Unit Cell: a = 3.59Å

hkl	d-spacing Å
111	2.073
200	1.795
220	1.269
311	1.082
222	1.036
400	0.898
331	0.824
420	0.803
422	0.733
511,333	0.691
440	0.635
531	0.607
600,442	0.598
620	0.568
533	0.548
622	0.541
444	0.518
551,711	0.503

VITA

Arnold Stephen Grot was born in Gary, Indiana, on August 25, 1949. He attended elementary schools in Northwest Indiana and was graduated from Andrean High School of Gary in June, 1967. In September of that year he entered Purdue University and received a Bachelor of Science degree in Engineering Sciences in June 1972.

He accepted a Graduate Research Assistantship at the University of Tennessee in September, 1972, and received the Master of Science degree with a major in Metallurgical Engineering in June, 1974. He is a member of the American Society for Metals, the Metallurgical Society of AIME, Tau Beta Pi, Sigma Pi Sigma, and Sigma Gamma Tau.

He is married to the former Nancy Sara Kleinbach of Cunningham, Washington.